1-1-2011

Astrochemical dynamics: Fundamental studies relevant to titan's atmosphere

Wilson Kamundia Gichuhi
Wayne State University,

ASTROCHEMICAL DYNAMICS:
FUNDAMENTAL STUDIES RELEVANT TO TITAN'S ATMOSPHERE

by

WILSON K. GICHUHI

DISSERTATION

Submitted to the Graduate School

of Wayne State University,

Detroit, Michigan

in partial fulfillment of the requirements

for the degree of

DOCTOR OF PHILOSOPHY

2011

MAJOR: CHEMISTRY (Physical)

Approved by:

_____

Advisor Date

_____

_____

_____

_____

DEDICATION

To Faith and Lincoln

ACKNOWLEDGMENTS

First and foremost, I would like to gratefully and sincerely thank my advisor, Prof. Arthur G. Suits for his guidance, understanding, patience and most importantly his unparalleled mentorship as well as keen insights into science that enabled me to complete my graduate studies. Through his rich experimental skills and knowledge, Prof. Suits encouraged me not only to grow as an experimentalist but also as an independent thinker. Indeed, his mentorship was paramount in providing a strong foundation that was consistent with my long-term career goals. Without Prof. Suits help, I would not have realized my dreams. For everything you have done for me, thank you ever so much.

I would like to thank all members of Suits research group, present and past, for being instrumental in providing an atmosphere of team-work in the lab which allowed many experimental challenges to be solved. In my initial years of joining the lab, Dr. Cunshung Huang and Silva Ruchira introduced and trained me on the principles of working with lasers, alignment, vacuum operations and two color laser experiments for diacetylene. In these initial experiments, Cunshung and Ruchira taught me how to manipulate the apparatus and carry out DC slice imaging experiments.

The Chemistry department at Wayne state has always had a wonderful team of staff and faculty. I am especially grateful to Diane Klimas who was so helpful in managing our Titan's workshops and other conferences in a very friendly and pleasant style. I thank Sharon Kelly, Melissa Barton, Erin Bachert, Deborah McCreless, Diane Kudla, Nestor Ocampo, Bernadette Miesik and Mary Wood for all their help throughout my PHD work.

I would also like to thank the current Suits group members: Nuradhika Herath, Armando Estillore, Lu Yan, Mike Hause, Bernadette Broderick, Chamara Abeysekera, Tarek Ghani, Laura Kiefer and Mike Doyle for all their help and assistance in the lab. Special thanks go to my committee members; Dr. Feig, Dr Wen Li and Prof. Rothe for their valuable assistance in preparing this thesis. I especially thank them for their input and accessibility without which it would have been impossible to finish the defense.

Finally, I would like to thank my wife Faith for her support, encouragement, quiet patience and unwavering love throughout my graduate work. Her tolerance of my unavailability, especially when our son Lincoln was born, is a testament in itself of her unyielding devotion and unconditional love. Together with Lincoln, the love of my wife Faith was undeniably the bedrock and pillar upon which the very last years of my PHD work have been built. I thank my parents and family members in Kenya for their moral support.

TABLE OF CONTENTS

LIST OF TABLES

LIST OF FIGURES

Current Thesis is based on the following Lead Publications:

Chapter 2

1. **Gichuhi, W.K**; and Suits A.G: "An Experimental technique to determine branching ratios of ion-molecule reactions at low temperature conditions"- Under Review in Rev. Sci. Instr; 2011.

Chapter 3:

2. Huang, C; Zhang, F; Kaiser, R.I; Kislov, V.V; Mebel, A.M; Silva R; **Gichuhi, W.K;** Suits, A.G; Photodissociation of the diacetylene dimer and implications for hydrocarbon growth in Titan's atmosphere'' *Astrophysical Journal,* 2010, 714 1249

Chapter 4:

3. **Gichuhi, W.K;** Mebel, A.M and Suits, A.G: "UV Photodissociation of ethylamine cation: A combined experimental and theoretical investigation", J. Phys. Chem. A 114, 51, 13296, 2011

Chapter 5:

4. **Gichuhi, W.K;** and Suits A.G: "Primary branching ratios for the low temperature reaction of state-prepared N_2^+ with CH_4, C_2H_2 and C_2H_4- J. Phys. Chem. A 115 (25), 7105, 2011
5. **Gichuhi, W.K**; and Suits A.G: "Low-temperature branching ratios for the reaction of state-prepared N_2^+ with acetonitrile"- Submitted to J. Phys. Chem. A, 2011

CHAPTER ONE

INTRODUCTION

1.1 Analogies and differences between Titan and Earth

The mildly reducing atmosphere[6] of Saturn's largest moon, Titan, has continued to attract enormous research studies due to its resemblance to the primordial Earth[7-9]. Titan was first discovered in 1655 by a Dutch astronomer Christiaan Huygens. It has a diameter of 5150 km, approximately 70% larger than the Earth's moon[10]. Initially, Huygens had believed that Titan was the largest of the planetary satellites, but this distinction was later found to belong to Jupiter's largest moon Ganymede[11, 12], making Titan to be the second largest satellite in the solar system. Like Earth, Titan's dense atmosphere is mainly composed of molecular nitrogen (N_2) (~95%). The other main constituents are methane (CH_4) (~4%), hydrogen (H_2), other traces of hydrocarbon and nitriles (<2%)[13]. With a surface temperature and pressure of approximately 94 K and 1.5 bar, respectively, Titan's atmosphere is nearly five times densier than the Earth's.

Despite the aforementioned differences between these two planetary bodies, several analogies can be drawn between them. For example, although Titan is much colder than the Earth, their vertical structure resembles each other, hence their layers are classified based on temperature characteristics[14]. Nevertheless, Titan's higher density makes its atmosphere to be much more extended from the surface than the Earth's. While the troposphere of Titan extends to around 40 km from the surface, the Earth's tropopause lies only 15 km above the surface. The warmest region of Titan's atmosphere i.e. the mesosphere, is extended to latitudes higher than 400 km (compared to 100 km for the Earth) but the shape looks very much the same[14]. Figure 1.1 shows the density and temperature profiles of Titan and Earth's atmospheres.

On Titan, CH_4 and H_2 are equivalent, respectively, to the terrestrial condensate water vapor (H_2O) and the non-condensate carbon dioxide (CO_2). Although CH_4 cycle on Titan is still poorly understood, its role can be compared to the role of water on Earth[15].

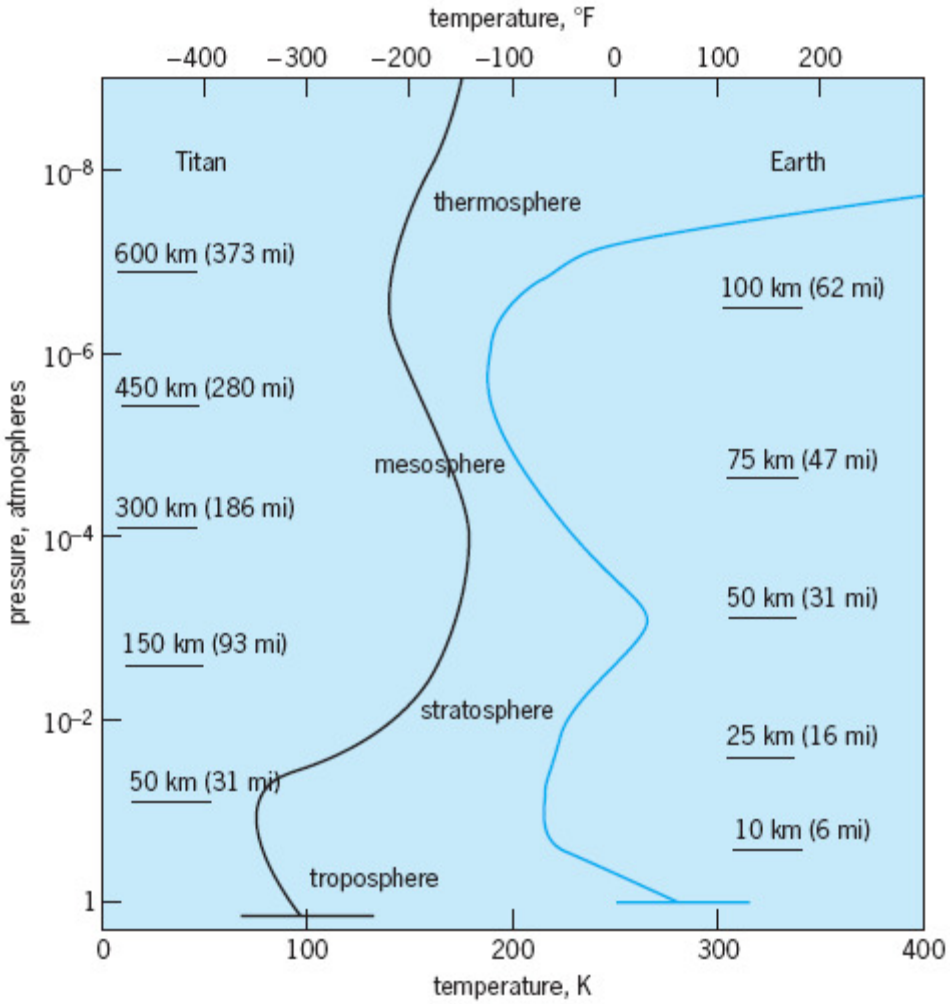

Figure 1.1: Physical structures of the atmospheres of Titan and Earth showing temperature and density profiles. The vertical axis is logarithmic pressure[3]

Based on the primordial noble gas composition measurements by the Cassini's Ion and neutral mass spectrometer (INMS)[16] and the Huygens Gas Chromatograph Mass spectrometer (GCMS)[17], it is speculated that Titan's atmosphere is secondary, just like the Earth's[1]. The major characteristic that makes Titan unique among the other solar

system's satellites (and the Earth) is its massive inventory of organic chemicals that constitutes its dense atmosphere.

1.2 Titan's Photochemistry

A combination of solar ultraviolet (UV) radiation and energetic particles from Saturn's magnetosphere (such as the suprathermal electrons) induces an active photochemistry that results in a chain of complex chemical reactions that lead to the formation of larger polyaromatic hydrocarbons (PAH), polyacetylene and other larger nitrile bearing species that constitutes the organic haze layers and aerosols whose formation mechanisms remain poorly understood to-date[18, 19]. Traditional laboratory approaches aimed at investigating the complex processes in Titan's atmosphere have involved electrical discharges[20-22] or UV radiation on simulated atmospheres[23-25] followed by analysis of the complex chemical products. In some cases, direct investigation of the underlying reactions has been pursued, albeit not under collisionless conditions in which the primary reaction products may be determined unambiguously.

In Titan's upper atmosphere, the photochemistry of neutrals and ions is strongly coupled[18], hence it is a worthwhile research effort to study the photochemistry of both the neutral composition that is mostly inherent in lower stratosphere as well as the rich ionosphere chemistry in Titan's ionosphere as revealed by the Cassini's Ion and Neutral Mass spectrometer (INMS). Furthermore, ion-molecule reactions in Titan's upper atmosphere[26] have recently been found to be much more important in Haze formation and hydrocarbon growth than it was initially thought. As such an accurate determination of primary branching ratios of nitrogen ion (N_2^+) reactions with the main minor neutral

components of Titan's atmosphere is also significantly important for accurate modeling of Titan's atmosphere.

In this thesis, we present a series of closely related fundamental photochemical studies as part of our comprehensive program aimed at investigating elementary reactions that can provide insights into the mechanisms that are responsible for the formation and growth of unsaturated hydrocarbon molecules and nitriles from the 'bottom up' in Titan's low temperature environment. Interpreted with the aid of high level ab initio calculations to characterize the relevant potential energy surfaces, the photochemistry measurements are all undertaken on cold, isolated molecules in molecular beams with the primary reaction products determined along with their translational energy distributions (and angular distributions in some cases). Towards the end of the thesis in Chapter 5, we present measurements of primary branching ratios of ion-molecule reactions of state-prepared N_2^+ cations with the main minor neutral components of Titan's neutral atmosphere. By examining the neutral photochemistry relevant to Titan's stratosphere, the ion chemistry that provides insights into the rich Titan's ionospheric chemistry and the ion-molecule reactions relevant to the upper ionosphere, this thesis provides detailed, integrated dynamical insights into the complex organic chemistry that is inherent in the strangely familiar world of Titan.

1.3 Origin of Titan's Nitrogen dominated atmosphere

Although nitrogen is ubiquitous on the atmospheres of terrestrial planets of Earth, Mars and Venus[1], its detection on a comparatively small and very cold moon of Titan by Voyager mission in 1980 was quite surprising. Generally, nitrogen in the atmosphere of planets and satellites can either have a primordial or a secondary origin depending on the

way it was initially delivered[1, 27]. The secondary origin means that N_2 could be a dissociation product of another nitrogen-bearing primordial molecule such as ammonia (NH_3). In sections 1.3.1 and 1.3.2, we give a brief review of the various possibilities of the origin of N_2 on Titan.

1.3.1 Direct Capture of N_2: Primordial N_2

Compared to Earth's oxidizing atmosphere, Titan's reducing atmosphere has methane (CH_4) as a greenhouse gas instead of carbon dioxide and free hydrogen gas instead of oxygen (O_2). Although not in similar proportions, these mixture of gases is a resemblance of the putative composition of the outer solar nebular which could be an indication that the N_2 on Titan's atmosphere is primordial, i.e. it was delivered as N_2 by the planetesimals that formed the satellite[1, 8]. Even though cold trapping of N_2 in the Titan forming planetesimals[28] was suggested earlier, the Huygens GCMS measurement of primordial argon (^{36}Ar) did not support this suggestion. A direct capture of N_2 would also be associated with ^{36}Ar given the fact that the two have similar trapping temperatures. The associated solar ratio for the $^{36}Ar/N_2$ in such a scenario would be 0.11. This is in contradiction with the GCMS[5] measured ratio of 2.1×10^{-7}. This clearly eliminates a direct capture of N_2 as the origin of Titan's N_2. Another implication of this measurement is that the planetesimals that formed Saturn's satellites, including Titan and Enceladus were certainly too warm for direct trapping of N_2. Thus, the N_2 on Titan must be secondary, produced by degassing of the icy planetesimals that formed the satellite[11].

1.3.2 Secondary formation of N_2 from primordial NH_3

For the terrestrial planets of Mars, Venus and Jupiter, N_2 is believed to be of secondary origin[29]. This is also believed to be the case for Titan. What this means is that

N_2 must have arrived on these solar system objects as an easily trapped condensed compound such as NH_3. The concept is also true for the other meteorites, comets and inner planets. For Earth and the meteolites, this conclusion is supported by the studies of $^{15}N/^{14}N$ ratio[30]. On the contrary, N_2, the dominant form of nitrogen in the outer solar nebula, was most probably included in the hydrodynamic collapse of surrounding nebula gases that deposited H_2 and He to Saturn[31]. According to the comets, icy planetesimals formed at temperatures beyond 32 K will not contain N_2, an additional suggestion in support of the secondary source for the origin of Titan's atmosphere[3].

With a density of 1.8 g/cm^{-3}, it is believed that Titan is composed of roughly 40 % ice by mass and the rest 60% being rock[32]. Ammonia is therefore believed to have been trapped initially in ice of Titan forming planetesimals. During the accretionary heating phase, volatiles were released to the atmosphere. Large quantities of water vapor, methane and ammonia are believed to have been present in Titan's primordial atmosphere[3]. Figure 1.2 (a) shows a photochemical scheme for the production of N_2 from NH_3 on Titan's primordial atmosphere while Figure 1.2 (b) presents a cartoon summarizing the processes that are thought to be involved in forming N_2 on Titan.

According to Figure 1.2 (a) the photolysis of NH_3 produces amidogen radical (NH_2)[1]. About one third of the dissociated NH_3 is recycled back by the reaction of the NH_2 radical with hydrogen atom (H). The remaining NH_2 radicals then react in a self recombination reaction to produce hydrazine (N_2H_4). Above 150 K, large amounts of N_2H_4 remains in the vapor phase. This leads to its dissociation forming an intermediate radical, hydrazyl (N_2H_3). The self-recombination of N_2H_3 radicals leads to the formation of N_2. However, below 150 K, little NH_3 is in the vapor phase and even small amounts

of N_2H_4 from it condenses, preventing the subsequent production of N_2. Apart from NH_3, large amounts of water vapor are also present at temperatures greater that 250 K. The photolysis of H_2O vapor therefore results in the production of highly reactive hydroxyl radicals (OH) and H atoms. The H atoms then react with NH_2 to form NH_3. Based on the cycle of reactions depicted in Figure 1.2 (a), the ideal temperature that is necessary to produce N_2 from NH_3 on primordial Titan is 150-250 K.

Although there is a general consensus that N_2 in Titan was produced from the dissociation of NH_3 as described above, the original source of NH_3 is less clear. Titan's forming planetesimals could have originated from Saturn's subnebula or as comets in the outer solar nebular[33]. However, if comets were the source of NH_3 on Titan, the $^{15}N/^{14}N$ ratio on Titan should be the same order of magnitude as in the comets, assuming that no escape of N_2 occurred over geological time.

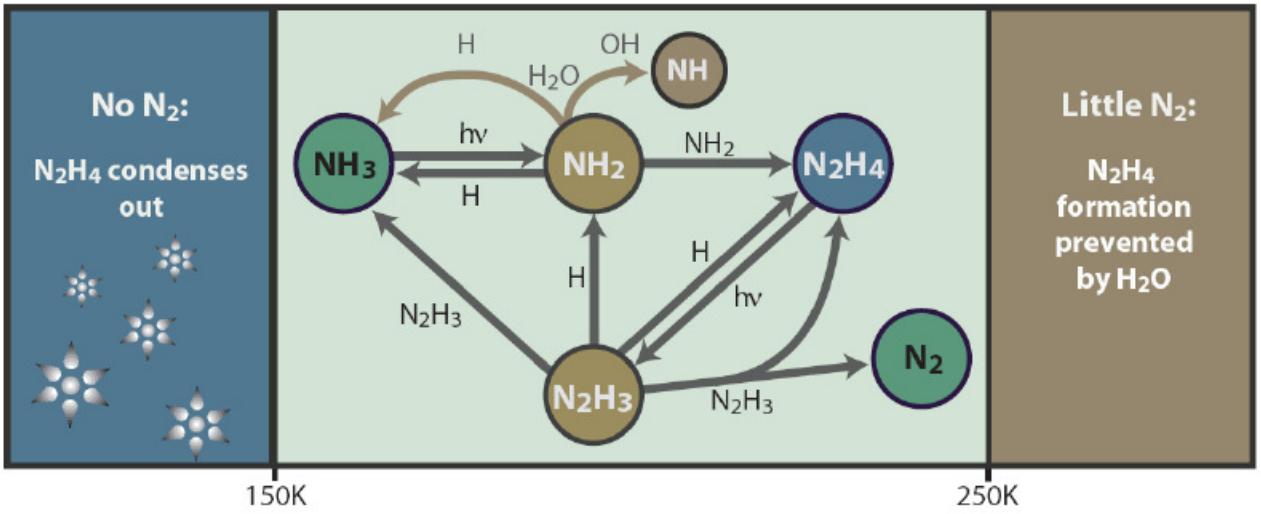

Figure 1.2 (a): Photochemical production of N_2 from NH_3 in Titan's primordial atmosphere.[1]

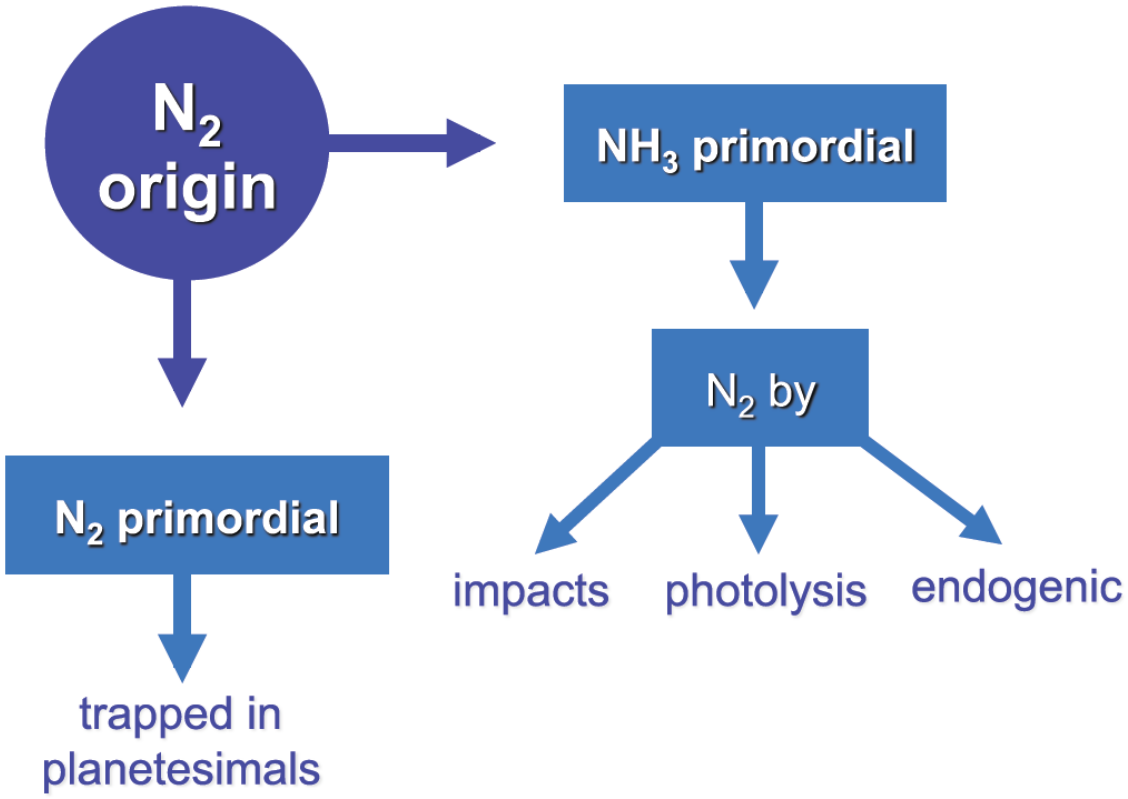

Figure 1.2 (b): A cartoon showing a summary of the postulated origin of N_2 on Titan's reducing atmosphere[1]

1.3.3 N_2 from impacts

In addition to NH_3 photolysis, the conversion and replenishment of N_2 from Titan's primordial NH_3 by impacts associated with Titan's accretion or the late heavy bombardment (LHB)[3, 34] has also been suggested as a possible origin of Titan's N_2. The possibility of shock-induced dissociation of ammonia from high velocity impacts during Titan's accretion was initially tested in a laboratory simulation experiment by McKay et al; in 1988[35]. In this experiment, a 1064 nm Nd-YAG laser was impacted on a mixture containing NH_3 and CH_4, generating large quantities of N_2. Although a creative idea, this

experiment resulted in the formation of other higher weight compounds that had m/z values greater than that of N_2. Furthermore, the shock tube experiment did not include water vapor that would inhibit the production of N_2, especially in the cooling phase of the shock. Seven years later, Griffith and Zahnle[36] suggested that Titan's N_2 atmosphere could have been a result of cometary impacts. This scenario relies on the fact that the source of N_2 comes from the comets that condense out of the solar nebula, not in the planetesimals that condensed from the Saturnian's subnebula to accrete Titan. The cometary hypothesis is based on the belief that N_2 was supplied originally in the form of complex organic molecules or molecular nitrogen. However, if, indeed, comets were the source of Titan's atmosphere, the D/H ratio on Titan should resemble that of comets; which is not the case. Thus, the comets as well as direct infusion of N_2 by comets are unlikely to be the source of N_2 on Titan. The cometary hypothesis is in further weakened by the fact that the comets are deficient in N_2 since the temperature in the region of their condensation between the orbits of Neptune and Uranus was too high (50-60 K) for trapping of nitrogen[37] . In a recent study, a new mechanism for the post-accretion formation of Titan's N_2 has been suggested and a laboratory investigation implemented[38]. The study reports on a hypothesis that proposes the conversion and replenishment of N_2 from NH_3 contained on Titan by impacts during the LHB. The results of these laboratory based impact experiments aimed at the determination of the efficiency of N_2 production from ammonium hydrate (NH_3-H_2O) ice have concluded that Titan, regardless of its thermal history, would acquire sufficient N_2 to account for the current atmosphere during the LHB and that most of the pre-LHB atmosphere would have been replaced by impact-induced N_2. So far, the results of this study are controversial since the Cassini-Huygens

data[5] does not show evidence of any such effects of cometary impact either in the atmosphere or on the surface of Titan. The presence of certain species on Titan such as primordial argon (^{36}Ar) are absent in comets. This provides an additional puzzle as to whether comets were responsible for N_2 during LHB.

1.4 Methane in Titan's atmosphere

As one of the most significant potential biomarkers in the solar system, CH_4 plays a central, controlling role in maintaining Titan's thick nitrogen atmosphere[1, 3, 15]. It is the source of haze layers that are responsible for the absorption of solar infrared radiation and the warming of the stratosphere by approximately 100-degree Celsius. Additionally, CH_4 is the source of hydrogen whose molecular collisions results in a 20 degree warming in Titan's troposphere[39]. Therefore, should Titan run out of CH_4, the atmosphere would collapse due to a drop in the temperature and the condensation of N_2 gas into liquid droplets. In summary, the three potential sources of methane on Titan includes: (i) direct delivery by Titan forming planetesimals; (ii) formation from primordial (non-methane) carbon and (iii) biological[1]. A biotic production of CH_4 that involves serpentinization reactions in Titan's interior has particularly been proposed as a major origin of Titan's atmospheric methane. There is another alternative scenario that suggests that methane was incorporated in Titan's planetesimals before its formation. The serpentinization reactions are not able to reproduce the Methane's Deuterium over hydrogen (D/H) ratio observed at present Titan's atmosphere. This process would require a maximum D/H ratio in Titan's water ice 30 % lower than the value likely acquired by the satellite during its formation, based on Cassini observations at Enceladus[40].

1.5. Titan atmosphere as a factory of Hydrocarbons

Having a massive atmosphere that consist of ~95% N_2 and ~4% methane[32], the solar radiation and charged particle collisions initiates chemical processes that break up these gas molecule. Despite being far from the sun and receiving only 1 % of the solar ultraviolet flux as compared to the Earth, photochemistry is the main driving force that makes it possible for Titan's atmosphere to have a thriving complex organic chemistry that leads to the formation of complex hydrocarbon molecules. At times, when Titan is in the vicinity of Saturn's magnetosphere, it is bombarded by charged particles such as the magnetospheric electrons which also contribute to the photoionization and dissociation of N_2 and CH_4. Simple hydrocarbons such as ethane, acetylene, diacetylene, hydrogen cyanide and cyanogen then readily form[41, 42]. Through a series of complex photochemical processes, more complex molecules such as propane, butane, polyacetylenes and cynanoacetylenes are then formed systematically[43, 44].

1.6 Haze formation

Starting with its initial discovery by Huygens in 1655, the detection of CH_4 in its atmosphere by Kuiper in 1944, the Voyager fly-bys in 1980 to the recent Cassini/Huygens space mission, Titan has been the subject of many studies aimed at understanding its climate, atmospheric dynamics and the important role of the haze that is formed in its atmosphere. The haze, having a well-defined structure, obscures Titan's surface from direct observations in the visible and is directly responsible for the orange color of Titan's atmosphere[18]. The haze particles are, in addition, believed to play an anti-greenhouse effect similar to that of the terrestrial atmospheric aerosols and clouds[29].

Nevertheless, the processes and mechanisms that control haze formation and its radiative properties have been the least and poorly understood to date. Figure 1.3 shows a picture of Titan's stratospheric haze as seen by the Cassini spacecraft.

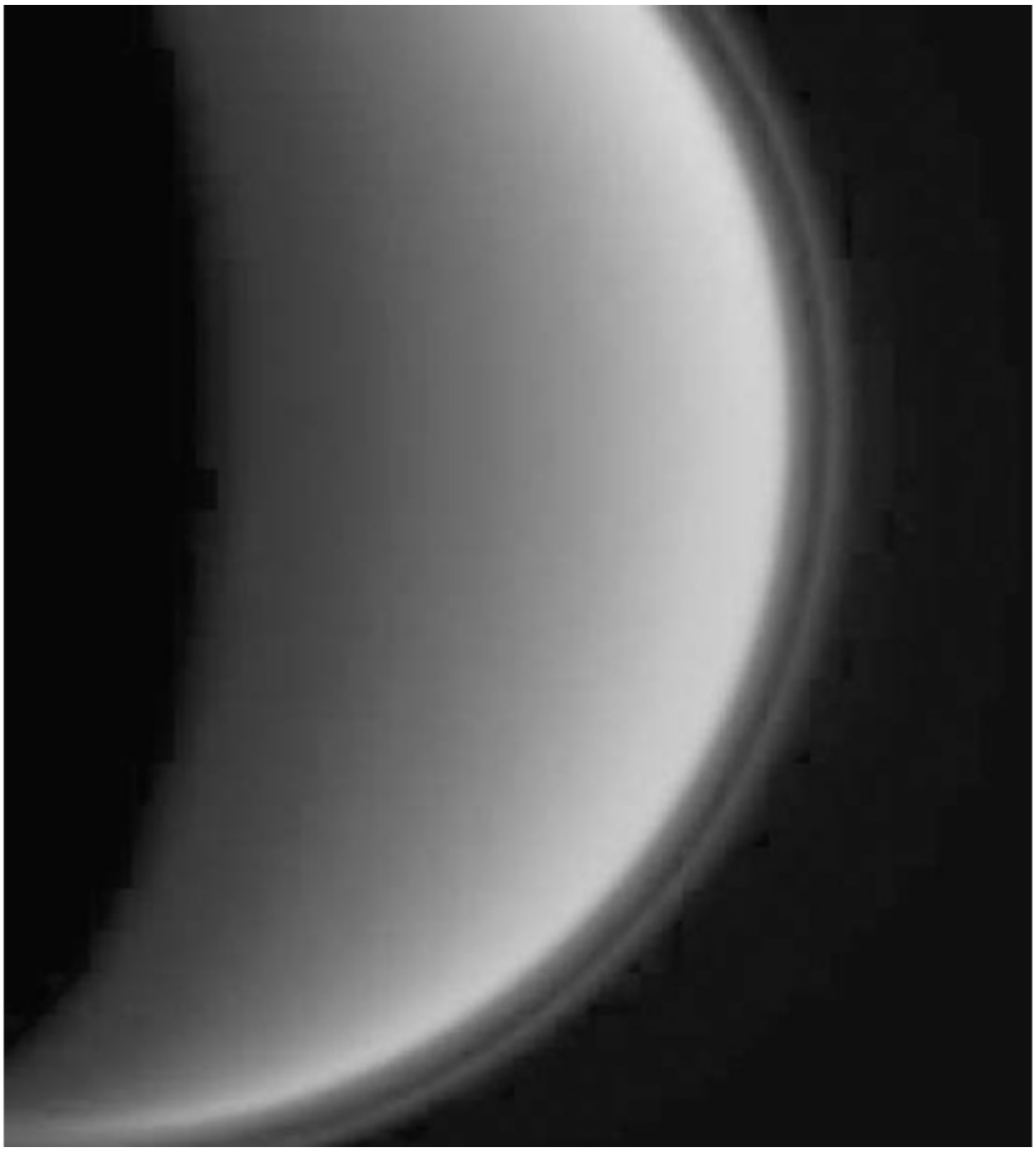

Figure 1.3: Image taken with the Cassini spacecraft's narrow-angle camera showing the complex structure of Titan's atmospheric haze layers. The Image was taken on 3 July 2004, at a distance of about 789 000 kilometers from Titan. (Image courtesy of NASA/JPL/Space Science Institute)

The entire chemistry that leads to the formation of the haze starts with the dissociation of N_2 and CH_4 through electron and photon impacts. In the upper atmosphere, primary processes leads to the formation of acetylene (C_2H_2) and hydrogen cyanide (HCN). Once these molecules are formed, they diffuse down to the lower levels where they allow the formation of higher hydrocarbons and nitriles[13]. CH_4 dissociation also occurs in the lower stratosphere through the photocatalytic processes involving C_2H_2 and other polynes.

1.7 Titan's stratosphere, neutral atmosphere and surface features

The composition of Titan's atmosphere from an altitude of ~140 km down to the surface was determined by the Cassini-Huygens probe GCMS after its successful landing[5]. Although the Voyager remote sensing instruments had already identified and measured several minor constituents in the tropopause and the stratosphere, the height profiles, isotope ratios and noble gas concentrations were not successfully retrieved from these data. It was therefore not possible to determine the fate of the photochemically produced gases in the upper atmosphere until the arrival of the Cassini orbiter. Figure 1.3 shows examples of averaged mass spectra obtained on; (a) the surface, (b) 130 to 120 km altitude and (c) 20 to 10 km altitude. The Huygens probe was also assigned to determine the extent to which simpler trace gases can form complex molecule, condensates or aerosols particles that ultimately precipitate on the surface. As can be seen from Figure 1.3, N_2, CH_4, H_2, ^{22}Ne, ^{36}Ar and ^{40}Ar were detected in situ in the lower surface. Kr and Xe could not be detected as they were below the detection limit of the instrument. Additionally, C_2H_6, C_2H_2, C_2N_2 and CO_2 were detected as they evaporated from the surface directly below the probe[28].

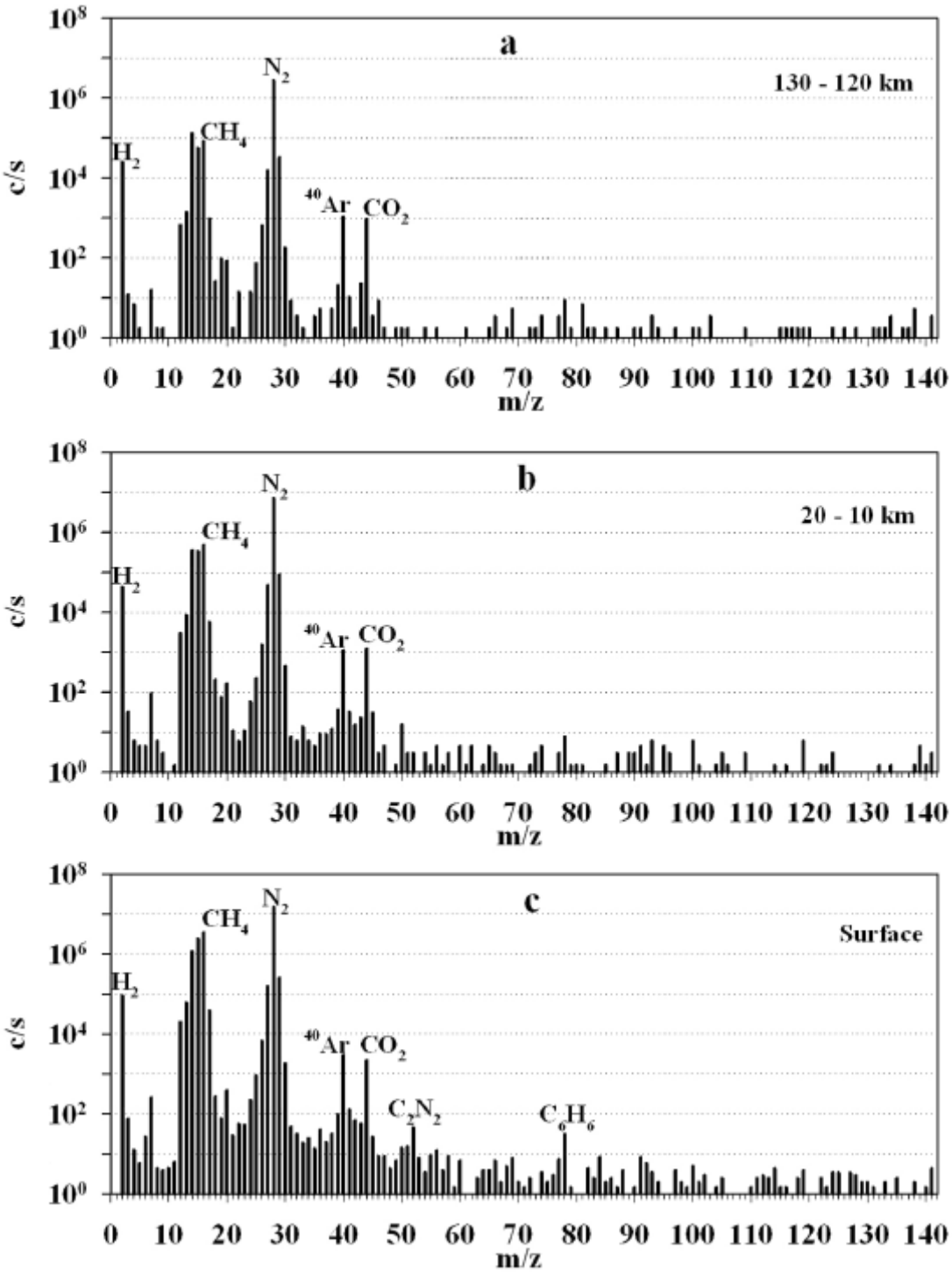

Figure 1.4. Examples of averaged mass spectra obtained at high, low altitude and on the surface; (a) Average from 130 to 120 km, (b) Average from 20 to 10 km, (c) Average surface spectra[5]

In addition to the GCMS results, the chemistry of Titan's neutral atmosphere has been a subject of a number modeling studies by several groups[42, 45, 46]. Figure 1.5 illustrates the basic chemical processes that constitute the active chemistry prevalent in the stratosphere[1]. On the left hand side, pathways for isolated CH_4 chemistry are shown. Primarily, CH_4 is dissociated by the Lyman-alpha radiation at 121.6 nm resulting in the formation of reactive methyl (CH_3), $^1CH_2$, $^3CH_2$ and CH radicals[47]. CH_3 is particularly produced at nearly 50% branching and it is indeed the precursor to all complex organics on Titan's atmosphere. As mentioned earlier, even though photolysis in the major contributor for CH_4 destruction in the upper atmosphere, below the stratosphere, catalytic destruction of C_2H_2 plays a crucial role in the irreversible destruction of CH_4.

As shown in Figure 1.5, further chemistry results in the formation of much heavier and stable hydrocarbons that includes C_2H_2, C_2H_4, C_3H_8, C_4H_{10}, polyacetylenes or polyynes ($C_{2n+2}H_2$, n= 1,2,3,…..etc). Although polyacetylenes higher than C_4H_2 have not been detected in Titan's atmosphere, perhaps due to their low vapor phase concentrations, Kaiser and co-workers have shown that triacetylene (C_6H_2)[48] can readily be formed in Titan's upper atmosphere from a reaction between C_2H and C_4H_2. This pathway has been suggested as a possible route to the synthesis larger hydrocarbons and polyacetylenes in Titan's low temperature and pressure conditions. The work presented in chapter three of this thesis show that the photodissociation of weakly bound van-der-waal complexes such as the diacetylene dimer[49] initiates atomic hydrogen loss and hydrogen transfer reactions forming two prototypes of resonantly stabilized free radicals (RSFRs), C_4H_3 and C_8H_3, respectively, via one step photoexitation pathway. These RSFRs represent hydrogenated polyynes which can neither be synthesized via traditional

photodissociation pathways of the diacetylene monomer nor via hydrogen addition to the polyynes. The photodissociation dynamics of mixed dimers involving acetylene, diacetylene and other trace constituents represent an overlooked reaction class that has the potential to synthesize more complex, RSFRs, considered to be major building blocks to polycyclic aromatic hydrocarbons in Titan's low-temperature stratosphere. The implication of these findings to Titan's neutral atmosphere will be discussed in detail in Chapter 3 of this thesis.

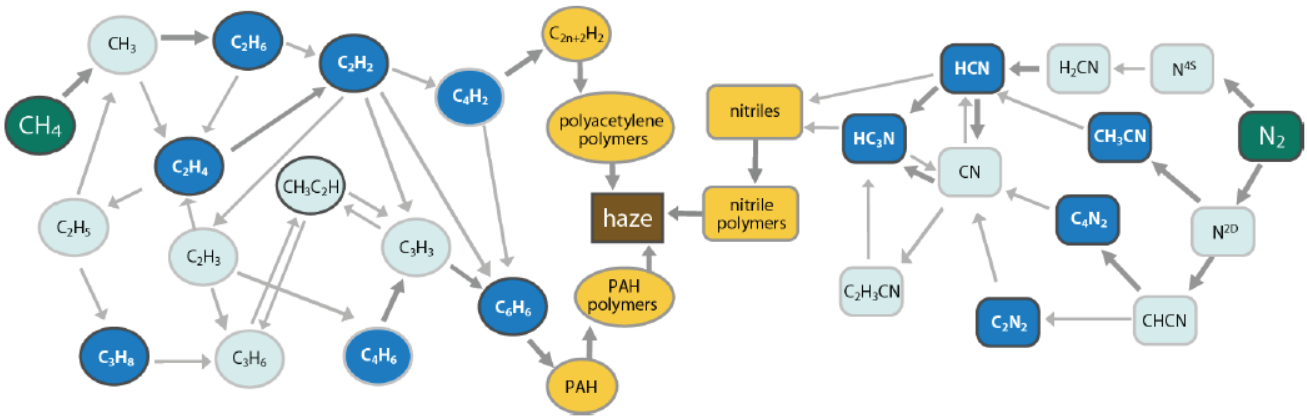

Figure 1.5: Basic schematic of coupled methane–ammonia chemistry in the neutral atmosphere of Titan below ~800 km, showing the production of stable hydrocarbons and nitriles, and subsequently the photochemical haze[1]

1.8 Titan's Ionosphere and Ion-molecule reactions

1.8.1 Composition of Titan's ionosphere

Prior to the Cassini tour of Titan's ionosphere, atmospheric models had suggested that the primary altitude of aromatic hydrocarbon formation (example benzene formation) occurs in the well-mixed portion of the atmosphere at around 750 km. This being the case, the models proposed that the process of aromatic hydrocarbon formation would be accompanied by hydrocarbon radical reactions with a much weaker source due to ion-neutral reactions near the ionospheric peak of 100 km[43]. The expectations prior to the Cassini orbiter were that benzene would be barely measurable at the lowest altitudes observable by Cassini's INMS (~950 km). Surprisingly, the INMS observed an unexpected abundance of hydrocarbon and nitrile species throughout the instruments mass range (1-100 Daltons)[16]. Even more surprising and unexpected was the measurement of up to 350 Daltons of positive ions by the Cassini plasma spectrometer (CAPS) ion beam spectrometer[16, 46]. Although not calibrated to measure negative ions, the CAPS electron spectrometer also, albeit at low resolution, reported an appreciable concentration of negative ions exceeding to over 10,000 Daltons[50].

Figure 1.6 shows the INMS measurements of the ion composition obtained during the Cassini's T40 flyby. The spectrum represents the average composition in the 1015–1050 km region of the atmosphere that was obtained near the time of closest approach. As it is also the case with other reducing environments, ionization in Titan's ionosphere flows from species whose parent neutrals have smaller proton affinities (PA) to species whose parent neutrals have larger PA. As such, proton exchange reactions drive the chemistry in the ionosphere of Titan resulting in the most abundant ions being essentially

protonated neutrals (closed shell ions) with the $HCNH^+$ ion being the most abundant[4, 46]. Radical cations such as $C_2H_4^+$, $C_3H_4^+$, NH_3^+ and HCN^+ are difficult to produce and even when they are formed, they are eliminated fast through reactions with the main neutral species as well as through electron-dissociative recombination. In summary, the INMS results presented in Figure 1.6 was a confirmation of a long-thought idea that a very rich chemistry is taking place in Titan's ionosphere.

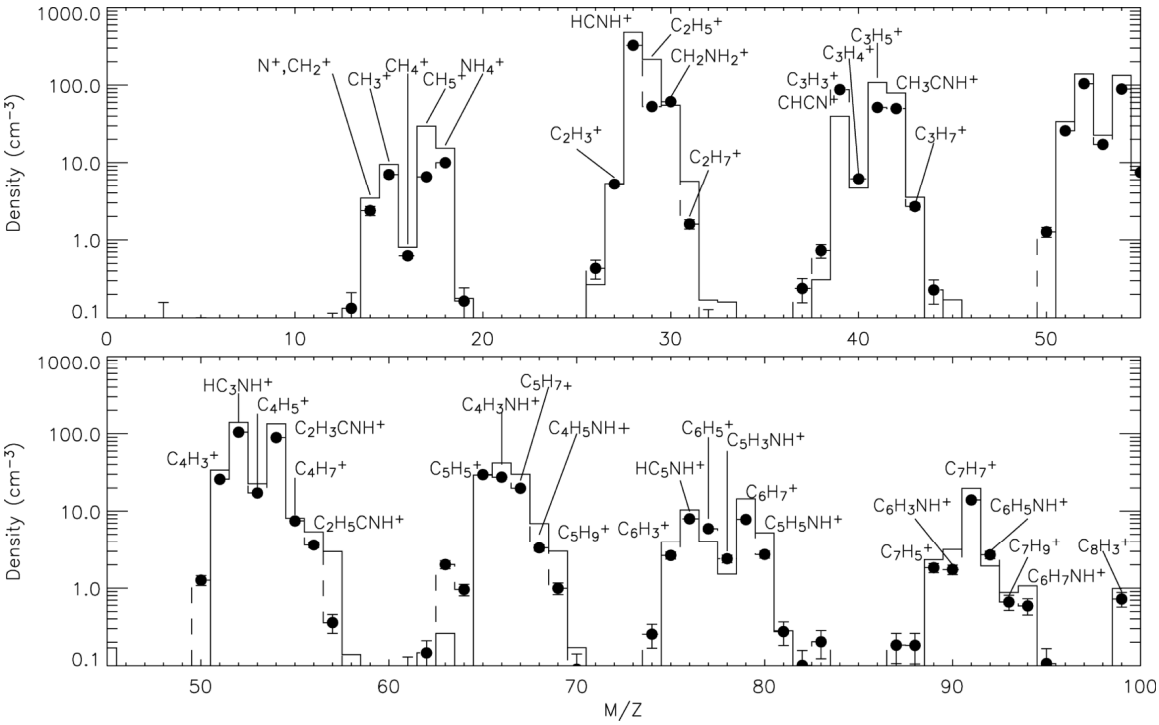

Figure 1.6: Positive ions mass spectrum measured during the T40 encounter, averaged between the altitudes of 1015 and 1050 km. The black dots show the INMS measurements, and the black line connects the points. Error bars represent the uncertainty due to counting statistics. They are smaller than the symbol size for larger densities. They do not include a systematic error of 20% due to calibration uncertainties. The dotted line represents the modeled spectrum with densities of selected neutrals tuned to reproduce the observations[4]

1.8.2 Ion-molecule reactions in Titan ionosphere and their role in Haze formation

Supported by the current modeling studies on Titan's ionosphere[2, 45, 51], the Cassini data have shown that ion chemistry and the accompanying relevant ion-molecule reactions are important in determining the abundances of trace neutral species and laying a strong foundation in understanding the mechanisms that lead to the formation of the haze layers and aerosols. Ionization in the upper atmosphere generates N_2^+ and N^+ in approximately equal abundances[52, 53]. Following the formation of N_2^+ and N^+, a network of ion-molecule reactions is initiated by the reactions of these ions with the next abundant molecule, CH_4. In Titan's mesosphere and thermosphere, N_2 and CH_4 are dissociated by a combination of extreme solar ultraviolet (EUV) radiation and energetic electrons from Saturn's magnetosphere according to reactions 1.8.2.1 to 1.8.2.7[42]. Figure 1.7 portrays a snap shot of the first key neutrals and the ion-molecule reactions that occurs in the ionosphere while reactions 1.7.2.1 to 1.7.2.3 represent the very first primary ion-molecule reactions that occurs in Titan's ionosphere.

$$N_2^+ + CH_4 \rightarrow CH_2^+ + N_2 + H_2 \quad \text{..……1.8.2.1}$$

$$\rightarrow CH_3^+ + N_2 + H \quad \text{……1.8.2.3}$$

(Rate constant k = 1.14 x 10^{-9} cm^3 s^{-1})

$$N^+ + CH_4 \rightarrow CH_3^+ + NH \quad \text{…… ……..1.8.2.3}$$

$$\rightarrow CH_4^+ + N\text{…….1.8.2.4}$$

$$\rightarrow HCNH^+ + H_2 \quad \text{…….. 1.8.2.5}$$

$$\rightarrow HCN^+ + H_2 + H\text{…….1.8.2.6}$$

(Rate constant k = 1.15 x 10^{-9} cm^3 s^{-1})

CH_2^+ and CH_3^+ product ions are unreactive with N_2 and will go on to react further with CH_4 and other neutral hydrocarbon species present in the atmosphere. New ions are then formed within the framework of secondary ion-molecule reactions and the ionospheric chemistry becomes complex very quickly as can be seen in Figure 1.7. The newly formed molecules diffuse to lower altitudes where they mix evenly with the atmosphere and contribute to the molecular abundances observed by the Voyager and the Cassini spacecrafts. As the molecules diffuse through the stratosphere, they are condensed. The aerosol layers formed by the condensation of these molecules in the stratosphere are believed to be one of the main sources of the Titan's characteristic orange haze.

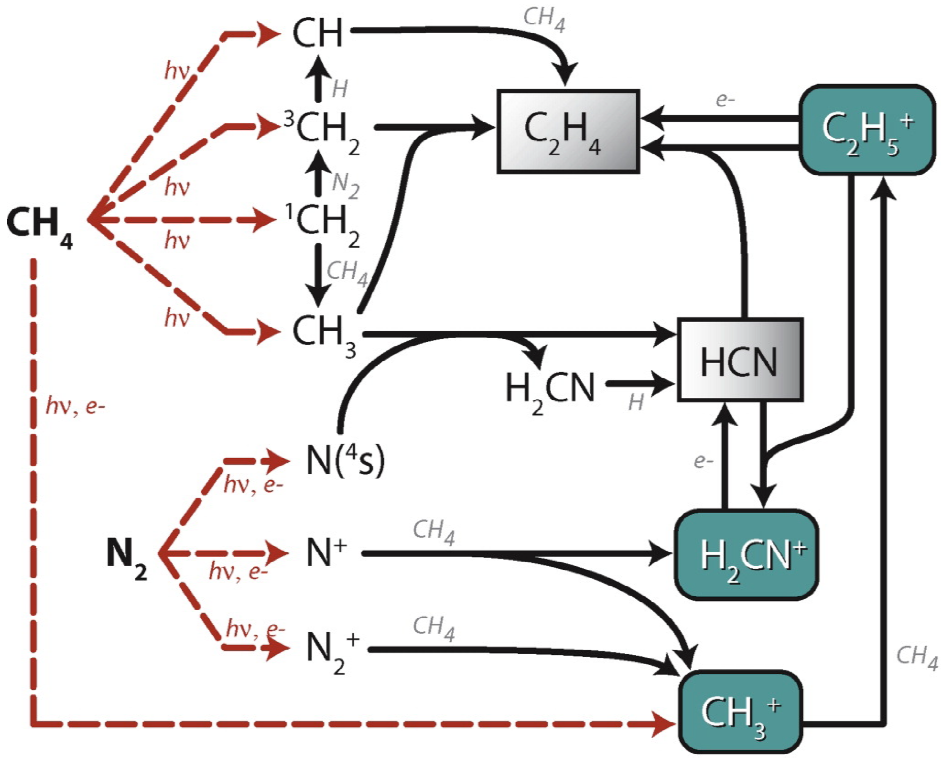

Figure 1.7: A snap shot of the first key neutrals and the ion-molecule reactions that occurs in the ionosphere[2]

In order to build an accurate model of Titan's ionospheric chemistry, it is of crucial importance to know the primary species present, the main primary reactions occurring, the main primary product channels, the rate of formation and destruction of each of the species present, the associated primary product branching ratios of these reactions and the other physical parameters (such as pressure and temperature) that govern the chemistry. Laboratory data acquired at well defined conditions is therefore very essential to the construction of an accurate model. In instances where the required laboratory data such as the reaction rates and BRs are unavailable, it is common to make estimates which usually make the models deficient as far as the full description of the planetary atmosphere is concerned. In a detailed uncertainty analysis of kinetic parameters of the ion-molecule reactions included in Titan's ionospheric models, Carrasco et al[54, 55]; have shown the uncertainty on the measured BRs as one of the limiting factors for accurate prediction of ion-density profiles in Titan's ionosphere.

The BRs of the main primary product channels associated with the ion-molecule reaction between N_2^+ and CH_4 have particularly been cited as a major contributor to the uncertainty in the models. Although Titan's ionosphere is a difficult environment to model because the chemistry is not uniform throughout, to-date, some models[2] have proved to be remarkably accurate in matching the observations provided by the Voyager and the Cassini missions. Needless to say, the insights that the models provide into Titan's ionosphere is useful, but their true accuracy cannot be valid without accurate laboratory determinations of important primary astrophysical quantities such as the BRs at low temperature and pressure conditions that closely resemble Titan's. As such, we show in chapter two how a modified ion imaging apparatus can be modified to measure

accurate BRs of ion-molecule reactions at well defined conditions of pressure and temperature that are close to Titan's. Finally, in Chapter five, we present BR measurements of state-prepared N_2^+ initiated ion-molecule reactions using the newly commissioned apparatus. In what we are calling *''Astrochemical dynamics''*, the development of such new methodologies that probe Titan's ion-molecule reactions at relatively low temperature regimes allows for direct and deeper dynamical information of such a complicated ionosphere to be inferred.

CHAPTER TWO

EXPERIMENTAL

2.1 Direct current (DC) slice ion imaging

For Ethylamine (ETA) cation dissociation, experiments are carried out using a velocity map imaging technique that is optimized for DC slice imaging. The technique has been described in detail elsewhere[56, 57], hence we only give a brief description here. The schematic diagram for the experimental set-up is shown in Figure 2.1. The resonance enhanced multiphoton ionization scheme (REMPI) that is used in the preparation of ETA cation is illustrated in Figure 2.2. In the 1+1 REMPI scheme, two photons of 233 nm laser light are used to prepare ground state ETA cation. Absorption of an additional photon from the same light leads to fragmentation of the state prepared ETA cation. Both ionization and dissociation occurs from the same laser pulse. The product ions are then accelerated through multilens velocity mapping assembly and impacted onto a dual microchannel plate array of 120 mm diameter that is then coupled to a p-47 phosphor screen. A narrow gate of about 80 ns was used to appropriately sample the central section of the distribution to implement the slicing condition. The resulting ion image was recorded by a CCD camera (Sony XC-ST50), 768 X 494 pixels) in conjunction with the IMACQ Megapixel acquisition program[58].

2.2. Modified Ion imaging apparatus

An overview of the imaging apparatus that has been modified to measure BRs is illustrated in Figure 2.3. The main modifications that makes the apparatus suitably adapted for BR measurements are the insertion of fine mesh nickel grids that covers the 2 mm diameter hole infront of the of the repeller plate, the removal of the skimmer, pulsing

of the repeller/extractor plates and the firing of the laser beam inside the source chamber at a very close distance (~1-2 mm) to the aperture of the supersonic nozzle.

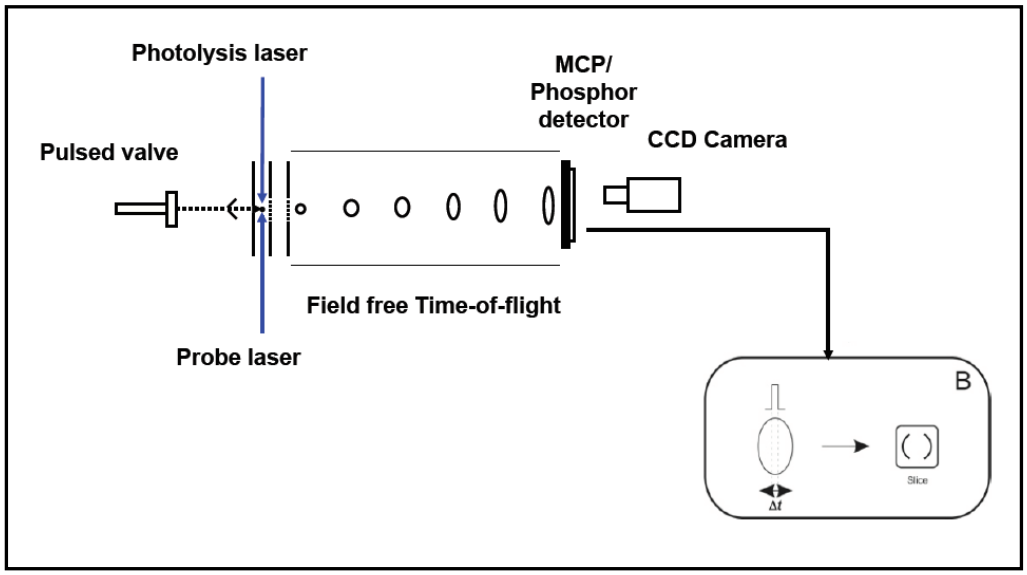

Figure 2.1: Schematic diagram for the ion imaging set up for the dissociation of Ethylamine cation. In this particular experiment, the same laser pulse was utilized for the preparation of the cation (REMPI laser) as well as for the dissociation of the state prepared cation.

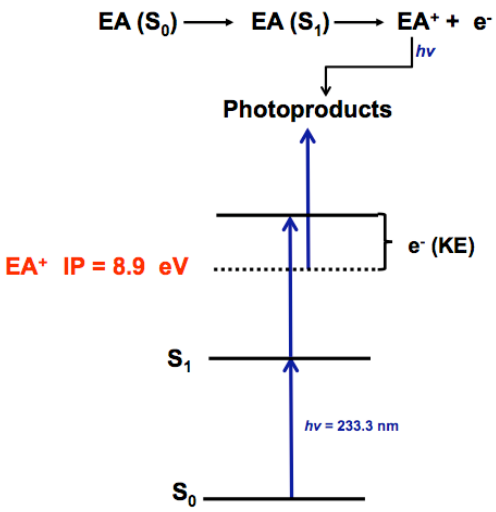

Figure 2.2: Excitation scheme for the 1+1 resonance enhanced multiphoton ionization (REMPI) of ethylamine cation at 233 nm.

The vacuum system and the chamber characteristics of the ion imaging experimental set-up have been reported in detail elsewhere[57], so in this description, we mainly focus on the new modification that allow us to measure low-temperature BRs in the collision region of the supersonic expansion. A 2-mm diameter conical nickel skimmer that is located 2.5 cm downstream of the supersonic nozzle was removed, leaving a larger diameter aperture that separate the main chamber from the source chamber. The removal of the skimmer allowed higher gas densities of the newly born ions to be extracted into the main chamber where the ion optics are housed. Removing the skimmer therefore enabled us to detect the newly born ions at an improved signal to noise ratio. Inside the source chamber, the general valve supersonic nozzle was mounted in the opposite geometry so that the flat surface was at a close proximity to the focused REMPI laser beam.

Following ionization of the neutral reactant gas through REMPI, the parent ions are accelerated out of the ionization region by the potential difference between the repeller and the extractor. The ion optics assembly consists of four thin electrodes (repeller, extractor, lens 1 and lens 2). The inside diameters for these electrodes are 2, 16, 32, and 40 mm with respective spacing of 1.8, 2.1, and 2.9 cm. This four lens configuration without the grids was initially designed to obtain optimum velocity mapping conditions[58] for ion imaging experiments. However, for our BR measurements, we configured and optimized our mass spectrometer in reference to the classic two field Wiley-McLaren design[59]. During the course of our experiments, the potential gradient applied across the repeller and the extractor was regularly adjusted in order to obtain a desired resolution in the time-of-flight data. The fine mesh nickel grid mounted in front

of the repeller provided homogeneous fields in the ion acceleration region. To ensure efficient extraction of newly born ions into the main chamber, a negative voltage bias of 50V and 30 V were applied to the repeller and the extractor plates, respectively. Positive voltage pulses of 700 V and 500 V were then applied to the repeller and the extractor, respectively, in order to propel the ions to the detector and allow for mass selection and detection. Both plates had the same delay time of 30-50 μs and a width that was varied between 8-30 μs depending on the arrival time of the respective ions. Once the ions were in the extraction volume, lens 1 could then be occasionally used to focus the ions onto the detector by adjusting its voltages from 300 V to 500 V. Right in front of the supersonic nozzle (~1 mm from the hole), the reactant N_2^+ ions were predominantly produced in their ground vibrational states via a 2 + 1 REMPI scheme at 202 nm[60].

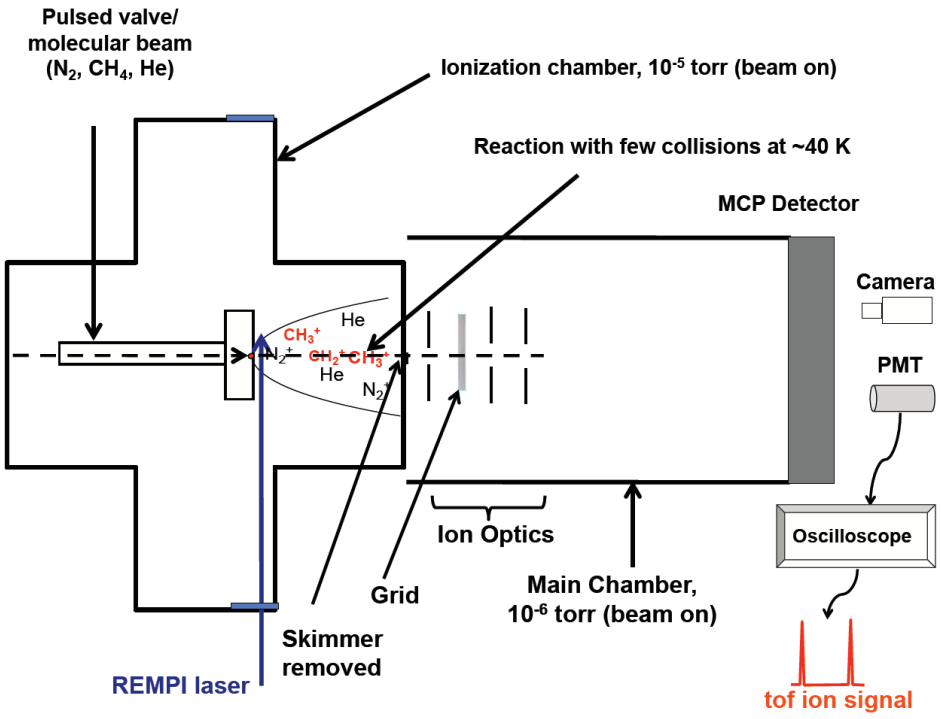

Figure 2.3: Schematic diagram of the experimental approach using the modified velocity map ion imaging apparatus

Both plates had the same delay time of 30-50 μs and a width that was varied between 8-30 μs depending on the arrival time of the respective ions. Once the ions were in the extraction volume, lens 1 could then be occasionally used to focus the ions onto the detector by adjusting its voltages from 300 V to 500 V. Right in front of the supersonic nozzle (~1 mm from the hole), the reactant N2+ ions were predominantly produced in their ground vibrational states via a 2 + 1 REMPI scheme at 202 nm[60].

In order to record the N_2 2+1 REMPI spectrum, the fundamental wavelength of the dye laser was scanned from 16,470 to 16474 cm^{-1}. Figure 2.4 top and bottom shows the experimental and simulated REMPI spectrum, respectively. The simulated spectrum was obtained by fitting the literature N_2 spectroscopic constants using the Pgopher program. There is a good agreement between the experimental and the simulated spectrum. A key point to note is that our main purpose in recording the REMPI spectrum presented in Figure 2 was to determine the rotational temperature. Under our experimental conditions therefore, a rotational temperature of 40 ± 5 K was determined after the fitting. The typical linewidth of the dye laser employed in our study was ~0.2 cm^{-1}. In addition to the pure N_2 spectrum, we also recorded the spectrum using the CH_3^+ signal that was formed from the reaction of N_2^+ with CH_4. Except for an increased intensity for the pure N_2 spectrum, the two spectra are similar which is indicative of the lack of rotational dependence on the BRs.

To make sure that the measured BRs were not sensitive to laser delay, reactant concentration, pulse valve delay, extraction voltages, laser power and other factors, the conditions of the experiment were broadly explored and optimized. This was necessary since the main aim of our new apparatus was to measure BRs that were exclusively from

primary reactions. The timing of the experiment was carefully arranged to eliminate any cluster or the occurrence of secondary reactions. At first, the laser fires. After a variable delay (ca.300 μs), the pulsed valve driver opens and the supersonic expansion begins. In this case, the laser firing is referenced as time zero. The ions then flow downstream for a second delay time until they arrive at the TOF mass detector. No ion signal was observed when the laser was off-resonance. Additionally, there was no signal of other products (e.g. He^+, C^+, CH^+, N^+) suggesting plasma formation in the nozzle. Figure 2.4 presents a TOF spectrum for the charge-transfer reaction between N_2^+ (v = 0) ions with Kr in the presence of Ar and He as buffer gases. There is no He^+ (m/z =4) or Ar^+ (m/z =40) signal in the spectrum which is a clear indication of an efficient CT that is purely induced by state-prepared ground state N_2^+ ions with no plasma or contribution from vibrationally excited N_2^+. The fact that we do not observe Ar^+ signal is, indeed, a further confirmation that N_2^+ ions are formed in the ground vibration state since we would expect to see an Ar^+ signal in an instance where vibration excited N_2^+ ions (v=1) are formed. The results on this TOF spectrum will be discussed further in the results and discussion section.

Containing the newly born ions, the unskimmed molecular beam was allowed to flow downstream into the main chamber where the ion optics are housed. It is in the main chamber where both the ion extraction and the detection were accomplished. The plates were externally triggered at 10 Hz. After the extraction of the product ions, the ion cloud was then accelerated toward a 120 mm diameter chevron-type microchannel plates (MCPs) coupled to a fast P-47 phosphor screen. A CCD camera (SONY XC-ST50), 768 X 494 pixels) was used to view the phosphor screen while a photomultiplier tube (PMT) captured the integrated TOF signal. In all our experiments, the MCP remained un-gated.

The PMT signal was then sent to an oscilloscope for averaging and the final data transferred to the computer. In order to get the BRs, the area under each peak was determined after fitting the peaks using Gaussian function. Figure 5 shows a TOF spectrum for the reaction of N_2^+ (v=0) with methane and a corresponding Gaussian fit. It should be mentioned here that the BRs obtained by a direct integration of the peak areas were not very different from the one obtained by fitting with the Gaussian. We therefore chose to use the Gaussian fitting as it gave more consistent BRs since it eliminated the uncertainty brought about by the tailing of the peaks at higher masses.

2.2.1 Rotational Temperature determination

The rotational temperature of 40 ± 5 was arrived at after a careful simulation based on the line-width of our dye laser. It is critical to mention that a supersonic jet is a non-equilibrium medium[61]. The non-thermal equilibrium properties of the jet are usually caused by a drop in the density and temperature with increasing distance from the nozzle. The thermal anisotropy inherent in free jet expansions therefore makes the definition of the reaction temperature complicated. Ideally, we would like to obtain experimental data on BRs where the reaction temperature remains nearly constant. As explained below, although we can confidently measure the rotational temperature and report the temperature under which the reactions take place, that temperature may not represent the real reaction time. To-date, its only in the CRESU experiment[62] where this uncertainty in the reaction time has successfully been eliminated. According to M.A Smith and co-workers[61], at distances not too close to the nozzle, the reaction temperature of the product ions is expected to be equal. The distance from our nozzle to the point of ion extraction was maintained at 1-2 mm. On the other hand, the bias voltage for our repeller and the

extractor are less that -50 V and we do not expect to have substantial stray field-induced velocity that would lead to significant uncertainty in the rotational temperature. As can be seen from Figure 2.4, our experimental rotational populations deviate somewhat from a pure Boltzmann distribution, a well-known fact that occurs in rotational cooling in supersonic expansions[63, 64]. However, this non-Boltzmann nature of our rotational distribution did not seem have any impact on our measured BRs as they were found to be independent on the rotational level populated.

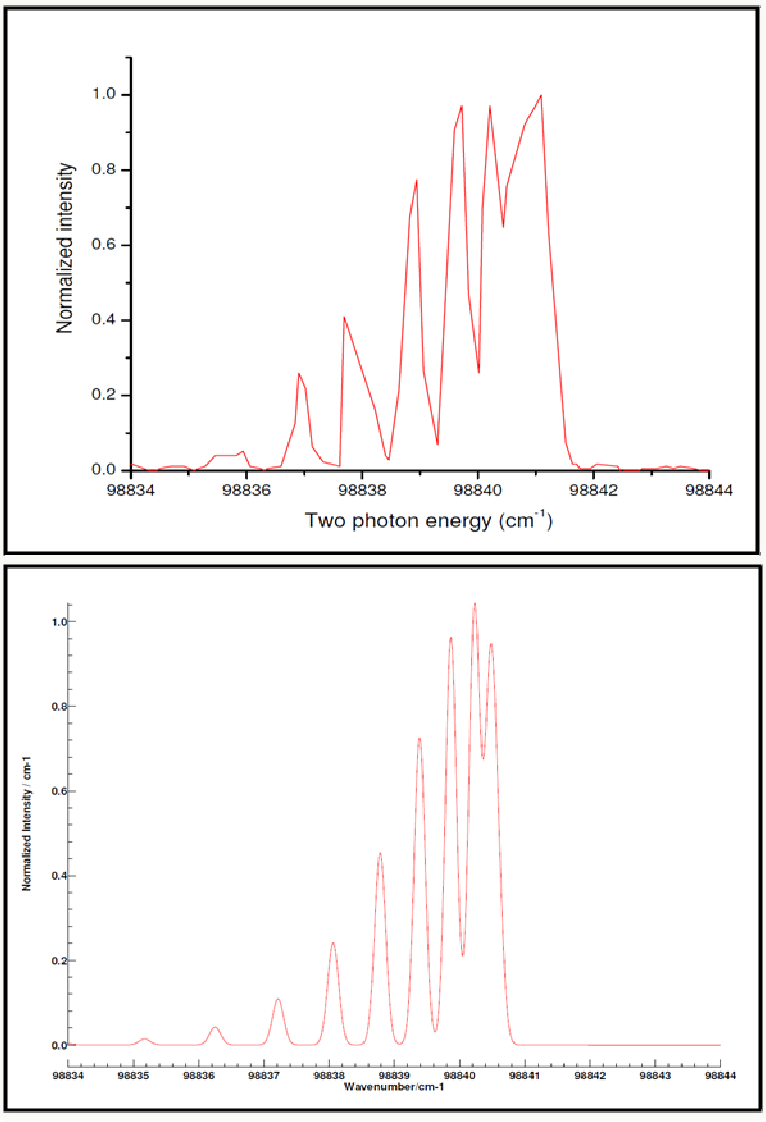

Figure 2.4: Experimental and simulated 2+1 REMPI spectrum of 40 ± 5 K rotational distributions of N_2 at 202 nm using a dye laser with a line width of ~0.2 cm^{-1} in the visible

It is worth pointing out here that although our rotational temperature was recorded in the early part of the expansion where the collision frequency and energy are possibly high due to the high density and high translational temperatures we do not anticipate that the translational temperature is so different from the rotational temperature. Indeed, in their detailed study of free jet flow reactor dynamics, Smith and co-workers have shown with minimum uncertainty that at distances not very far from the nozzle, the rotational temperature of the ion is expected to be in equilibrium with the translational temperature. The main uncertainty of the free-jet low temperature measurements is due to poor understanding of rotational relaxation and equilibrium in free jet expansions.

2.2.2 Charge transfer reaction

The TOF spectra presented in Figure 2.5 demonstrate the performance of the apparatus in measuring primary BR in a CT reaction between N_2^+ and Kr. The reaction of N_2^+ (v=0) with Kr is expected to produce Kr^+ as the only product channel, hence this serves as an ideal system for testing our new set-up in terms of any possible contribution of Kr collisions with N_2^+ (v=1) vibrationally-excited states. This experiment provides further corroborative evidence that there is no plasma-induced chemistry to hinder primary BR measurements. At thermal energy, this reaction exhibits anomalous vibrational energy dependence[65]. A dramatic vibrational enhancement has particularly been observed using the selected-ion flow technique (SIFT) coupled with a laser-induced fluorescence (LIF) detection scheme[66]. The measured rate constants are 1.0 (±0.6) X 10^{-12}, 2.8 (±0.3) X 10^{-12}, 2.1 (±0.2) X 10^{-11}, 5.1 (± 0.2) X10^{-11} and 8.3 (±0.4) X 10-^{11} $cm^3molecule^{-1}s^{-1}$ for N_2^+ v=0, 1, 2, 3 and 4, respectively. In spite of the large exothermicity, the reaction of the N_2(v=0) is so slow compared to the other N_2^+(v≥1)

states. To eliminate any speculation that the more reactive N_2^+ (v≥1) states were involved in any of our reactions, we used a He/Ar/Kr mixture in this experiment. The N_2^+ (v=0) + Ar CT reaction[67] is slightly endothermic (0.178 eV) and is known to be extremely slow at 300 K with an associated rate constant of 2 X 10^{-13}cm^{-3}molecule^{-1}s^{-1}, hence it is not expected to an observable channel at our low-temperature conditions. However, the rate constants for the N_2^+ (v=1-4) + Ar reactions are large and nearly independent of vibrational excitation[68]. In particular, the N_2^+ (v=1) + Ar reaction[68] is nearly resonant and very fast with an associated rate constant of 4 X 10^{-10} cm^{3}molecule^{-1}s^{-1}. Therefore, in the presence of any N_2^+ (v=1), Ar is expected to be much more reactive than Kr. The fact that we do not observe any Ar^+ signal is a very clear indication of the pure state-specific nature of the low temperature N_2^+-induced ion-molecule reactions performed in our newly commissioned experimental set-up.

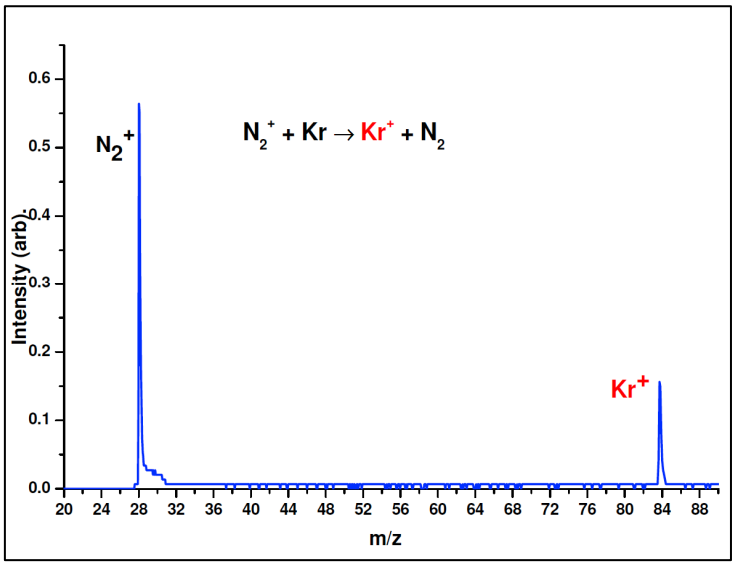

Figure 2.5: Time-of-flight spectrum of the charge transfer reaction of state-prepared N_2^+ (v=0) with Kr in the presence of He and Ar as buffer gases.

2.2.3. Hydrogen transfer reactions

Figure 2.6 (a) and (b) shows a TOF spectrum of ion-molecule reaction involving $H_2^+ + H_2$ and $N_2^+ + H_2$, respectively. The reaction of H_2^+ with H_2, being one of the simplest, well studied ion-molecule reactions where both atom and PT can occur[69, 70], provides an excellent system to use as a test case for the performance of our new apparatus. On the other hand, the reaction of N_2^+ with H_2 allows us to probe a fast PT reaction involving a combination of a heavier reactant ion (N_2^+) with a lighter neutral molecule (H_2). In the case of $H_2 + H_2$ system, both PT and atom transfer processes are expected to contribute to the observed H_3^+ signal but for the purpose of demonstrating the performance of the apparatus, we show the overall TOF that has a possible contribution from both processes without considering the use of deuterated species. H_3^+ ions are formed by a direct mechanism where the bond rupture can occur at either reactant if there is a rapid equilibration of charge states. This mechanism is consistent with the dynamics that are anticipated from the qualitative features of the potential energy surface and the results of the previous trajectory calculations. Previous crossed beam, merged-beam and integral cross section studies of the $H_2^+ + H_2$ reaction also justify the aforementioned mechanism. All these previous experimental studies were done at high collision energies. At E_c =1.5 - 3.5 eV and with vibrational cold H_2 as the reactant (v=0), the fraction of the available energy that appears as product recoil is estimated to be 31 - 32% with no strong dependence on collision energy. This means that just like in case of a typical exoergic reaction on an early downhill potential surface, two thirds of the available energy goes into internal excitation of H_3^+. The TOF spectrum presented in Figure 6 (a) is a clear indication of the superior collection efficiency of both the reactant H_2^+ as well as the

product H_3^+ ions that is inherent in our apparatus. This is a particularly significant factor for the H_3^+ product signal due to the large exoergicity (1.74 eV) between the zero point levels.

The $N_2^+ + H_2$ reaction has been studied by a variety of ion-molecule techniques[71, 72]. It is a representation of an exothermic (ΔH = - 2.5 eV) atom transfer reaction that is characterized by the formation of a single product channel as can be clearly seen from out TOF spectrum. Randeniya and Smith[73] have also reported kinetic energy dependent rate constants for this reaction at temperatures between 8-15 K using a flow jet reactor. In this study a minor product channel of $N_2H_2^+$ (< 5%) was observed. This channel was attributed to the occurrence of ternary association reaction in the beam. We did not observe any m/z 30 in our TOF, which is an additional evidence of the ability of our apparatus to exclusively measure primary branching of H-transfer type of reactions. In other related previous studies of this reaction[71], N_2^+ ions were prepared by electron bombardment and REMPI via high vibrational levels where electronically excited N_2^+ ions were possible. In those ion-molecule experiments, H_2^+ and N_2^+ ions were observed; albeit at very low branching. Our TOF spectrum with only a single N_2H^+ product channel is a further confirmation that our N_2^+ preparation scheme is free from any possible contribution from the excited state N_2 that can result in other processes such as CT leading to the formation of $H_2^+(v')$ and N_2^+ (v'). It is worth mentioning here that even though only one product channel is reported in the TOF spectrum, there is no doubt that our new strategy can be applied to determine product BRs of PT reactions where multiple product channels are involved.

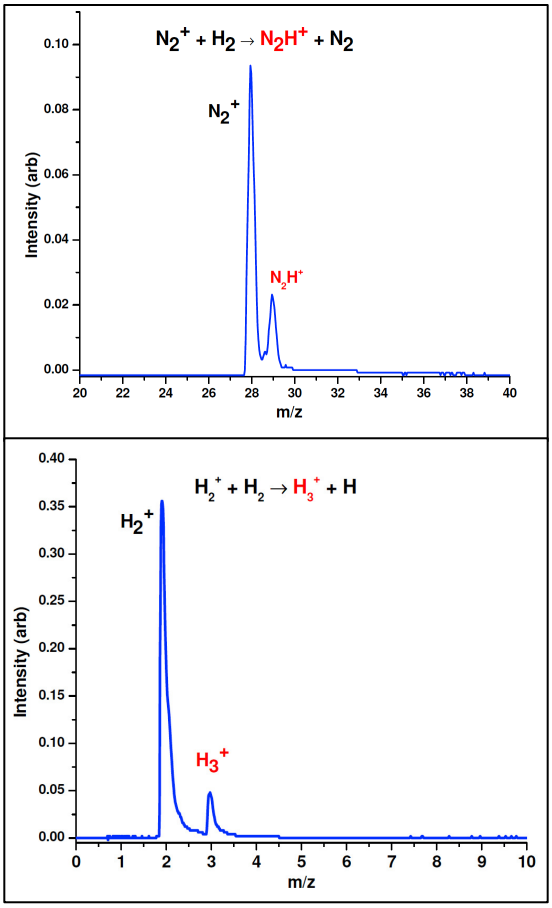

Figure 2.6: Time-of-flight spectrum of the (a) Hydrogen atom transfer resulting from the reaction of state-prepared N_2^+ ions (v=0) with H_2 and (b) H_3^+ formation from the reaction of H_2^+ with H_2 at 201 nm

2.3. Conclusion

We have presented a new, quick and reliable experimental approach that is capable of determining primary product BRs of ion-molecule reactions involving CT, dissociative CT, PT and AT processes. The technique combines state-selective ion preparation with reaction in the course of supersonic nozzle expansion where the BRs are measured at low temperatures; albeit at non-thermal equilibrium conditions of the supersonic jet. The measured BRs are independent of the rotational levels of the reactant

ion. The most critical factor in achieving high resolution TOF data in the present technique is the correct timing of the repeller and the extractor lenses with respect to the laser and pulse valve delays. This approach can be extended to routinely measure primary BRs where multiple product channels of dissociative charge transfer, proton transfer and atom transfer reaction are present.

CHAPTER THREE

DIACETYLENE DIMER PHOTODISSOCIATION

3.1. Introduction

As mentioned in Chapter one, Titan's atmosphere exhibits an extensive aerosol haze believed to be composed of hydrocarbons and nitriles formed from its dense atmosphere[74-76]. Photochemistry and impact from magnetospheric electrons are believed to initiate a series of reactions involving the significant fraction of methane in the atmosphere. These pathways ultimately yield complex hydrocarbons and carbon-nitrogen based compounds through a series of reactions involving radicals and ions. These processes have remained poorly understood to date, although the haze is known to play a vital role in Titan's energy balance and atmospheric dynamics.

Diacetylene (C_4H_2), the first of the series of polyynes, has long been recognized as a key species in Titan's atmosphere because it absorbs light at much longer wavelengths, where the solar flux is significant[75, 76] than acetylene, ethane or other important trace constituents of the atmosphere. Figure 3.1 present model profiles of ethynyl radical (C_2H), acetylene, diacetylene, triacetylene and tetra-acetylene in Titan's atmosphere. Diacetylene molecule has long been thought to be central to the formation of higher polyynes and polycyclic aromatic hydrocarbons (PAHs) that partially comprise the haze layer in Titan's upper atmosphere[76]. Reactions of metastable, electronically excited diacetylene were believed to play an important role in the formation of Titan's haze[77-83]. Recent work has suggested, however, that owing to its short lifetime and low dissociation rates, metastable diacetylene may not be significant in haze formation on Titan[79]. In this chapter, we present an experimental and theoretical study of the photodissociation of the

diacetylene *dimer* under collisionless conditions, and show evidence that its photochemistry represents a novel, overlooked source of resonantly stabilized free radicals (RSFRs) in Titan's atmosphere. These are considered crucial building blocks in the synthesis of polycyclic aromatic hydrocarbons (PAHs). Furthermore, the diacetylene dimer is just one example of a class of van-der-Waals complexes involving unsaturated hydrocarbons and nitriles that are likely to be sufficiently abundant to contribute to the hydrocarbon growth in Titan's atmosphere upon photochemical activation.

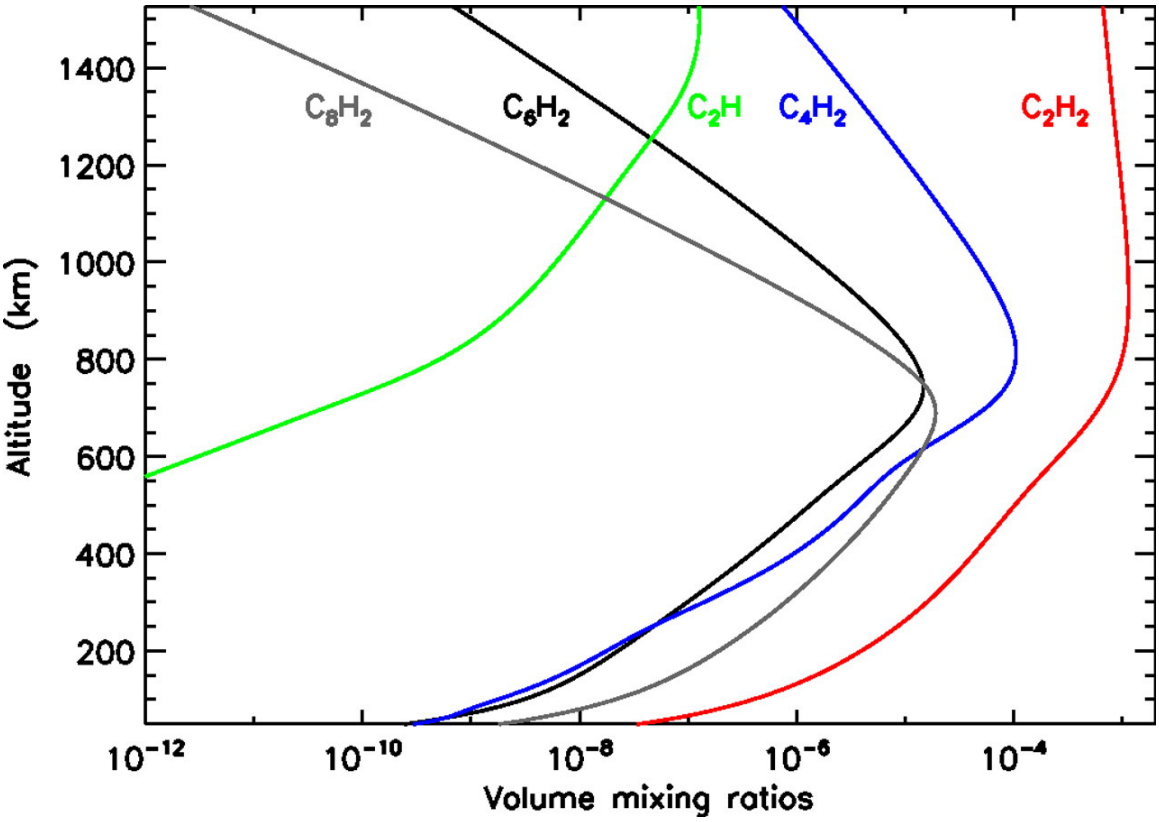

Figure 3: Model profiles of ethynyl radical (C_2H), acetylene (C_2H_2), diacetylene (C_4H_2), Triacetylene (C_6H_2) and tetraacetylene (C_8H_2). PNAS, 106, 3816078

3.2. Experimental and computational Methods.

Experimental

The crossed molecular and ion imaging techniques employed in the dimer dissociation were described in detail elsewhere, hence only the most pertinent and important details will be described here. In the crossed molecular beam experiment, a pulsed molecular beam of diacetylene seeded in argon carrier gas was generated by supersonic expansion of a 5% mixture through a piezoelectric pulsed valve operating at 60 Hz and 80 μs pulses with 500 Torr backing pressure. A four-slot chopper wheel located between the skimmer and the cold shield selects a segment of the seeded beam with a peak velocity of 567 ±2 m s^{-1} and a speed ratio S of 8.3 ±0.1. The expanded beam was skimmed twice before entering the main chamber, where it was crossed at 90° by a 193 nm photolysis laser. The time-of-flight spectra of the photo fragments were recorded in the plane of both molecular and laser beams using a rotatable quadrupole mass spectrometer with an electron-impact ionizer. Typically, the TOF spectra were recorded at lab angles in the range of 12°-35°. For all experiments, the delay time between the pulsed valve and the laser was set such that the diacetylene dimer signal was maximized relative to monomer and higher clusters. In trial experiments the laser was linearly polarized using a series of quartz plates at Brewster's angle. None of the photochemical signals were found to vary with laser polarization, so the experiments shown here were conducted with the laser unpolarized.

Diacetylene was synthesized using the method developed by Armitage et al[84]. C_4H_2 was produced and collected in a cold trap at –70 °C. After the synthesis, the sample was immediately transferred to a cylinder by slowly warming up the sample under

vacuum. The cylinder was then filled to a total pressure of 3 bars with argon to produce 5% diacetylene mixture. The infrared absorption spectrum and mass spectrum showed high purity (> 99.5 %) using this synthesis.

The analysis of the TOF spectra at different laboratory angles was performed with a forward convolution program[85]. A simulation of all measured TOF spectra was generated using an input center-of-mass P (E) distribution which was then convoluted over various instrument parameters such as beam velocity, laboratory angle, divergence of the beam and so on. The P(E) distribution was iteratively adjusted until a satisfactory simulation was achieved.

The diacetylene dimer photodissociation to the product at m/z = 51 ($C_4H_3^+$) was also performed in DC slice imaging experiments. Total translational energy distributions were derived from the sliced images by direct integration in velocity space, followed by conversion of the velocity distributions to translational energy[86]. After carefully tuning the delay time between the diacetylene molecular beam and laser firing, the diacetylene dimer segments in the molecular beam were picked up and dissociated at 193 nm. Multiphoton ionization of the C_4H_3 product by the 193nm laser allowed for detection. We were unable to detect m/z = 99 with this approach. Our detection of m/z = 51 may be through accidental 1+1 resonances, so the inability to detect m/z = 99 is not particularly surprising, as such resonances may not be available. Alternatively, ionization may not compete effectively with dissociation of the C_8H_3 neutral or other decay pathways in this case.

Computational details

Vertical excitation energies and transition dipole moments of diacetylene dimers were calculated using the equation-of-motion coupled clusters (EOM-CCSD) method[87, 88] with Dunning's augmented polarized triple-zeta correlation-consistent (aug-cc-pVTZ) basis set[89] . For several lower energy excited states, we have also carried out internally-contracted multireference configuration interaction MRCI calculations with Davidson's corrections for quadruple excitations (MRCI+Q) and with active spaces including 8 electrons distributed on 8 orbitals (8,8) and 16 electrons on 12 orbitals (16,12). The (16, 12) active space involved all π electrons of the two diacetylene monomer units. The MRCI calculations were performed with the same aug-cc-pVTZ basis set. We considered two different structures of the diacetylene dimer, T-shaped and parallel-slipped; their optimized geometries were taken from the most accurate results by Hopkins et al[90]. at the CCSD(T)/TZ2P(f,d)++ level of theory. Transition dipole moments were also computed at the complete-active-space self-consistent field CASSCF (16,12)/aug-cc-pVTZ level of theory[91, 92]. For comparison, similar EOM-CCSD, MRCI, and CASSCF were performed for the isolated diacetylene molecule. In this case, we used (4, 4) and (8, 10) active spaces for MRCI and CASSCF. All ab initio calculations of excitation energies and transition dipole moments were carried out employing the MOLPRO 2006 program package[92]

To unravel the reaction mechanism for the formation of the observed C_8H_3 + H and C_4H_3 + C_4H products in photodissociation of diacetylene dimer, we performed *ab initio* calculations of the ground state potential energy surface of C_8H_4 for various pathways leading from $(C_4H_2)_2$ to the products. Since the reaction paths lead from the species with a closed-shell singlet wave function (in the dimer) to the products having

overall open-shell singlet wave functions, relevant intermediates and transition states may have a biradical character and therefore the use of multireference methods for the electronic structure calculations is required. Hence, we carried out geometry optimization and vibrational frequency calculations for various C_8H_4 species by employing the CASSCF approach with the active space consisting of 12 electrons distributed on 10 orbitals and the 6-311G** basis set, CASSCF(12,10)/6-311G**, and utilizing the Dalton 2 program package. Then, single-point relative energies were refined at the CASSCF optimized geometries using the multireference second-order perturbation theory CASPT2 method implemented in MOLPRO 2006 [2] with the same active space and the cc-pVTZ basis set.

3.3. Results

The diacetylene dimer was generated in a supersonic molecular beam, with photodissociation products probed via photofragment translational spectroscopy using two complementary approaches: universal mass spectrometric detection after electron impact ionization[85] and non-resonant multiphoton ionization of the neutral products employing imaging detection[86]. The irradiation of the diacetylene beam at 193 nm gave rise to strong signals that were found to be associated with the photodissociation of the diacetylene dimer. Utilizing a universal mass spectrometric detector, signal at a variety of mass-to-charge ratios (m/z) could be attributed to two reaction channels with unique contributions observed at m/z = 51 ($C_4H_3^+$) and m/z = 99 ($C_8H_3^+$) (Figure 3.1). For completeness, we should mention that the dimer dissociation channel to form two diacetylene monomers (m/z = 50) was also observed. However, it is not discussed here in detail since the main interest of this project is to investigate the formation of RSFRs from

the diacetylene dimers. Formally, channels at m/z = 51 ($C_4H_3^+$) and m/z = 99 ($C_8H_3^+$) correspond to the hydrogen loss and hydrogen transfer reactions 3.1 and 3.2, respectively, in the photodissociation process:

$$(C_4H_2)_2 + h\nu_{193nm} \rightarrow C_8H_3 + H \quad \text{.....3.1}$$

$$(C_4H_2)_2 + h\nu_{193nm} \rightarrow C_4H_3 + C_4H \quad \text{.....3.2}$$

When examined as a function of the delay time between the pulsed molecular beam valve and the laser, the profiles of the product signals closely tracked the dimer appearance at m/z=100, but not that of the monomer or higher clusters. These data are shown in Figure 3.2.

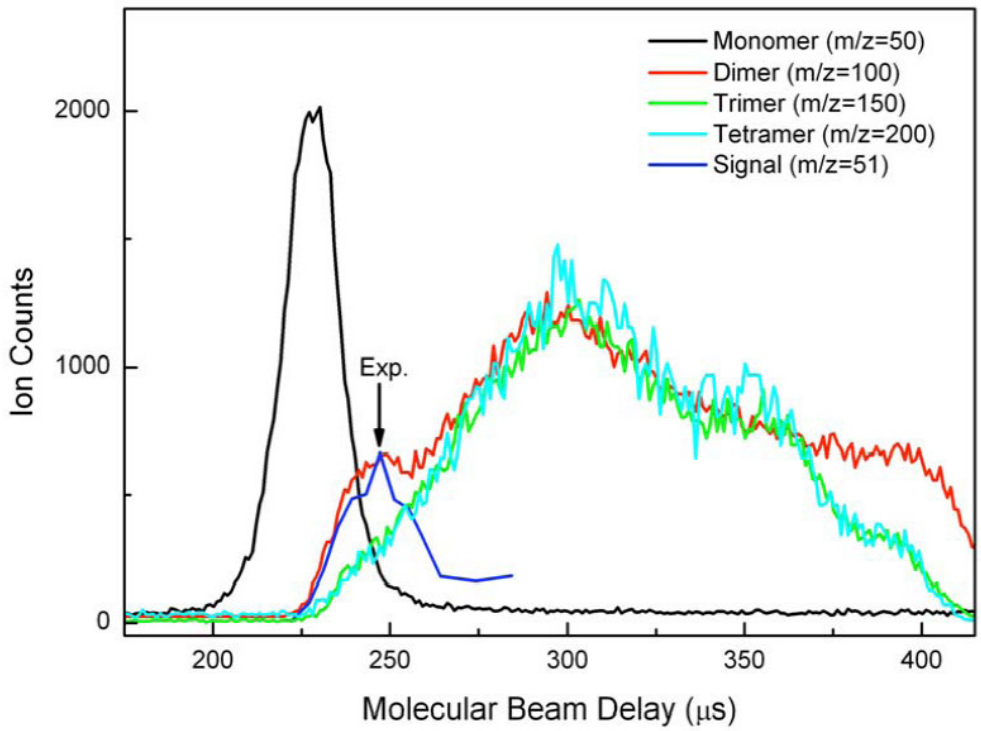

Figure 3.2: Signals on-axis in the molecular beam at indicated mass vs. delay between laser and pulsed valve. The monomer contribution has been reduced by a factor of 80, while the other contributions have been normalized at long delay times.

Representative time-of-flight (TOF) spectra at m/z = 51 and at m/z = 99 are shown in Figure 3.3. This signal corresponds to products following hydrogen atom transfer from one diacetylene molecule to the other (reaction (2); m/z = 51) and from the hydrogen atom loss from the dimer (reaction (1); m/z = 99), respectively. The Newton diagrams are also shown to rationalize the maximum scattering range of the heavy reaction products of reactions (1) and (2). In these diagrams, the velocity of the diacetylene dimer beam is 567 m s^{-1}; the limiting circles depict the maximum recoil velocity calculated from the excitation energy at 193 nm and the reaction energies of the corresponding reaction channels 3.1 and 3.2 as discussed in detail below. A forward convolution routine was used to fit the experimental data. Here, TOF spectra at m/z = 99 (C_8H_3) and m/z = 51 (C_4H_3) had to be fitted with a counter fragment of m/z = 1 (H) and m/z = 49 (C_4H) (reactions (1) and (2), respectively); the total mass of both reaction products of channels (1) and (2) of 100 amu also indicate that this signal originates from the diacetylene dimer. Likewise, the TOF spectra at m/z = 99 and 49 are distinct and do not overlap, demonstrating that at least two distinct channels are open in the photodissociation of the diacetylene dimer at 193 nm. This finding alone demonstrates that both channels lead to heavy hydrocarbon products of the gross formula C_8H_3 (reaction (1)) and C_4H_3 (reaction (2)). The corresponding center-of-mass translational energy (P(E)) distributions for both channels are also shown in Figure 3.3. The simulated TOF spectra are shown as the solid lines, and the circles are the experimental data.

The product at m/z = 51 ((C_4H_3)) was also detected in a separate DC sliced ion imaging experiment. The image of the $C_4H_3^+$ (m/z = 51) photofragment was recorded and is shown as an inset in the center-of-mass translational distribution of m/z = 51 in Figure

3.3. In this case, the translational energy distributions were obtained by direct integration of the imaging data[86]. Both translational energy distributions extracted from photodissociation experiments in the two different experimental setups agree well, and show both a distribution maximum peaking away from zero translational energy, but also a high energy cutoff at about 2.3 kcal mol^{-1}. Therefore, the TOF spectra recorded at m/z = 51 and data fitting support evidence of channel 3.2, i.e. the formation of two radical products with the gross formulae of C_4H_3 and C_4H.

The TOF spectrum recorded at m/z = 99 ($C_8H_3^+$) obtained with the universal detector shows that the atomic hydrogen loss channel, reaction 3.1, is also open in the photodissociation process. It is important to stress that we did not observe any signal at m/z = 99 at angles larger than 12°. At smaller laboratory angles, the signal was contaminated by background coming from the molecular beam itself. For m/z=99, we thus only show the TOF spectrum at 12°. The total translational energy obtained from the forward convolution fitting is also shown in Fig. 3.3; data are not reported below 13 kcal mol^{-1} because the results at 12° are not sensitive to slower recoiling fragments. In contrast to the translational energy distribution for the hydrogen atom transfer channel (reaction 3.2), the translational energy distribution for the hydrogen atom loss channel 3.1 exhibits a broad distribution and extends to a higher kinetic energy release of about 25 kcal mol^{-1}.

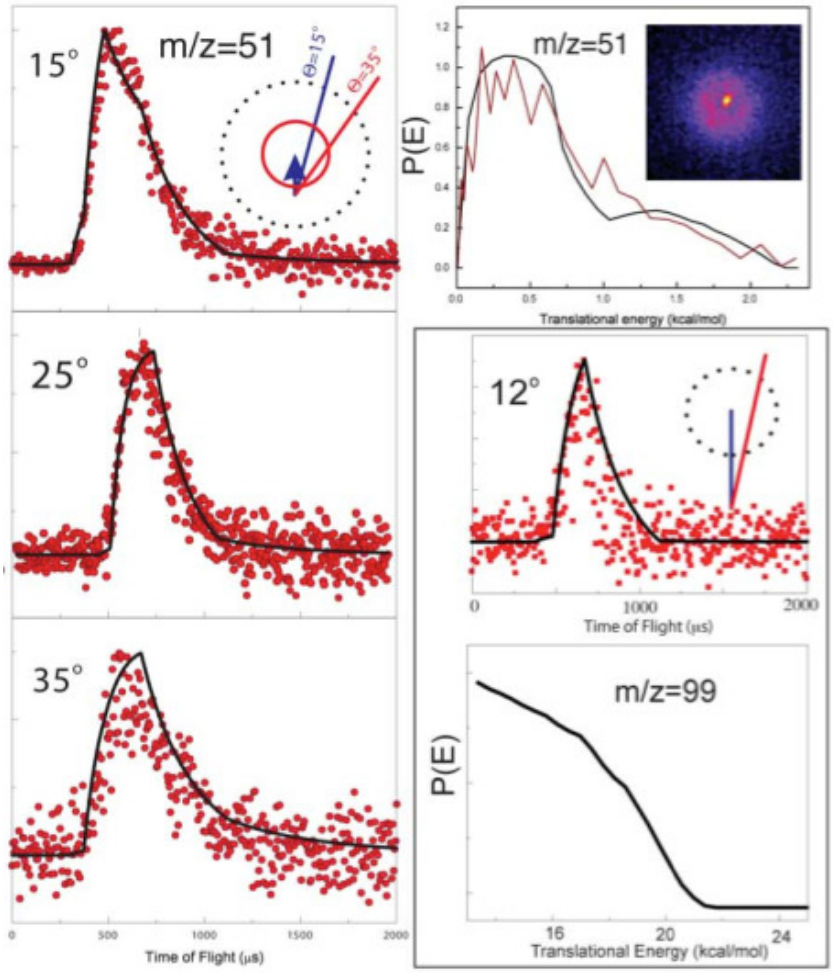

Figure 3.3: Representative TOF spectra recorded at mass-to-charge (m/z) of m/z = 51 ($C_4H_3^+$) and m/z = 99 ($C_8H_3^+$) fragments taken at indicated laboratory angles. The circles represent the data, while the solid lines depict the simulation based on the P(E)s, also shown in the figure. For the m/z = 51 case, ion imaging results are also shown, with the derived P(E) indicated by the lighter line.

Having established the existence of two pathways 3.1 and 3.2 to form two open-shell hydrocarbon radicals in the photodissociation of diacetylene dimers, via hydrogen transfer and hydrogen loss, of the generic formulae C_8H_3 and C_4H_3, we now examine the underlying photodissociation dynamics by considering the experimental results in light of high-level electronic structure calculations. This also helps to establish the extent to

which the newly formed molecules belong to the class of resonantly stabilized free radicals (RSFRs). This link is crucial to suggest possible structures of the isomers produced and to transfer these findings from the laboratory to the 'real' atmosphere of Titan. Earlier high-level electronic structure calculations by Hopkins et al.[90] suggest that the diacetylene dimer can either exist in a T-shaped or parallel-slipped configuration (Figure 3, Hopkins et al. 2007[90]). The T-shaped dimer belongs to the C_{2v} symmetry point group whereas the parallel-slipped dimer has C_{2h} symmetry. The results of these calculations[90] give binding energies of T-shaped and parallel-slipped dimers of 1.63±0.08 kcal mol^{-1} and 1.33±0.12 kcal mol^{-1}, respectively, relative to two separated diacetylene monomers, making the T-shaped structure slightly more stable than the parallel-slipped one. According to the present *ab initio* calculations, electronic transitions in the dimers at 193 nm include excitation to the 1^1B_2, 2^1A_1, 3^1A_2, and 4^1A_2 states for the T-shaped form and 1^1B_u, 2^1A_u, 2^1A_g, and 2^1B_g for the parallel-slipped structure. Here the transitions to the 1^1B_2, 2^1A_1, 1^1B_u, and 2^1A_u states are electronically allowed, but those to 3^1A_2, 4^1A_2, 2^1A_g, and 2^1B_g are forbidden. Nevertheless, a strong vibronic coupling induced by the CCC and CCH bending modes is expected to contribute significantly to oscillator strengths of all these transitions and to make them vibronically allowed. The calculated vertical excitation energies for these states are about 5.5-5.6 eV; based on calculations of Franck-Condon factors, their absorption spectra represent vibrational progressions with the origin around 5.2-5.3 eV (the adiabatic excitation energy) and spaced by about 2300 cm^{-1}. Therefore, in addition to the electronic excitation, the absorption of a 193 nm photon produces vibrational excitation of the normal modes corresponding to the

symmetric stretch of two triple carbon-carbon bonds coupled with the single carbon-carbon bond stretch with the frequency of about 2300 cm^{-1}.

The electronic structure calculations suggest further that photochemical activation by a 193 nm photon (148 kcal mol^{-1}) is likely followed by internal conversion (IC) to the (highly vibrationally excited) ground electronic state. Similarly to diacetylene monomer[79], IC is expected to be fast. Figure 3.4 shows the stationary points on the potential energy surface involved in the photochemistry of the diacetylene dimer. On the ground state potential energy surface, the individual diacetylene molecules within the dimers can be coupled via a carbon-carbon bond formation of at the C4-C4 and C4-C3 positions leading to biradical intermediates **[i1]** and **[i2]**, respectively, with **[i1]** being thermodynamically more stable by 15 kcal mol^{-1} compared to **[i2]** is important to stress that the energy of the transition states involved lie lower than the total available energy of the system. Formally, the parallel-slipped dimer correlates with the transition states leading to **[i1]** and **[i2]**. However, since the binding energies of the T-shaped and parallel-slipped dimers are low and the interaction between their monomer units is weak, isomerization between both structures is expected to be facile. The barrier for the parallel-slipped $\rightarrow$ T-shaped rearrangement cannot exceed 1.3 kcal mol^{-1} (the binding energy of the parallel-slipped structure), but it is likely to be much lower. Both **[i1]** and **[i2]** intermediates can isomerize via hydrogen shifts leading to **[i3]** and **[i4]**, respectively. Due to the change of the wave function character from the biradicals to the closed shell singlets, both structures are significantly more stable than **[i1]** and **[i2]**. Once again, the inherent barriers to hydrogen migration range well below the total available energy.

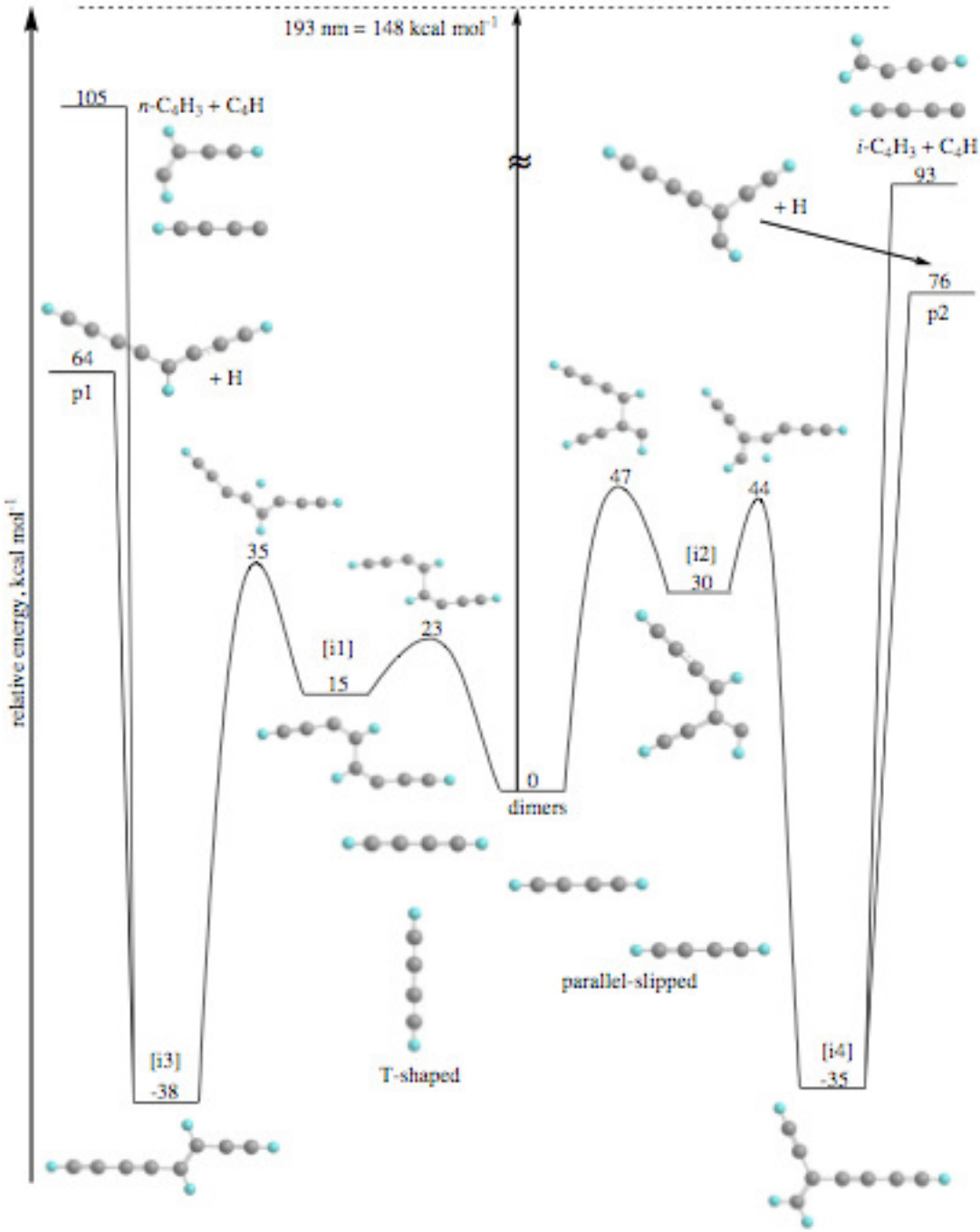

Figure 3.4: Potential energy surface involved in the photochemistry of the diacetylene dimer at 193 nm. The energies were calculated at the CASPT2(12,10)/cc-pVTZ//CASSCF(12,10)/6-311G**$^{+}$ ZPE(CASSCF(12,10)/6-311G**) level of theory.

The absolute barrier heights of 14–20 kcal mol^{-1} are reasonable when compared to similar closed shell, unsaturated hydrocarbon molecules (Mebel et al. 2006)). What is the fate of these reaction intermediates? Considering reactions (1) and (2), intermediate **[i3]** can either lose a hydrogen atom from the C3 position leading to a doublet C_8H_3 radical **p1** or undergo carbon-carbon bond rupture forming the n-C_4H_3 plus C_4H radicals. In intermediate **[i4]**, two decomposition pathways were identified as well: an atomic hydrogen loss leading to a C_8H_3 isomer **p2** and also a carbon-carbon bond rupture forming the i-C_4H_3 radical plus the 1,3-butadienyl radical (C_4H). All processes involve only simple bond ruptures without exit barriers. Note that among the C_8H_3 isomers, **p1** is thermodynamically more stable by about 12 kcal mol^{-1} compared to **p2**. The overall processes to form these isomers from the diacetylene dimers were found to be endoergic by 64 and 76 kcal mol^{-1}, for **p1** and **p2**, respectively. These energies are well below the total available energy of the system of 148 kcal mol^{-1}.

Considering the experimental data for the hydrogen loss channel (reaction 3.2), the corresponding center-of-mass translational energy distribution (Figure 3.3) is broad, and around 80% of the available energy goes to internal excitation of the C_8H_3 products. This is consistent with the hydrogen loss translational energy distribution observed in the monomer[79], but those have only been reported at higher excitation energies, around 10.2 eV and above. This again highlights the important distinction between these monomer and dimer systems: the hydrogen atom elimination threshold for the dimer is 2.5 -3.0 eV lower than for the diacetylene monomer. This is because the weak van-der-Waals bond in the dimer becomes a covalent bond in the product radical, thus gaining the bond energy and compensating partly for the large endoergicity of the bond fission. For the hydrogen

atom transfer channel, which leads to two C4 radical species, the center-of-mass translational energy distribution is extremely low (<2 kcal mol^{-1}). This finding suggests that the effective transfer occurs with little direct interaction between the two monomers. This mechanism may be analogous to the dynamics of deuterium atom release reported in water dimer photodissociation[93]. A closer investigation of the overall reaction threshold exposes unique features of the dimer photodissociation. Here, the atomic hydrogen transfer mechanisms in the dimer, giving two C4 radicals, have a threshold of only 4.12 eV. No analogous channel exists in the monomer. A number of C_4H_3 product isomers are accessible[94]; the lowest energy pathways are shown in Fig. 3.4 implying most likely formation of n-C_4H_3 or i-C_4H_3. The very low observed translational energy release does not rule out any of these. It should be noted that such reactions of dimers are not unprecedented. Previous studies have demonstrated "sequential" and "concerted" dissociation of van der Waals complexes such as hydrogen iodide (HI) clusters[95], dimers of carbonylsulfide (OCS) and carbondisulfide (CS_2), and the molecular oxygen (O_2) dimer. An overview of this literature is given in a recent study by Vidma et al.

3.4. Discussion

Our combined experiments and calculations provide evidence that upon photolysis at 193 nm, the diacetylene dimer exhibits two unique reaction pathways leading to resonantly stabilized free radicals (RSFRs), pathways that are absent in the photodissociation of the diacetylene monomer. These are: the synthesis of the C_8H_3 isomers **p1** and/or **p2** via atomic hydrogen loss processes (reaction 3.1) and the formation of n-/i-C_4H_3 isomers plus C_4H via carbon-carbon bond rupture in the reaction

intermediates (reaction 3.2). Both pathways involved an initial formation of a carbon-carbon bond between the monomer units in the T-shaped and parallel-slipped dimer on the ground electronic state surface followed by an intermolecular hydrogen transfer. These processes represent direct evidence that the photoexcitation of weakly bound van-der-Waals structures such as the diacetylene dimer can lead to a *hydrocarbon growth*, in this case to the formation of RSFRs. This is in strong contrast to the diacetylene monomer, in which only *photodestruction* to the C_4H radical plus atomic hydrogen was observed.

Having verified hydrocarbon growth to form resonantly stabilized free radicals (RSFRs) in diacetylene dimer upon photoexcitation at 193 nm, we apply our findings now to the atmosphere of Titan. Previous models of Titan's atmosphere underline the crucial importance of RSFRs in the underlying reaction schemes leading to PAH formation[18, 76]. Here, radicals such as C_4H_3, C_6H_3, and C_8H_3 were postulated as important transient species formed via addition of a hydrogen atom to a polyyne such as diacetylene (reaction (R1); Table 3.1). However, two major factors inhibit these reactions. First, classical activation barriers of the addition processes range from 2 to about 10 kcal mol^{-1}. Considering the temperature in Titan's stratosphere of about 120 K, the significant activation energy blocks the addition process at the outset. Secondly, the $[C_4H_3]^*$ reaction intermediate is internally excited; under the low pressure regime in Titan's stratosphere of 10 mbar, a collisional stabilization of this complex via reaction (R2) by a bath molecule from the atmosphere, predominantly molecular nitrogen, is unlikely at these temperature and pressure conditions. A recent calculation by Klippenstein & Miller[96]

suggested very small rate constants of only about 1.8×10^{-26} cm^6s^{-1} at 250 K to form C_4H_3 isomers.

Considering the C_8H_3 radicals, the situation is even more complicated. Here, recent studies indicated that polyynes such as the tetraacetylene precursor itself (HCCCCCCCCH; C_8H_2) can be synthesized via fast, barrierless reactions of diacetylene with ethynyl radicals (CCH) as formed in the photodissociation of acetylene at wavelengths less than 217 nm, followed by a consecutive reaction of a second ethynyl radical with triacetylene (HCCCCCCH; C_6H_2) (reaction sequence (R4)–(R7)). The overall reaction (R8) formally converts two acetylene and one diacetylene molecule to tetraacetylene plus four hydrogen atoms. Alternatively, a reaction sequence could involve the reaction of photolytically generated 1,3-butadienyl radicals (reaction (R9)) with a diacetylene molecule (reaction (R10). In analogy to reactions (R1) and (R2), the tetraacetylene molecule could only add a hydrogen atom over a significant barrier (reaction (R12)) followed by stabilization of the reaction intermediate (R13). Although the initial formation of tetraacetylene is fast, once again the hydrogen atom addition and stabilization of the intermediate, reactions (R12) and (R13), under Titan's atmospheric conditions are blocked. Therefore, the postulated reaction sequences (R1) – (R14) cannot lead to the formation of RSFRs in Titan's atmosphere due to the large activation energy, inefficient three-body processes, and the inherent small rate constants.

Table 3.1: Reaction schemes in Titan's atmosphere postulated to be involved in the formation of resonantly stabilized free radicals via hydrogen atom addition and three body reaction sequences.

(R1)	$C_4H_2 + H \rightarrow [C_4H_3]^*$	(R4)	$C_2H_2 + h\nu \rightarrow C_2H + H$
(R1)	$[C_4H_3]^* + M \rightarrow C_4H_3 + M'$	(R5)	$C_2H + C_4H_2 \rightarrow C_6H_2 + H$
		(R6)	$C_2H_2 + h\nu \rightarrow C_2H + H$
		(R7)	$C_2H + C_6H_2 \rightarrow C_8H_2 + H$
(R3)	$C_4H_2 + H \rightarrow C_4H_3$	(R8)	$2\,C_2H_2 + C_4H_2 + 2\,h\nu \rightarrow C_8H_2 + 4\,H$
(R9)	$C_4H_2 + h\nu \rightarrow C_4H + H$	(R12)	$C_8H_2 + H \rightarrow [C_8H_3]^*$
(R10)		(R13)	$[C_8H_3]^* + M \rightarrow C_8H_3 + M'$
(R11)	$2\,C_4H_2 + h\nu \rightarrow C_8H_2 + 2\,H$	(R14)	$C_8H_2 + H \rightarrow C_8H_3$

The diacetylene dimer is just one example of an overlooked reaction class involving van-der-Waals complexes consisting of polyynes and possibly cyanoacetylenes and aromatics that are likely to be sufficiently abundant to contribute to hydrocarbon growth in Titan's atmosphere upon photochemical activation. Analogous behavior is expected for acetylene, for example, and this is supported by calculations of the acetylene plus acetylene potential energy surface . The acetylene dimer has an even stronger bond than the diacetylene dimer; therefore, the mixing ratios are expected to be much higher in Titan's atmosphere for acetylene than diacetylene. Based on calculated equilibrium constants, we estimate a dimer mixing ratio of 6×10^{-14} for diacetylene dimer and 1×10^{-7} for the acetylene dimer in Titan's atmosphere at the 10 mbar level. The mixed acetylene-diacetylene dimer binding energy is comparable to that of diacetylene, but owing to the higher acetylene abundance on Titan, the mixed dimer mixing ratio is expected to roughly half that of the diacetylene monomer itself.

3.5. Conclusions and implications to Titan's atmosphere

The photodissociation of weakly bound van-der-Waals clusters of acetylenes and polyyacetylenes offer a mechanism to synthesize resonantly stabilized free radicals – building blocks toward the formation of PAHs - via a versatile *one step pathway* in Titan's low tempertature atmosphere. This presents a novel, neglected reaction class in chemical models simulating the growth of PAHs and of the organic haze layers on Titan and elsewhere in the outer solar system. Consequently, given the profound differences in photochemical behavior shown here, it is likely that the photodissociation of polyyne dimers such as reactions 3.1 and 3.2 leads to a more efficient formation of RSFRs than consecutive reactions involving hydrogen addition and three body reaction sequences (R1) – (R14) in Titan's atmosphere. As the mixing ratios vary strongly with temperature and pressure, it will be important to include these complexes together with the wavelength-dependent quantum yield in future photochemical models to gauge the full extent of their role in the hydrocarbon growth on Titan.

CHAPTER FOUR

PHOTODISSOCIATION OF ETHYLAMINE CATION

4.1 Introduction

Despite being in its infancy, research on Titan's ionospheric chemistry has been a subject of intense scrutiny [97-101] since the surprising revelation of its rich chemical composition by the Ion Neutral Mass Spectrometer (INMS) on board the *Cassini* spacecraft [102, 103]. The work presented in this chapter has been guided by the hypothesis that primary photodissociation of ions under collisionless conditions, in concert with high-level ab initio calculations, can allow us to investigate the formation mechanisms, reaction pathways, and properties of key species detected by Cassini, even if the subject photodissociation per se may not be directly relevant. We will expand on this point in the Discussion.

Studies on the photodissociation of ethylamine (ETA) cation in the ultraviolet (UV) region are rather scarce. As one of the first members of simple alkyl amines, ETA Rydberg states are similar to those of methylamine but due to the presence of additional carbon atoms, the number of dissociative 3s Rydberg states in ETA is higher [104, 105,33]. In a series of classical investigations by Lorquet and Leclerc[104] using quantum mechanical treatments, it was demonstrated that $CH_3CH_2NH_2^+$ ions, in their ground state, dissociate into a CH_3 radical and a $CH_2NH_2^+$ ion when the vibrational energy in the C-C bond exceeds 0.9 eV. Using a time of flight mass spectrometer, multiphoton dissociation of ETA cation at 450 and 532 nm was found to yield m/z = 28, 30, and 44 as the major peaks with m/z=30 dominating at both wavelengths [106]. No parent ion was observed at 450 nm while at 532 nm, the m/z = 44 and m/z 28 signals were found to increase.

Inarguably, since the electronic clouds of α- C atom in the ion shifts towards N atom, no other fragmentation pathway is expected to compete with the β- (C-C) bond, as was also demonstrated by an electron impact ionization study of aliphatic amines[107]. Bodi et al., [107] in a Threshold Photoion Photoelectron Coincidence Spectroscopy (TPEPICO) study, reported that the dominant reaction generates $CH_2NH_2^+$ + CH_3 and H-loss product channels, with the H-loss product channel accounting for less than 10 %. The onset for H-loss was calculated to be 9.627 eV, 135 meV below the computed onset for the CH_3 loss. The conclusion from this observation was that the H-loss channel was slow, probably as a result of tunneling. In another related study aimed at obtaining an accurate heat of formation of ethylidenimmonium cation ($CH_3CHNH_2^+$), Harvey and Traeger [108] found the H-loss to be the lowest energy fragmentation pathway of EA cation with an appearance energy of 9.61 eV. However, no direct laboratory investigation of ETA cation dissociation in the UV under collisionless conditions in a molecular beam has been reported. In addition, no theoretical investigations have mapped out a detailed potential energy surface with the various primary and secondary reaction pathways, some of which leads to direct observation of product channels that have been detected in Titan's ionosphere.

Prior to the ethylamine cation study, our group had investigated the photodissociation of methylamine cation as a potential starting molecule to explore the features of the potential surface that may lead to the formation of species that are relevant to Titan's ionosphere [98]. It is reasonable to envision that although ETA cation has not been detected in Titan's upper atmosphere, it is yet another excellent starting molecule that can aid in understanding the ion-molecule reactions related to the formation and

reactions of the dominant $HCNH^+$ ion and other isomers depicted on its potential energy surface. In this paper, therefore, we present results on ETA cation photodissociation as a second prototypical amine cation with a rich potential surface that has several primary and secondary product channels that can readily be investigated experimentally using our Direct current (DC) slice imaging technique via 1+1 resonance enhanced multiphoton ionization (REMPI) strategy.

To this end, a combined experimental and theoretical investigation on ETA cation dissociation at 233 nm using Direct current (DC) slice imaging and high level ab initio calculation, respectively, is reported. These experimental results on the photodissociation of ETA cation are not intended to document the full suite of related photochemical processes in Titan's ionosphere. Nevertheless, within the theoretical realm provided by the high level ab initio calculations, the ion imaging results strive to reveal and explore important aspects and isolate key reaction pathways and phenomena on the potential surface. Although primary photodissociation of the cation is our main goal in this study, our motivation comes from, on one hand, the need to identify important secondary decomposition reaction pathways on the potential surface, and on the other hand, our interest to explore excited state dynamics such as the $HCNH^+$ formation that is reported in this paper. The implications for the chemistry of $HCNH^+$ formation and haze formation in Titan's atmosphere will also be considered.

4.2 Experimental and Computational Details

Experimental

Ethylamine cation dissociation was carried out using a velocity map imaging apparatus[58, 109] that was optimized for DC slice imaging[58, 110]. Since the details of this technique have been discussed in details elsewhere and in Chapter two only the important features that are key to the Ethylamine cation experiment will be briefly mentioned here. A pulsed supersonic molecular beam containing ~1% ethylamine (stated purity >99.0%) seeded in Helium was expanded from a pulsed valve into a differentially pumped source chamber at a backing pressure of ~ 2 bar. The wavelength of the laser light employed in this study was produced by frequency doubling of the output of a tunable, narrow-linewidth (0.07 cm^{-1}) OPO laser system (Spectra-Physics MOPO HF). The MOPO HF was pumped by the third harmonic of a seeded Nd:YAG laser operating at 10 HZ. The vertically polarized laser beam was then focused (20 cm focal length) into the interaction region. The laser polarization was parallel to the detector plane, while the typical output power employed was ~ 0.1 mJ /pulse. Calibration of the ion images was achieved by using experimentally obtained images of CO ($v=0$, $J=65$) in the photodissociation of OCS at 230 nm under identical conditions.

Computational details

Molecular geometries and vibrational frequencies of local minima and transition states of $CH_2CH_2NH_2^+$ cation were calculated at the hybrid density functional B3LYP/6-311** level of theory[111,112] using the GAUSSIAN 98 package[113].

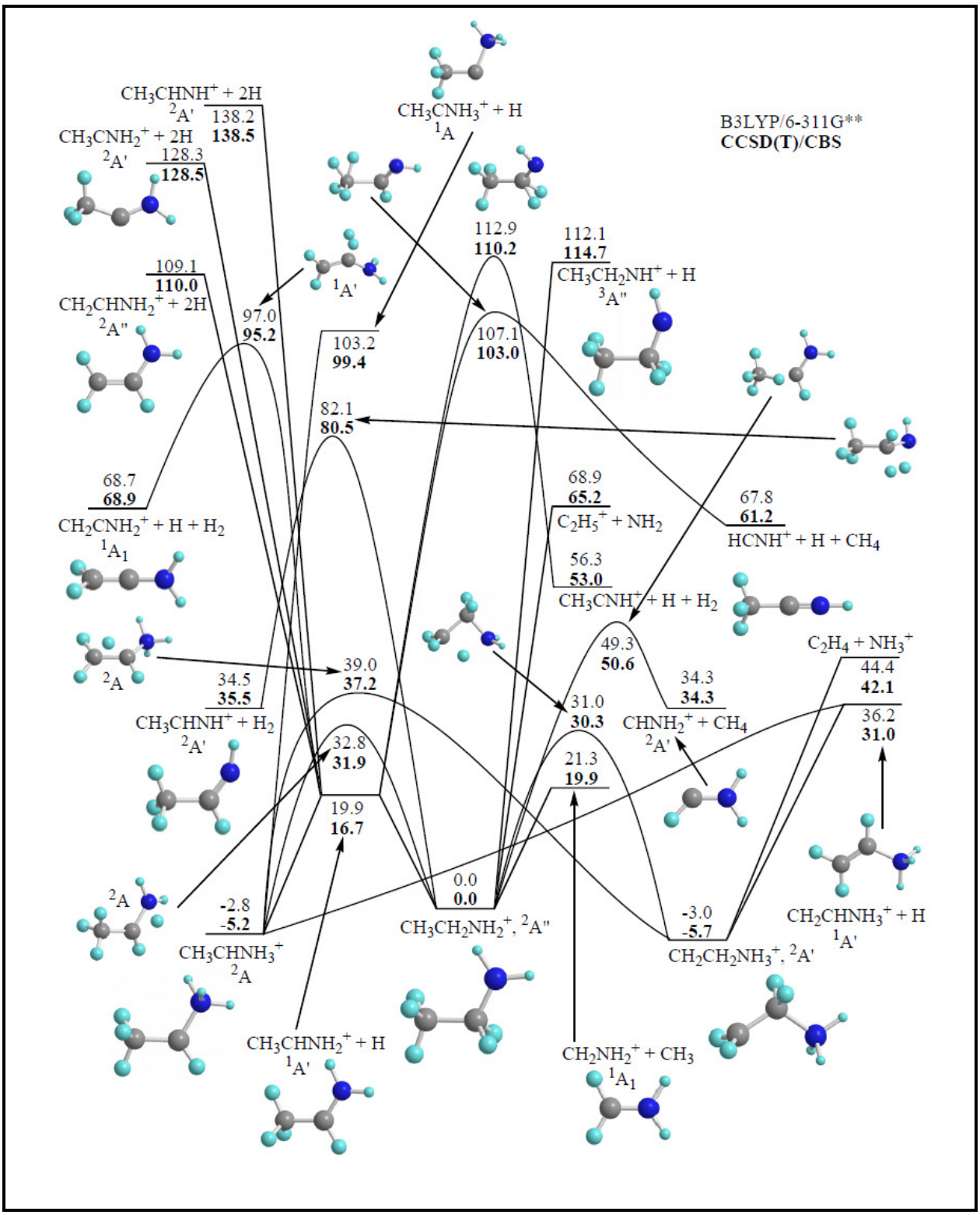

Figure 4.1: Stationary points on the potential energy surface involved in the photochemistry of the ethylamine cation at 233 nm. The energies were calculated at theB3LYP/6-311** and **CCSD (T)/CBS** level of theory. Energy values are in kcal/mol.

Relative energies of various isomers and species on the ground state potential surface of ETA cation were refined utilizing the coupled cluster CCSD(T) level of theory[114-117] with Dunning's correlation-consistent cc-pVDZ, cc-pVTZ, cc-pVQZ, and cc-pV5Z basis sets[118] and with further extrapolation to the complete basis set (CBS) limit[119]. The CCSD(T) calculations were performed using the MOLPRO package[120]. The results of the calculations are summarized in Figure 4.1, which will guide our presentation and discussion of the experimental results.

4.3 Results

Ethylamine exhibits a broad, structured absorption spectrum between 219 nm to 240 nm, with the most intense peaks appearing at 229.5 and 233.4 nm[105, 121]. The lowest lying singlet excited states of ethylamine are expected to be n-3s Rydberg in character[121, 122]. One photon excitation of neutral ETA at 233.3 nm is associated with the first member of the amine-wagging vibrational progression[105]. In this case, we suspect that ionization from the Rydberg level is dominated by the diagonal (v+=v') transition, although we have not confirmed this with photoelectron spectroscopy. The absorption of an additional 233 nm photon by the state-prepared ETA cation leads to subsequent fragmentation, where both primary and secondary product channels are observed. The main channels observed in our experiment are H-loss and formation of $HCNH^+$.

H-loss Channel. The H-loss ion image and the corresponding total translational energy distribution are presented in Figure 4.2. The ion image has two components, both of which have an isotropic angular distribution. This ion image gives a bimodal total translational energy distribution upon analysis. The total available energy at 233.3 nm is 123 kcal/mol. In the bimodal translational energy distribution, one component extends to

the limit of the available energy for formation of the $CH_3CHNH_2^+$ product but drops off on the low energy side at about 11.5 kcal/mol. A second slow component peaks at very low energy (2.3-4.6 kcal/mol) and drops rapidly at 11 kcal/mol and beyond. Based on the potential energy surface profile presented in Figure 1, two H loss pathways are possible: one is the lowest energy process of all, with a threshold of about 17 kcal/mol: this clearly corresponds to the outer ring in the H-loss image. There is a "hole" in the image for that product, because any of that isomer formed with less than ~20 kcal/mol in translation can undergo secondary decomposition via several pathways and cannot remain bound. The second, very slow isomer must then correspond to the triplet $CH_3CH_2NH^+$ product channel at high energy. The H-loss translational distribution is consistent with simple bond fission without an exit barrier following an internal excitation to the ground state of the cation.

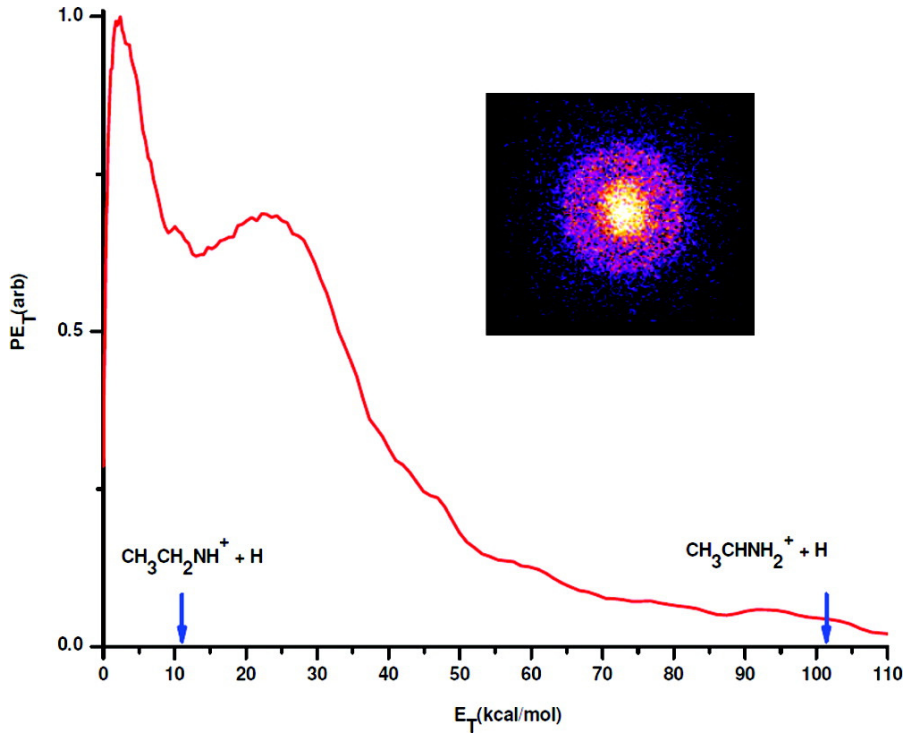

Figure 4.2: H-loss ion image and the associated translational energy distribution for ethylamine cation dissociation at 233 nm.

Formation of m/z=42. Figure 4.3 shows the DC sliced ion image and the associated translational energy distribution for the formation of m/z =42 product channel. The results show an isotropic angular distribution which is typical of ground state statistical dissociation following internal conversion. In order to understand and identify the dissociation pathway leading to the formation of m/z = 42 in our experiment, we turn to the stationary points and reaction pathways of the ground state cation presented in Figure 1. The m/z=42 product must come from loss of H followed by loss of H_2. As this involves a secondary (3-body) decomposition process, we cannot directly reconstruct the total translational energy from measurement of one fragment only.

However, as the initial step is loss of H, we assume negligible translational energy in the m/z=43 product, and obtain the translational energy distribution in Figure 3 by assuming H_2 as the cofragment. Starting from the H loss product $CH_3CHNH_2^+$, there are two possible routes for the formation of m/z 42. One of these involves H_2 loss over a barrier of 95 kcal/mol , with a reverse barrier of 25 kcal/mol. From our total available energy of 123 kcal/mol, we find that this channel is open. A perusal of the total translational energy distribution presented in Figure 3 show the distribution peaking away from zero, with a maximum peak at 5.8 kcal/mol that extends all the way out to 45 kcal/mol; the maximum limit for the formation of $CH_2CNH_2^+$ product channel. On the other hand, the $CH_3CHNH_2^+$ isomer can undergo H_2 loss through a barrier of 110 kcal/mol to form $CH_3CNH^+ + H_2$, a reverse barrier of 57 kcal/mol. Although this channel is about 16 kcal/mol below the $CH_2CNH_2^+ + H + H_2$ channel, the barrier associated with it is 15 kcal/mol higher than that the former; therefore, it is not expected to be competitive. Our DC sliced ion imaging results eliminates this product channel as it

would have be expected to show a large fraction of this barrier energy in translation, which we do not observe.

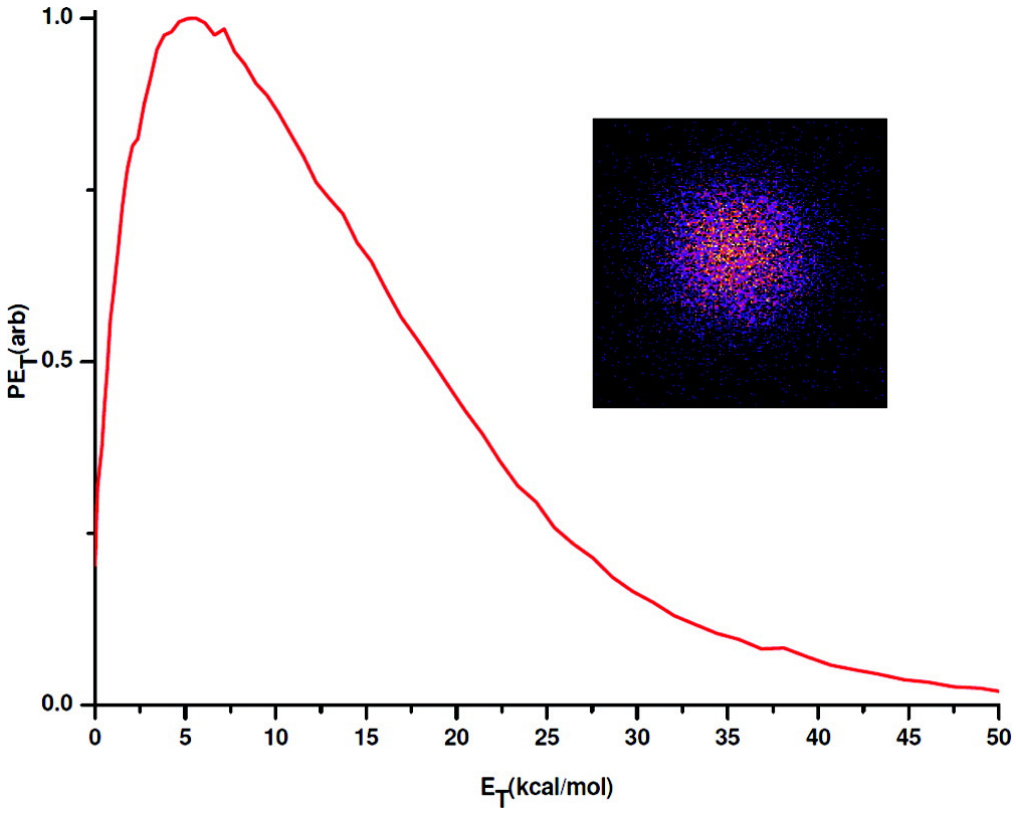

Figure 4.3: $H+H_2$ loss image and the associated translational energy distribution for $CH_3CH_2NH_2^+$ cation dissociation at 233.3 nm

Formation of m/z=28 ($HCNH^+$). We now turn to the results for the formation of the m/z=28 ($HCNH^+$) product channel. Apart from the parent ion (m/z=45) signal, m/z=28 was observed as the most intense peak in our time-of-flight spectrum. It is worth mentioning that the dissociation of $CH_3CH_2NH_2^+$ cation was investigated at wavelengths ranging from 230 nm to 234 nm, but we only show the results of 233.3 nm as, no wavelength dependence was found. At all the investigated wavelengths, $HCNH^+$ formation remained the dominant channel, even at very low laser powers much less than

0.1 mJ. In Figure 4.4, the DC sliced ion image and the associated translational energy distribution for the formation of m/z=28 are presented. As in the case of m/z=42 discussed above, we neglect the initial recoil in any initial H loss step and simply assume m/z=16 for the cofragment mass. The ion image has two distinct components, with the faster component showing an appreciable anisotropy. The inner portion of m/z=28 image does not exhibit any anisotropy and peaks at very low energy of 2.3 kcal/mol, dropping off to a limit of 4.2 kcal/mol. The faster component in the m/z=28 image peaks at 4.6 kcal/mol and extends out to 35 k cal/mol. From the potential energy profile presented in Figure 1, m/z=28 can be readily be identified as $HCNH^+$ formation. The $HCNH^+$ can be formed via several pathways, one of which is through the secondary decomposition of $CH_3CHNH_2^+$ to yield $HNCN^+ + H + CH_4$. If we consider the ground state dissociation of $CH_3CHNH_2^+$, the H_2 loss channel to form $CH_2CNH_2^+ + H + H_2$ is expected to be much more significant than the $HCNH^+ + H + CH_4$ channel. Even at internal energies of 130 and 140 kcal/mol, the RRKM branching of $HCNH^+ + CH_4$ /H_2CCNH_2 is calculated to be 1:7 and 1.5:6, respectively. The fact that we see appreciable anisotropy in the faster component of the $HCNH^+$ image is an indication that either excited state dynamics or multiphoton dissociation are involved.

The angular anisotropy parameters describing the angular distributions are obtained by fitting the angular distributions from the ion image to an even order polynomial expansion:

$$I(\theta) \alpha 1 + \beta_2 P_2(\cos\theta) + \beta_4 P_4(\cos\theta) + \beta_6 P_6(\cos\theta) \quad \text{..... (4.1)}$$

where θ is the angle between the laser polarization vector and the recoil velocity vector. Figure 4.5 (a) shows the angular distribution of the faster components of the $HCNH^+$ ion

channel. This angular distribution is well fitted using only the second order Legendre polynomial, giving a beta value of 0.57. The measured anisotropies integrated over the entire image from the fast to slow components are presented in Figure 4.5(b). It is clear that $HCNH^+$ ion image exhibits significant energy dependence in the angular distribution. There is a steady decrease in β with decreasing radius (velocity). A one-photon process can be fully described including only the P_2 *(cos θ)* term in equation 1. Since our experiment employs very low laser powers, and given this excellent fit including only the P2 term, we believe HCNH+ is the product of single photon dissociation and thus probably represents a direct dissociation process from an excited electronic state. These results on $HCNH^+$ formation will be discussed further in the Discussion section.

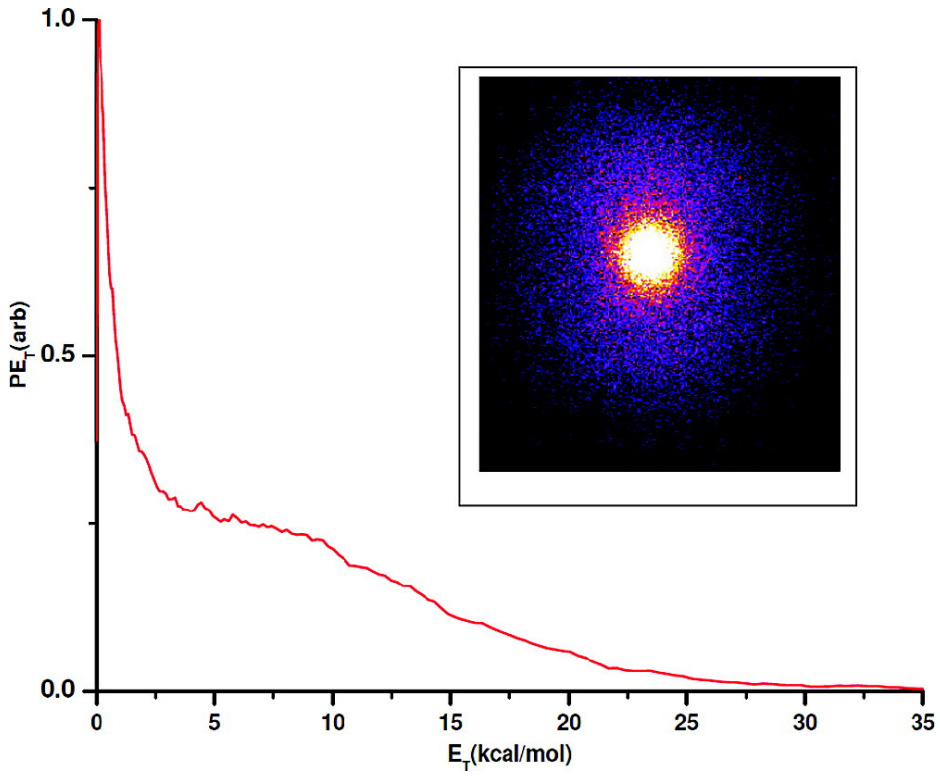

Figure 4.4: $HCNH^+$ image and the associated translational energy distribution for $CH_3CH_2NH_2^+$ cation dissociation at 233.3 nm

(a)

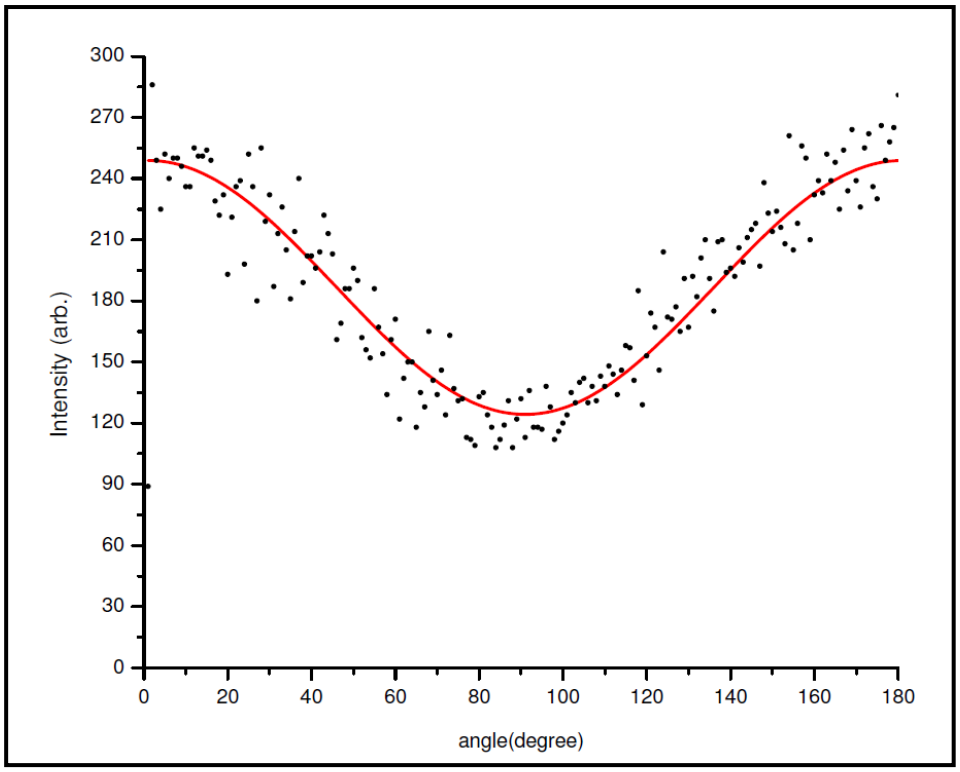

(b)

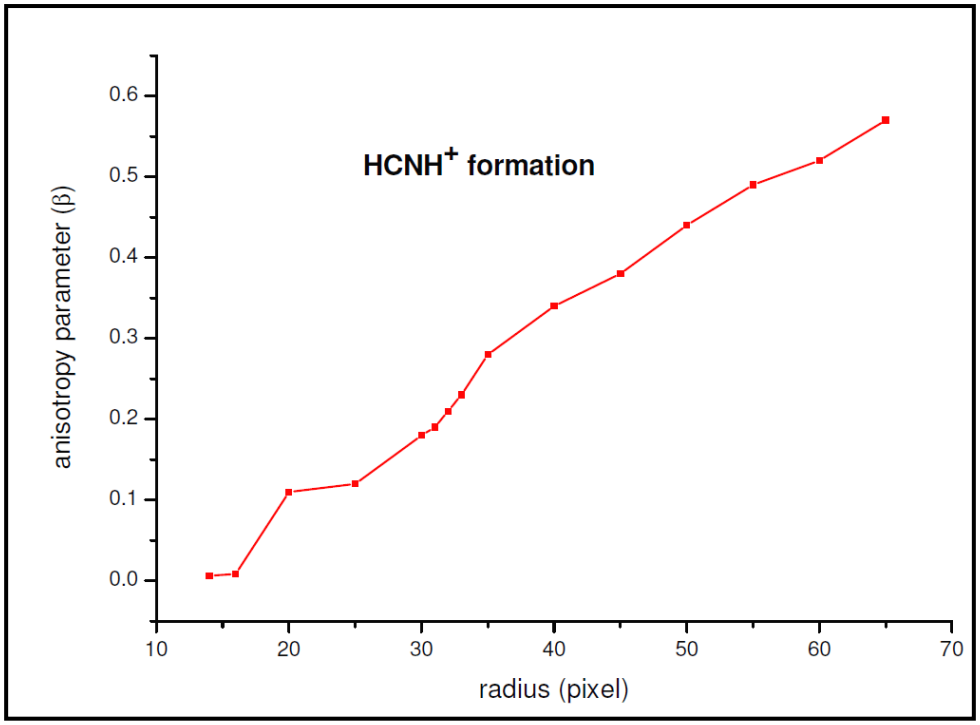

Figure 4.5: (a) Angular distribution of $HCNH^+$ ion. Solid lines correspond to the best fit with second order Legendre polynomial term **(b)** Anisotropy parameter, β, versus velocity for $HCNH^+$ product channel following 233.3 nm dissociation of ETA cation.

4.4 Discussion

The ion imaging results, having identified the H-loss and $HCNH^+$ ion formation as the main primary and secondary dissociation product channels, respectively, can now be examined in light of the high-level ab initio calculations presented in Figure 4.1. The stationary points and dissociation asymptotes for the ground state potential energy surface of ETA cation have been calculated at CCSD(T)/CBS and B3LYP/6-311G** level of theory. It is clearly seen that $CH_3CH_2NH_2^+$ can undergo isomerization through rearrangements to more stable distonic $CH_2CH_2NH_3^+$ and $CH_3CHNH_3^+$ isomers. The barrier heights associated with these rearrangements are 30.3 and 31.9 kcal/mol and the $CH_2CH_2NH_3^+$ and $CH_3CHNH_3^+$isomers are 5.7 and 5.2 kcal/mol lower in energy than $CH_3CH_2NH_2^+$, respectively. Earlier theoretical work on the potential energy surface of methylamine cation reports a similar isomerization of $CH_3NH_2^+$ to $CH_2NH_3^+$ cation, with an associated barrier height of 7.6 kcal/mol [123]. The lowest primary dissociation channel of $CH_3CH_2NH_2^+$ is H loss to form $CH_3CHNH_2^+$ at a reaction energy of 16.7 kcal/mol. ETA cation can also lose an H-atom from the NH_2 group to yield a triplet species $CH_3CH_2NH^+$ + H. The triplet $CH_3CH_2NH^+$ cation is located at 98.0 kcal/mol above the singlet $CH_3CHNH_2^+$ product. The other primary channel is the formation of $CH_2NH_2^+$ + CH_3, a process that involves a barrierless cleavage of the β-C-C bond with a reaction energy of 19.9 kcal/mol. CH_4 can also be eliminated through a primary photodissociation process to yield $CHNH_2^+$ cation via a barrier of 50.6 kcal/mol. The reaction energy involved in this process is 34.3 kcal/mol, with the process requiring the breaking of a C-C bond and a significant rearrangement through the $HCNH_2^+$ transition state structure. Another primary decomposition product of ETA cation is located at 65.2 kcal/mol above

the parent cation and involves the loss of NH_2 to form the $C_2H_5^+$ cation. Although this channel occurs without an exit barrier, its contribution in the dissociation of ETA cation is not as competitive as the H-loss process that is located 48.5 kcal/mol lower in the potential surface. Within our available energy of 123.3 kcal/mol, $CH_3CH_2NH_2^+$ can also lose H_2 through a barrier height of 80.5 kcal/mol to form CH_3CHNH^+.

We now consider the various secondary dissociation pathways presented in the potential energy profile presented in Figure 4.1. Once the $CH_3CHNH_2^+$ cation is formed via H loss, it is expected to undergo secondary decomposition through H_2 loss to form $CH_2CNH_2^+ + H + H_2$. This process occurs with a barrier of 78.5 kcal/mol (above the H loss product) and involves significant rearrangements. $CH_3CHNH_2^+$ can also undergo barrierless H loss to yield $CH_2CHNH_2^+$, $CH_3CNH_2^+$ and CH_3CHNH^+ isomers that are located at 93.3, 111.8, and 121.8 kcal/mol above $CH_3CHNH_2^+$, respectively. Among the three H-loss channels from $CH_3CHNH_2^+$, the first is expected to be the most important. The formation of $CH_3CNH^+ + H + H_2$ and $HCNH^+ + H + CH_4$ represent two other pathways in which $CH_3CHNH_2^+$ cation can undergo decomposition. The former channel involving H_2 loss occurs with a barrier of 93.5 kcal/mol and is located at 36.3 kcal/mol above $CH_3CHNH_2^+$ while the latter process involving CH_4 loss takes place with a barrier of 86.3 kcal/mol and is 8.2 kcal/mol higher than the H_2 loss channel.

H-loss channel. From our combined experimental and theoretical results on $CH_3CH_2NH_2^+$ cation dissociation at 233.3 nm, one photon dissociation leads to the formation of several primary and secondary product channels in which the primary loss of an H atom to form the singlet $CH_3CHNH_2^+$ ion is the lowest of all. The presence of two components in the ion image and the corresponding bimodal total translational

energy distribution presented in Figure 4.2 is indicative of the formation of triplet and singlet H-loss species that are separated by 98 kcal/mol. Once the singlet $CH_3CHNH_2^+$ cation is formed, it is amenable to further secondary decomposition through H-loss, H_2 loss and CH_4 loss to form m/z=43, 42, and 28, respectively. Further dissociation of the triplet species on $CH_3CH_2NH^+$ is not energetically allowed. The fast component of the H-loss product channel corresponds to the outer part of the ion image. The presence of a 'hole' in this outer ring suggests the occurrence of secondary decomposition of $CH_3CHNH_2^+$ cation via several pathways. The features of the translational energy distribution presented in Figure 4.2 are consistent with barrierless ground state statistical dissociation of ETA cation following internal conversion. The first excited states of ETA cation are calculated to be about 2.67 eV above the ground state of the cation[104]. Immediately above the first excited state of ETA cation, there exist numerous other low-lying excited states that are separated by an average energy spacing of about 0.15 eV [124]. At our excitation energy, there are thus many excited electronic states that can facilitate rapid nonradiative electronic relaxation. It is therefore plausible that the absorption of one 233.3 nm photon by ETA cation will lead to subsequent dissociation in the ground state. The lack of anisotropy on the ion image suggests that the lifetime may be long relative to the rotational period of the molecule or that there is a geometry change during the dissociation.

Formation of m/z=42. Turning to the results on the formation of m/z =42 presented in Figure 4.3, one can clearly see that the translational energy distribution peaks away from zero and falls off at high translational energy limit of 45 kcal/mol. Within our total available energy of 123.3 kcal/mol, it is possible to overcome the barrier

leading to the formation of $CH_2CNH_2^+ + H + H_2$. Typically, the ion image associated with dissociation via a barrier should peak away from zero energy as this repulsive energy release is converted to translational energy. The presence of slow m/z=42 products that may result from other multiphoton dissociation processes that are not discussed in this report may contribute to the observation of slow components in the m/z=42 image.

$HCNH^+$ formation. The m/z = 28 image shown in Figure 4.4 and the corresponding translational distribution are quite interesting. Generally, this kind of bimodal distribution is a clear indication of a photodissociation process resulting from a superposition of two phenomena accompanied by two different translational energy releases, such as in the case of 1,1-difluoroethene dissociation [125]. The slow part of the distribution, represented by the inner ring of the image, has a narrow kinetic energy release peaking near zero and falling off at a very low translational energy release of 16-18 kcal/mol. As mentioned earlier in this manuscript, one of the central questions raised by our experimental results is the absence of the CH_3 loss channel to yield $CH_2NH_2^+$. One possible explanation would be a rapid decomposition of the initially formed $CH_2NH_2^+$ product ions via H_2 loss to yield $HCNH^+$ product. In an earlier unimolecular decomposition study of $CH_2NH_2^+$, H_2 loss was found to be accompanied by a small fraction of kinetic energy since the $HCNH^+$ formed has bending excitation carrying away the available energy [126]. The average rate constant for the formation of $HCNH^+$ ions from $CH_2NH_2^+$ was calculated to be $6.0 \times 10^4\ s^{-1}$ [126]. If, in our experiment, $CH_2NH_2^+$ loses H_2 to form $HCNH^+$, we expect the inner part of the image to be representative of this process. Indeed, a dissociation pathway involving H_2 loss from $CH_2NH_2^+$ is expected to

occur via a barrier of 92.3 kcal/mol as demonstrated in our earlier results on methylamine cation [98]. In principle, secondary decomposition of $CH_2NH_2^+$ does not seem a convincing explanation for the dominance of the slow part of $HCNH^+$ product channel since the process would be too expensive energetically. A major observation to note, however, is the complete disappearance of the angular anisotropy of this inner ring which strongly suggests that the decay pathways of the slow and faster $HCNH^+$ product channel ion are not the same. We turn now to the faster, anisotropic component of the $HCNH^+$ image in Figure 4.5. Such anisotropy is unusual, if not unprecedented; in dissociation of polyatomic radical cations, as internal conversion and dissociation from long-lived lower-lying states is the general rule. Instead, these results suggest direct dissociation via an excited state as aruged earlier. As shown by the results in Figure 4.1, the fast $HCHN^+$ could result from secondary decomposition of $CH_3CHNH_2^+$. The image accompanying this process should have a 'hole' as this channel has an exit (reverse) barrier of 41.8 kcal/mol. We do not anticipate that this process would be as competitive as the H,H_2 loss channel. At this stage, the participation of excited state dynamics can be postulated as a likely explanation for the formation of the fast $HCNH^+$ ions since multiphoton dissociation is ruled out by the low laser powers and the good fit to the second order Legendre polynomial. Unfortunately, Figure 1 can provide no insight into dissociation pathways on the excited state, and such calculations are extremely challenging. We also note we are puzzled by the absence of the $CH_2NH_2^+$ channel in our experiment. Further theoretical studies, including a full account of the excited state processes involved, will be helpful to clarify this.

4.5 Conclusions

In summary, we report, via a combined experimental and theoretical investigation, results on the dissociation of ETA cation at 233 nm. As the main primary channel observed, the H- loss image has a translational energy distribution with a bimodal structure that correlates well with the formation of singlet $CH_3CHNH_2^+$ and triplet $CH_3CH_2NH^+$ species on the ground state potential surface of the cation. In addition to H loss, CH_3 loss to yield $CH_2NH_2^+$ is expected to be an important primary channel according to theoretical results, but we do not observe it in our experiment. $HCNH^+$ is formed as a dominant secondary channel with a bimodal translational energy distribution. The appearance of a significant angular anisotropy on the outer region of the ion image is suggestive of a direct excited state decay pathway for this fast portion of the distribution, which is a significant portion of the overall yield. $CH_2NH_2^+$ decomposition to $HCNH^+$ occurs at a very high energy so it does not seem a likely explanation for the dominance of this product. The formation of $CH_2CNH_2^+$ is also observed as a minor channel resulting from secondary decomposition of $CH_3CHNH_2^+$.

CHAPTER FIVE

LOW TEMPERATURE BRANCHING RATIO MEASUREMENTS OF ION-MOLECULE REACTIONS USING STATE PREPARED N_2^+ IONS

5.1 Ion-molecule reaction of State-prepared N_2^+ ions with CH_4, C_2H_2 and C_2H_4

5.1.1 Introduction

The gas phase study of state-specific ion-molecule reactions[127] has provided an essential cornerstone for the fundamental understanding of unimolecular and bimolecular reaction dynamics[128]. State-specific ion-molecule reaction experiments[129-130] have, in addition, been very useful in developing accurate models of plasma environments and planetary atmospheres through the determination of absolute state-selected cross sections[131,132] and product BRs.[133,134] Application of powerful methods that probe ion-molecule reactions under single collision conditions[135-136] and reaction kinetics at the relevant temperatures are key to developing a comprehensive picture of ion-molecule reaction dynamics.[137-138] A great challenge facing these approaches, however, is obtaining accurate branching ratios at the low temperatures characteristic of the atmospheres of the outer planets and their satellites.

Although important contributions to the study of ion-molecule reaction dynamics have been achieved by the use of state-prepared ions as the precursor reactant species in ion-molecule reactions[130], accurate determinations of BRs of the various product channels have remained a challenging subject of considerable interest due to their critical role in the accurate modeling of chemically active and reducing planetary atmospheres such the dense nitrogen-rich atmosphere of Titan.

As more concrete and detailed chemical information, such as from Cassini's Ion and Neutral Mass spectrometer (INMS)[139,140] has emerged, efforts to provide accurate models of Titan's upper atmosphere have in parallel necessitated the need for accurate and up-to-date laboratory measurements of BRs of the crucial ion-molecule reactions that are important in the ionosphere.[141,133,142]. A substantial number of laboratory studies have been devoted to the accurate determination of BRs of N_2^+ reactions with the minor hydrocarbon constituents of the upper atmosphere, such as CH_4, C_2H_2 and C_2H_4.[133] New experimental data are clearly required to provide accurate quantitative comparison between the *in-situ* observations of the Cassini orbiter and the proposed models. Indeed, for a thorough understanding of the *astrochemical dynamics*[143] in Titan's chemically active atmosphere, new approaches to laboratory measurements of important astrophysical quantities such as the BRs at well-defined conditions need to be developed. To this end, we report on the low temperature BR measurements of ion-molecule reactions of state-prepared N_2^+ ions with CH_4, C_2H_2 and C_2H_4. In these studies we have developed a simple but powerful approach that quickly provides the subject BRs at conditions close to those relevant for Titan's ionosphere.

The three main pathways for the reactions of N_2^+ with CH_4^+ are:

$$N_2^+ + CH_4 \rightarrow CH_4^+ + N_2 \qquad \Delta H^o = -2.97 \text{ eV} \ldots\ldots\ldots\ldots\ldots\ldots 5.1.1$$

$$\rightarrow CH_3^+ + N_2 + H \qquad \Delta H^o = -1.19 \text{ eV} \ldots\ldots\ldots\ldots\ldots 5.1.2$$

$$\rightarrow CH_2^+ + N_2 + H_2 \qquad \Delta H^o = -0.41 \text{ eV} \ldots\ldots\ldots\ldots\ldots 5.1.3$$

$$\rightarrow N_2H^+ + CH_3 \qquad \Delta H^o = -2.86 \text{ eV} \ldots\ldots\ldots\ldots\ldots 5.1.4$$

The N_2H^+ ion product channel has only been observed in the studies of McEwan et al.[142] and Nicolas et al.[131] The channels leading to the formation of CH_3^+ and CH_2^+ product

ions have been previously investigated using Ion Cyclotron Resonance (ICR), selected ion flow tube (SIFT) and free jet flow reactor techniques where both the rate coefficients and the BRs were measured.[134,133] However, the BR measured by Randeniya and Smith [144] at 8-15 K differ by 10% from the room temperature value.[133] The critical role of N_2 photoionization in Titan's atmosphere and its subsequent contribution to the formation of complex organic molecules has also triggered a series of related photocell EUV experiments by Imanaka and Smith. [145,146] These studies have demonstrated that the photoionization of N_2^+ at 60 nm can lead to the formation of CH_3^+ product ions with a subsequent production of complex organic species. However, the conclusions of Smith and Imanaka studies are somewhat limited as to the description of initial chemical reaction mechanisms and the primary branching where ion-molecule reactions are expected to be the dominant processes that determine the subsequent chemistry. This is due to the fact that in a photocell, the generation of neutral complex organic molecules is a result of coupled sets of photodissociation, photoionization, ion-molecule reactions, electron-ion recombination and neutral-molecule reactions.

Whereas the BR measurements for the $N_2^+ + CH_4$ reaction has been subject of considerable scrutiny both at room temperature and at low temperature conditions, the BR data of the various product channels in the reactions of N_2^+ ions with C_2H_2 and C_2H_4 remain insufficiently investigated. Previous work by Anicich et al.[134,133] has generally reported the thermal rate coefficient and BRs using the SIFT technique. For the $N_2^+ + C_2H_2$ reaction, the most recent study[133] reported a single non-dissociative charge transfer channel leading to the sole formation of $C_2H_2^+$ product ions. A product branching ratio[134] of 0.37:0.03:0.60 for the formation of $C_2H_2^+$, NCH^+ and N_2H^+ product ions reported in

Anicich's at al.'s earlier study[134] was believed to be largely in error due to the presence of impurities and secondary collisions. As for the $N_2^+ + C_2H_4$ reaction, a model by Anicich et al.[133] predicted that the $C_2H_3^+$ and $C_2H_2^+$ product ions are formed with an overall BR of 0.64:0.36, respectively, although there is as-yet no experimental support for this determination. This ratio was obtained without invoking HCN^+ and $HCNH^+$ ions in the model, although they were observed in Anicich's et al. experiments.

In the present study, we report for the first time the product branching ratios of state-prepared N_2^+ ion-molecule reactions with CH_4, C_2H_2 and C_2H_4 in a supersonic molecular beam expansion where the characteristic rotational temperature is 40 ± 5K and only a few collisions are present. This work is related to a number of previous studies. Pollard and coworkers[147] used REMPI production of H_2^+ to study $H_2^+ + H_2$ albeit in crossed beams at superthermal collision energies with an eye to the dynamics. Glenewinkel-Meyer and Gerlich[148] examined the use of REMPI production of state-selected H_2^+ in single beam and merged beam reaction with H_2 and examined many of the underlying experimental issues, but their focus was on using the approach to determine rate constants and cross sections. More recently, Belikov et al.[149] extended the approach described by Glenewinkel-Meyer and Gerlich[148] to study state-specific reactions of HBr^+ at low temperature. They obtained rate constants for several different channels as a function of initial spin_orbit state and rotational level. Our approach is similar, although our focus is simply on determining the branching ratios, and we prepare our reactants in the collision region of the expansion

The BR determinations provide direct insights into the underlying fundamental mechanisms accompanying the non-resonant dissociative charge-transfer reactions which

can further assist in the accurate modeling as well as a better understanding of the astrochemical dynamics in Titan's ionosphere. Finally, these branching ratio measurements have been undertaken as a test-case for our newly-commissioned experimental approach that combines state-selective ion preparation with reaction in the course of the nozzle expansion.

5.1.2 Experimental

The experiments were carried out using a modified velocity map imaging mass spectrometry apparatus (VMIMS) that was described in detail in Chapter 2. Here, only the details pertinent to the N_2^+ initiated ion-molecule reactions will be highlighted are pulsed on. The reactant N_2^+ ions were produced via a 2+1 REMPI scheme[150]. In this scheme, two photons of the 202 nm laser light are used to excite the ground N_2 molecule to the intermediate $a''\ {}^1\Sigma_g^+$ Rydberg state. The wavelength calibration of the laser light was achieved by using a wavemeter (Coherent Wavemaster). The precise frequency of the tripled light used corresponded to the transition to the lowest rotational level ($J=0$) of the $a''\ {}^1\Sigma_g^+ \leftarrow X^1\Sigma_g^+$ (0, 0) band of N_2, measured to be 49420.29 cm^{-1}. Absorption of an additional photon from the same laser pulse allows the production of N_2^+ ions. The $a''\ {}^1\Sigma_g^+$ Rydberg state possesses a ground state N_2^+ core[151-152] and has been shown to ionize exclusively via $\Delta v=0$ [153]. Consequently, this REMPI produces N_2^+ ions that are entirely in the ground vibrational state of the cation. We observed no dependence of the branching on the rotational level excited, so these spectra were all obtained on the lowest, most populated level, giving N_2^+ in low rotational levels. The tunable 202 nm light used to prepare the N_2^+ ions was generated by frequency tripling of the output of a tunable, narrow-line width (<0.075 cm^{-1}) OPO laser system (Spectra-Physics MOPO HF). The

MOPO HF was pumped by the third harmonic of a seeded Nd:YAG laser operating at 10 HZ. Approximately 50 mJ/pulse of horizontally polarized 607 nm light with 10 ns pulse width and < 0.075 cm^{-1} bandwidth was produced. The MOPO output was then doubled in an angle tuned KDP crystal and then finally frequency tripled in BBO crystal to produce vertically polarized 202 nm light. The tripled light was then focused with a 16 cm lens into the ionization chamber where the reactions of N_2^+ ions with the target neutral molecule took place.

5.1.3 Results

$N_2^+ + CH_4$ reaction

The time-of-flight mass spectrum for the reaction between N_2^+ (v=0) ions with CH_4 is presented in Figure 5.1. The spectrum was accumulated up to 1200 shots at 10 Hz with the accumulated intensity of the CH_3^+ and CH_4^+ product ions being measured and monitored for over a period of 15-20 minutes to ensure that there was no change in the BRs. In order to eliminate the occurrence of secondary reactions, CH_4 concentrations were kept low at ~1%. The obtained mass spectra were then fitted using Gaussian functions and the integrated area of the peaks used to calculate the BRs presented in Table 5.1. The results summarized in Table 5.1 give an overall branching ratio of 0.83: 0.17 for the formation of CH_3^+ and CH_2^+ product ions, respectively. Although it is energetically possible to form the CH_4^+ ion, this non-dissociative charge transfer was not observed in our experiment. Even at very low collision energies, the integral cross section for this channel is below 0.1$Å^2$ as has already been reported by Nicolas et al.[131]

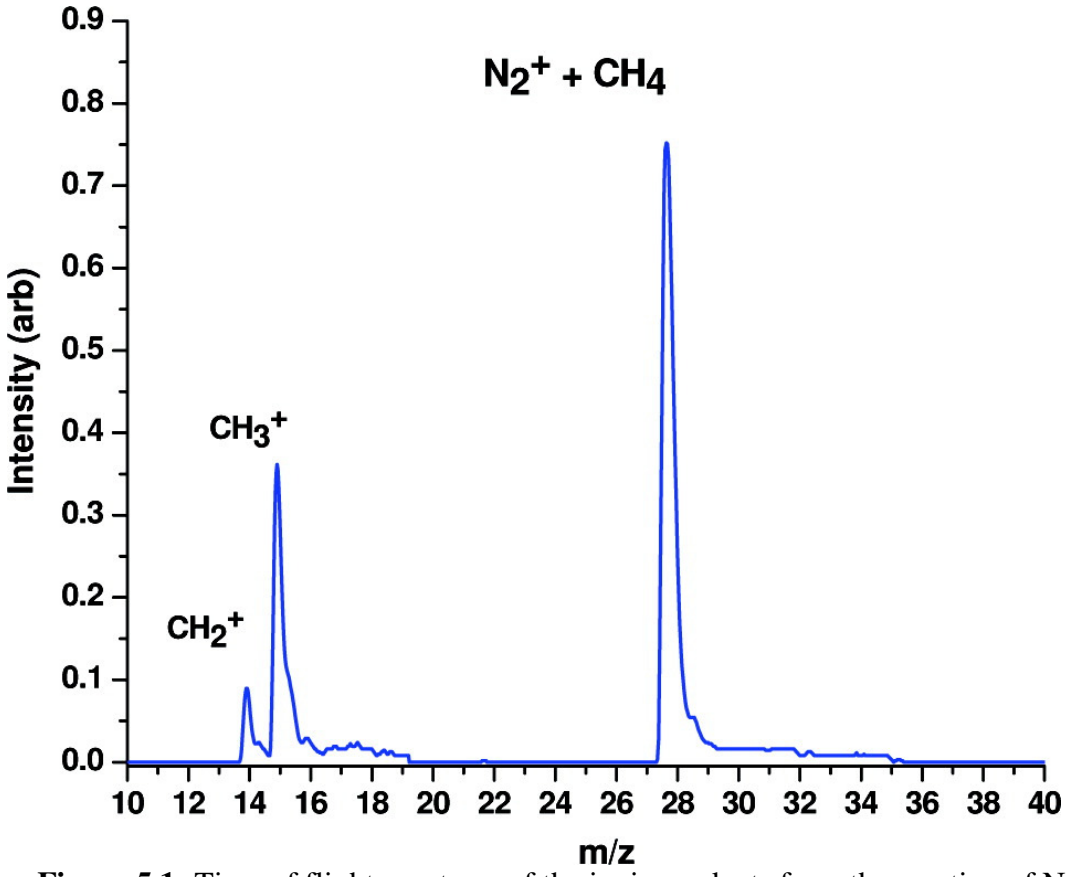

Figure 5.1: Time of flight spectrum of the ionic products from the reaction of N_2^+ (v=0) with methane.

In order to gain more insight onto the dynamics of the dissociative charge-transfer reaction of state-prepared N_2^+ ion with CH_4, it important to consider the dissociation pathways and the fragmentation pattern of CH_4^+ ion as reported by Stockbauer[154] and Bombach.[155] The ionization energy of CH_4 is 12.61 eV while the dissociation energy of CH_4^+ leading to the formation of CH_3^+ + H channel is 1.64 eV.[156] The removal of an electron from CH_4 molecule leads to the formation of nascent CH_4^+ product ions in a triply degenerate $^2T_2$ state.[157] Due to the Jahn-Teller effect,[157] the nascent CH_4^+ cation then undergoes deformation to lower ^2T_g symmetry structure. Between 13.8-16.4 eV, the CH_4^+ (^2T_g) ion exhibits a breakdown pattern[158] that leads to the formation of CH_4^+ product ions only below 14.3 eV. Above 14.3 eV, the branching ratio to the CH_4^+ product

ion decreases due to the appearance of CH_3^+ ion. The CH_4^+ product ion disappears above 14.5 eV. The threshold for the formation of CH_2^+ product ions is 15.2 eV, with its branching increasing with an increase in the internal energy. Taking into account that the ionization energy (IE) of N_2 is 15.58 eV[159], this means that a significant amount of the 2.97 eV reaction exoergicity is deposited into CH_4^+ ion in form of internal energy. On the basis of this reported fragmentation pattern of CH_4^+ ion below 16 eV, the absence of a CH_4^+ ion peak in our mass spectrum is a confirmation that CH_4^+ formation becomes insignificant as $CH_3^+$and CH_2^+ ions are formed due to an increase in the internal energy of the parent CH_4^+ product ion . The IE for Ar[159] is very close to that of N_2, it is therefore worth comparing our present results to those of $Ar^+ + CH_4$ reaction reported by Tsuji et al.[160] In the $Ar^+ + CH_4$ reaction, Tsuji et al.[160] observed the formation of CH_3^+ and CH_2^+ product ions as the only primary channels, with an overall branching ratio of 0.85:0.15, respectively. This branching is very close to our present BR value for the formation of CH_3^+ and CH_2^+ product ions in the $N_2^+ + CH_4$ reaction which is in turn, indicative of a similar charge transfer reaction mechanism. In addition, our BR is also in reasonable agreement to the earlier reported values at low temperature[144] and room temperature conditions[133].

$N_2^+ + C_2H_2$ reaction

The time-of-flight spectrum presented in Figure 5.2 shows the formation of $C_2H_2^+$ ion as the only primary product channel in the $N_2^+ + C_2H_2$ reaction. This is in agreement with the previous room temperature measurements by Anicich et al.[133] using flowing afterglow-selected ion flow tube (FA-SIFT) technique. The single charge transfer channel was observed to proceed with an overall rate constant of 5.50 X 10^{-10} cm^{-3}/s. The IE of

C_2H_2 is 11.4 eV[159]. This gives a value of 4.19 eV as the total amount of internal energy that can efficiently be transferred to the $C_2H_2^+$ in a N_2^+ + C_2H_2 collision and hence become available for bond-breaking in the parent $C_2H_2^+$ cation.

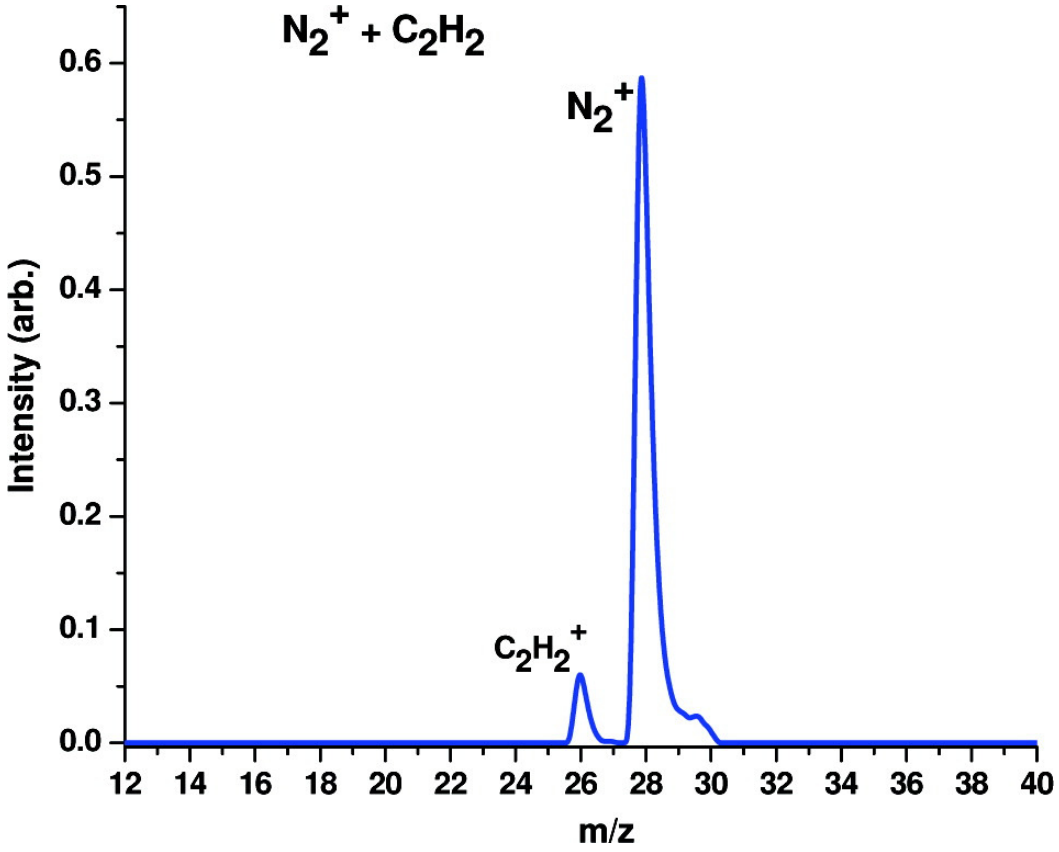

Figure 5.2: Time of flight spectrum of $C_2H_2^+$ product ion from the reaction of N_2^+ (v=0) with acetylene.

The appearance energy for the lowest energy dissociation channel in $C_2H_2^+$ (i.e., the formation of C_2H^+ ion) is 17.3 eV[159,161]. This value is higher that the ionization energy of N_2^+, hence it is not energetically possible to induce C-H bond dissociation in $C_2H_2^+$ through a dissociative charge-transfer reaction with N_2^+. Our present results are also in reasonable agreement with the almost isoenergetic Ar^+ + C_2H_2 reaction[160] where $C_2H_2^+$ product ion was observed as the only product channel. The formation of $C_2H_2^+$

($^2\prod_u$) in the $N_2^+ + C_2H_2$ reaction can simply be understood as an efficient charge-transfer reaction that occurs without an energy barrier in a direct long-range encounter.

$N_2^+ + C_2H_4$ reaction

Figure 5.3 presents the associated time-of-flight spectrum for the $N_2^+ + C_2H_4$ reaction. The main peaks observed in this experiment correspond to the formation of $C_2H_3^+$ and $C_2H_2^+$ product ions at a branching ratio of 0.74:0.26 (as shown in Table 5.1).

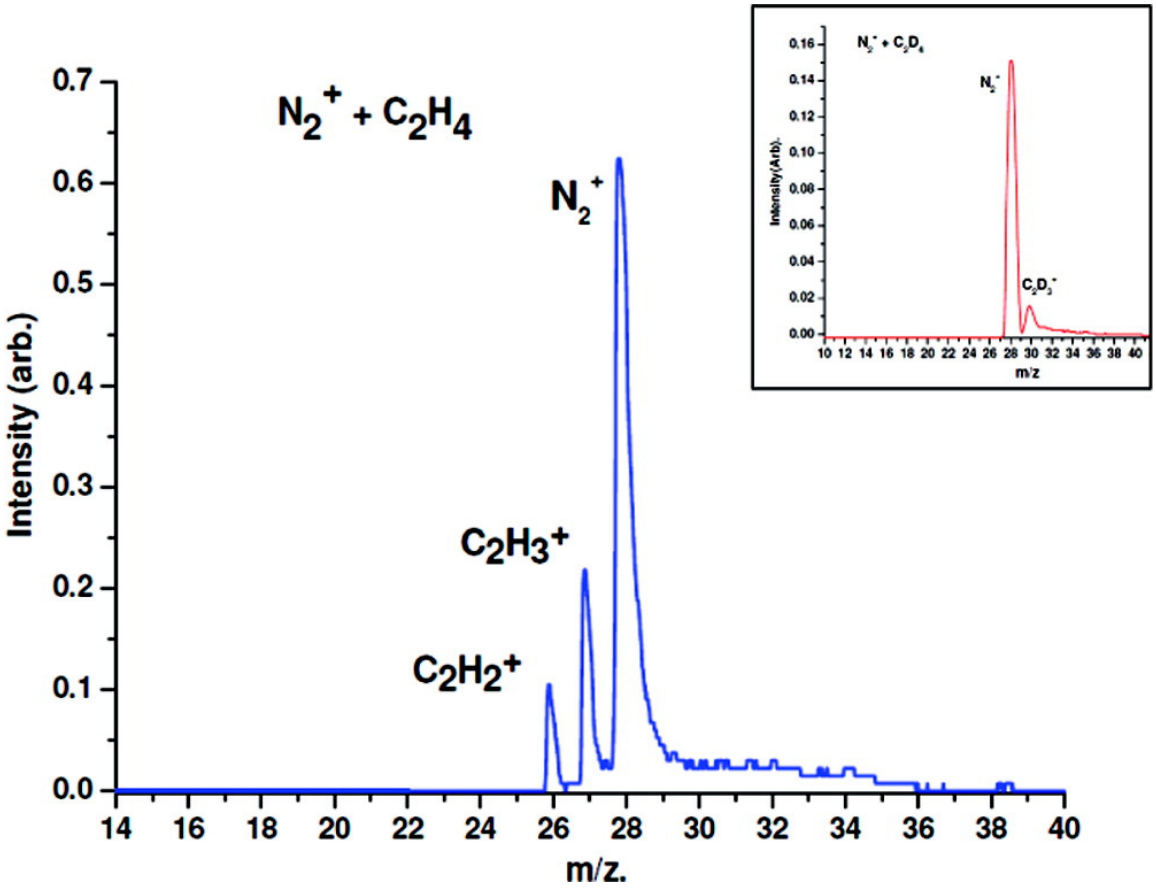

Figure 5.3: Time-of-flight spectrum of the product ion channels from the reaction of N_2^+ (v = 0) with C_2H_4. Inset shows the spectrum for reaction with C_2D_4, confirming the absence of $C_2D_4^+$ product.

Table 5.1: Branching ratios for the formation of various product ion channels observed upon the reaction of N_2^+ (v=0) with CH_4, C_2H_2 and C_2H_4. The branching ratios are an average of at least six independent measurements under similar conditions with $\pm 2\sigma$ error.

Reaction	Product ion	Branching ratio
$N_2^+ + CH_4$	CH_3^+	0.83 ± 0.02
	CH_2^+	0.17 ± 0.02
$N_2^+ + C_2H_2$	$C_2H_2^+$	1
$N_2^+ + C_2H_4$	$C_2H_3^+$	0.74 ± 0.02
	$C_2H_2^+$	0.26 ± 0.02

At this point, it may be worthwhile to take into consideration the electronic states of $C_2H_4^+$ ion that may be involved in the charge- transfer reaction below 15.58 eV, the limit for our recombination energy. The four main $C_2H_4^+$ precursor states that may be involved are X^2B_{2u}, A^2B_{2g}, B^2A_{2g}, and C^2B_{3u}.[162,163] The removal of an electron from any of these states results in C-H bond (s) rupture. As mentioned by Tsuji et al [160] in the $Ar^+ + C_2H_4$ ion-molecule reaction, the CT reaction in C_2H_4 predominantly leads to an efficient population of a pre-dissociative $C_2H_4^+$ state that lies at about the 15.3 eV energy range.

From the C_2H_4 breakdown diagram [155], $C_2H_4^+$ ion can only be formed below 13.3 eV. The production of the parent ion starts to decrease above 13.0 eV due to the appearance of $C_2H_3^+$ and $C_2H_2^+$ product ions. In the $Ar^+ + C_2H_4$ reaction for example, the

formation of $C_2H_4^+$ non-dissociative CT channel was negligible with a reported BR of 0.04 as compared to the $C_2H_3^+$: $C_2H_2^+$ BR of 0.76:0.20. This reported BR for the formation of to $C_2H_3^+$ and $C_2H_2^+$ product ions was found to increase with an increase in the internal energy of the parent $C_2H_4^+$ ion. The present 0.73:0.27 BR for the formation of $C_2H_3^+$ and $C_2H_2^+$ product ions, respectively is not very different from the one observed for the $Ar^+ + C_2H_2$ reaction in Tsuji et al.'s work [160]. We do not anticipate that $C_2H_4^+$ product channel would be formed, as it is expected to undergo a rapid decomposition to $C_2H_3^+$ and $C_2H_2^+$ product ions. To gain deeper insights onto the dynamics of this N_2^+ ion-molecule reaction, these results will be discussed further in the following section by invoking the photoionization and the state-specific photodissociation dynamics results of $C_2H_4^+$ cation as reported in earlier studies.

5.1.4 Discussion:

$N_2^+ + CH_4$ reaction: dissociative charge transfer and the branching ratios

Despite the uncertainty in the BR measurements by different techniques and workers, it is generally accepted that the mechanism accompanying this reaction is a simple capture process followed by dissociative charge-transfer. It is instructive to discuss our results in relation to the earlier results of $Ar^+ + CH_4$ reaction by Tsuji et al. [160] In the $Ar^+ + CH_4$ reaction, the dissociative charge transfer leading to the formation of CH_3^+ and CH_2^+ product ions is thought to involve a non-adiabatic transition between two non-resonant charge states ; $Ar^+ + CH_4$ and $CH_4^+ + Ar$. As indicated by the magnitude of the total cross-section, there is a large non-adiabatic coupling between these two charge transfer states. On reaching the first relevant crossing that has a high probability, Ar^+ and

CH_4 charge transfer occurs with unit probability resulting in an immediate dissociation of the nascent CH_4^+ ion. Although a detailed potential energy surface for the reaction N_2^+ + CH_4 is not currently available, it is likely that the dissociative charge transfer reaction proceeds via a non-adiabatic coupling just as in the Ar^+ + CH_4 case. In an earlier study, Nicolas et al.10 proposed that the formation of CH_2^+ and CH_3^+ ions proceeds via a separated sequential process. In this case, an impulsive single-electron transfer is later accompanied by CH_4^+ ion dissociation.

Using a flow jet reactor, Randeniya and Smith [144] obtained a CH_3^+: CH_2^+ branching ratio of 0.80: 0.20 at 30 K, a value that is very close to our present 40 ± 5K value of 0.83:0.17. The room temperature branching ratio of 0.88: 0.12 reported by Anicich et al.[133] differs by about 7% with our value. It is critical to mention that the CH_3^+: CH_2^+ branching ratio does not depend significantly on the collision energy, an indication that the kinetic energy is not efficiently converted into internal energy of the CH_4^+ ion. As previously noted in the Nicholas et al. study, this behavior is also a confirmation of the strong coupling between the two aforementioned charge-states (N_2^+ + CH_4 and CH_4^+ + N_2).

Charge transfer in N_2^+ + C_2H_2 reaction

High resolution He I photoelectron spectroscopy shows that the adiabatic ionization energies corresponding to $X^2\prod_u$, $A^2\sum_g^+$ and $B^2\sum_u^+$ states of $C_2H_2^+$ ion are 11.403, 16.297 and 18.391 eV[163], respectively. There also exist regions of autoionizing Rydberg series that converge to vibrationally excited levels of the electronic ground state at regions 2 eV above the ground state. It is plausible that these autoionizing Rydberg states act as the precursors to the non-dissociative charge transfer reaction that lead to the

sole formation of $C_2H_2^+$ product ion. Since the threshold for the appearance of the lowest H-loss dissociation channel, $C_2H^+ + H$, is above the recombination energy of N_2^+ ion (15.58 eV), the only accessible electronic state in a C_2H_2 collision encounter with N_2^+ is the $X^2\prod_u$ ground state. As no chemical bond is broken in $C_2H_2^+$ ion, the appearance of a single peak as displayed in Figure 2 is as a result of a CT process that occurs over comparatively long distances in an electron transfer that is accompanied by no appreciable momentum change. Considering the N_2^+ ion recombination energy of 15.58 eV and the strong C-H bond in $C_2H_2^+$ cation, the non-dissociative CT channel leading to the formation of $C_2H_2^+$ product ion is expected to be the only primary process. This is consistent with our observed unity measurement of the branching for this reaction.

$N_2^+ + C_2H_4$ reaction: dissociative charge transfer and the branching ratio

Our time-of-flight mass spectrum shown in Figure 3 represent the first unambiguous experimental study identifying $C_2H_3^+$ and $C_2H_2^+$ as the major primary product channels in the $N_2^+ + C_2H_4$ charge transfer reaction. The branching ratio for the formation of $C_2H_3^+$: $C_2H_2^+$ product ions as summarized in Table 5.1 is 0.74:0.26, respectively. In their most recent work, Anicich et al.[133] performed careful modeling of the $N_2^+ + C_2H_4$ reaction and followed the reactions over a significant flow range. Whereas the HCN^+ and $HCNH^+$ channels reported earlier by Anicich et al. were omitted in the model, the non-dissociative charge-transfer channel was also not identified. A branching ratio of 0.64:0.36 for the $C_2H_3^+$: $C_2H_2^+$ product channels was obtained from the model.

Our BR measurement differs by ~9% from that inferred from the model. In order to get more insight into $N_2^+ + C_2H_4$ dissociative charge transfer reaction that leads to the

observed branching ratio, it is beneficial to consider the excited states of $C_2H_4^+$ cation that may be involved. As mentioned earlier, below 16 eV the four $C_2H_4^+$ accessible sates are: X^2B_{3u}, A^2B_{3g}, B_2A_g and C^2B_{2u} states at 10.51, 12.45, 14.45, and 15.87 eV, respectively[164]. On the other hand, the appearance energies for the formation of $C_2H_3^+$ and $C_2H_2^+$ ions are 13.3 and 13.0 eV, respectively[164]. This clearly shows that at a total N_2^+ recombination energy of 15.58 eV, the $C_2H_3^+$ and $C_2H_2^+$ ions have thresholds that are associated with the X^2B_{3u}, and A^2B_{3g} as the possible precursor electronic states.

We note here that in order to have a clear picture of the dynamics involved in the CT reaction of N_2^+ + $C_2H_4^+$, one cannot overlook the underlying photodissociation dynamics of the $C_2H_4^+$ cation and the associated branching as exemplified in a number of previous studies. Indeed, a detailed state-selected ion imaging study on $C_2H_4^+$ cation dissociation by Kim et al. [165] has established that the $C_2H_4^+$ cation undergoes fragmentation that leads to H-loss and H_2 elimination as the main primary processes. Consistent with the previous single-photon ionization mass spectrometry and threshold-photoelectron-photoion coincidence (TPEPICO) studies[154], Kim et al.[165] found the H elimination channel to be much more favorable than the H_2 loss channel. It is interesting to note that just as in these photochemistry experiments, the most preferred dissociative CT channel in our present study is the H-loss channel leading to the formation of $C_2H_3^+$ product ion. Although Ar^+ is more energetic than N_2^+ ion (15.76 recombination energy versus 15.58 eV), its reactions with $C_2H_4^+$ provides an additional platform for obtaining a qualitative picture of the charge-transfer mechanism for the reactions of N_2^+ with C_2H_4. The Ar^++ C_2H_4 study[160] reported a branching of 0.76:0.20:0.04 for $C_2H_3^+$:$C_2H_3^+$:$C_2H_4^+$ with a conclusion that the $C_2H_3^+$ and $C_2H_3^+$ ions are produced though a near-resonant

charge transfer mechanism without significant momentum transfer. Consequently, two charge transfer mechanisms in the $Ar^+ + C_2H_4$ reaction are inferred; one is the dominant near-resonant dissociative charge transfer leading to the formation of $C_2H_3^+$ and $C_2H_2^+$ ions while the other is the minor non-resonant non-dissociative charge transfer leading to the formation of $C_2H_4^+$ parent ions. In the $N_2^+ + C_2H_4$ reaction, we propose that just as in the case of $N_2^+ + CH_4$ reaction, the collision encounter between N_2^+ ions and the C_2H_4 molecule lead to an efficient dissociative charge transfer involving a non-adiabatic transition between two non-resonant charge states of $N_2^+ + C_2H_4$ and $C_2H_4^+ + N_2$. Detailed theoretical studies on the potential energy surface for the reaction $N_2^+ + C_2H_4$ would be required to validate our proposed mechanism but owing to the similarities between the recombination energies of Ar^+ and N_2^+ ions, this interpretation appears quite plausible. Our qualitative arguments can further be supported by the fact that we do not observe the parent $C_2H_4^+$ ion.

5.2 Reaction of state-prepared N_2^+ ion with Acetonitrile

5.2.1 Introduction

As one of the possible building blocks of biomolecules[166], Acetonitrile (CH_3CN) was first discovered in Titan's atmosphere via ground-based mid microwave sub-mm spectroscopy. A disk-averaged vertical profile mole fraction of the order of 10^{-8} was revealed above 150 km[167]. This profile was found to increase slowly with altitude up to 500 km. CH_3CN has also been found to be ubiquitous in laboratory experiments simulating Titan's atmosphere[168]. The mole fraction of CH_3CN calculated by two recent models appears to be in close agreement[139, 168]. These two models propose the insertion of

N (^{2}D) into C_2H_4 as the major route leading to the production of CH_3CN. Although the possible role of CH_3CN and other related cyano compounds in Titan's ion-molecule reactions has not received much attention in the past, we seek to report on the low temperature product BRs of N_2^+ reaction with CH_3CN as an initial attempt understanding the fate of other closely related unsaturated trace constituents in Titan's atmosphere upon a collision encounter with the dominant N_2^+ cation. Utilizing the SIFT technique, Wincel et at;[169] reported room temperature rate coefficient and product BRs for the reaction of N_2^+ cation with CH_3CN. For a period of more than 20 years, no further experiments on N_2^+ reaction has been undertaken and the existing BRs are largely in error due to the use of inaccurate dissociation thresholds for CH_3CN^+ cation and the possible involvement of electronically excited N_2^+ cations. We expand on this in our discussion on the BRs.

Figure 5.4 shows some of the energetically allowed ionization and fragmentation pathways for CH_3CN. The lowest energy values associated with the production of CH_2CN^+, $CHCN^+$ and CCN^+ are 14.4 eV, 15.9 eV and 20.0 eV[170], respectively. Studies on acetonitrile molecular cation dissociation have also been carried out using several mass spectrometric techniques[171-173]. Using mass-analyzed ion kinetic energy spectrometry, Choe[172] has for example obtained the kinetic energy distribution for the H-loss channel that leads to the formation of CH_2CN^+ product ion and perfomed Density functional theory calculations to investigate the isomerization and dissociation pathways of the ground state CH_3CN^+ cation. In this experiment, only the H- loss product was observed, agreeing with the previous experimental results.

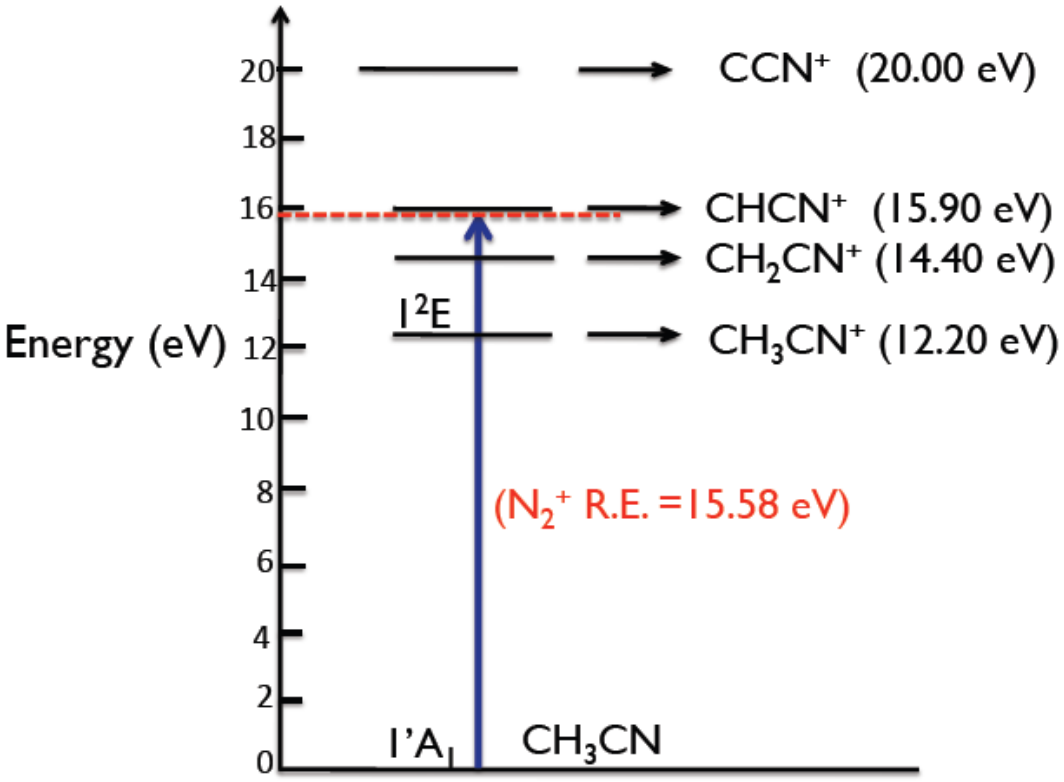

Figure 5.4: Energy diagram showing the possible dissociation channels of acetonitrile cation in a charge transfer reaction involving N_2^+ cation with a total recombination energy of 15.58 eV

5.2.2 Charge transfer, H-loss channels and the branching ratios

Figure 5.5 shows the time of flight profile associated with the reaction of N_2^+ cation with CH_3CN at 202 nm. Here, we neglet the N_2^+ peak and show only the H-loss and charge transfer product ion peaks at m/z 40 and 41, respectively. Taking the recombination energy of N_2^+ cation to be 15.58 eV and considering the associated

dossociation thresholds as presented in Figure 5.3, the only two possible primary product channels possible in a charge transfer reaction involving N_2^+ with CH_3CN are:(i) Charge transfer leading to the formation of the parent cation and (ii) the H-loss product. This is indeed consistent with our results as opposed to the Wincel et al[169] results where the H_2 loss product was observed. In the Wincel's experiment, the N_2^+ ions were prepared by bombandment with an electron beam of gas mixtures of CH_3CN + M (M= Ar, H_2, N_2, CO, CO_2 and CH_4 at pressures ranging from 0.01 to 0.4 torr and temperatures between 305 K and 345 K). This method of preparing N_2^+ cations resulted in the production of long-lived excited ions of N_2^+ ion that reacted with CH_3CN forming CH_2CN^+ product ions. Table 5.2 gives a summary of Wincel's et al;[169] banching ratio and our present low temperature BR.

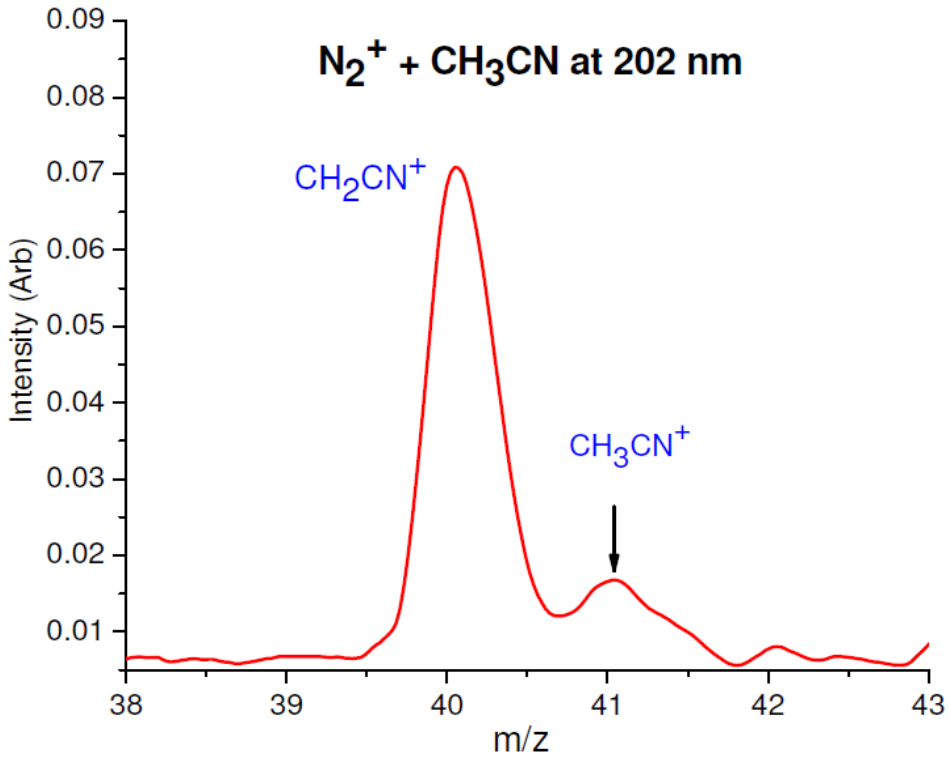

Figure 5.5: Time of flight spectrum of CH_2CN^+ and CH_3CN^+ product ions from the reaction of N_2^+ (v=0) with acetonitrile.

Using our new low temperature technique, we obtain a branching ratio of 0.95:0.05 for the formation of CH_2CN^+ and CH_3CN^+ product ions, repectively. The branching ratio seems to overwhelmingly favor the formation of the H-loss product channel just like is the case of Choe's experiment[172] where the H-loss product was observed to be the dominant channel. RRKM model calculations based on the obtained potential energy surface predict that CH_3CN^+ cation interconverts to CH_2CNH^+ and CH_2NCH^+ followed by dissociation to a cyclic $C_2H_2N^+$ via an cyclic $C_2H_3N^+$ intermediate near the threshold[172]. The H-loss kinetic energy distributionn in Choe's experiment seems broader and different than the typical statistical distribution associated with a simple bond cleavage. One possibility for this large KER is a considerable reverse barrier which is commom in some direct bond cleavage reactions to produce cations with aromatic stability.

Table 5.2. BRs for the formation of various product ion channels observed upon the reaction of N_2^+ (v=0) with CH_3CN. The branching ratios are an average of at least six independent measurements under similar conditions with ±2σ error

Reference	Product Ion/Channel	BR
Wincel et al; (1988)	$CH_3CN^+ + N_2$	0.15
(SIFT technique)	$CH_2CN^+ + H + N_2$	0.65
	$CHCN^+ + H_2 + N_2$	0.20
Current Study (2011)	$CH_3CN^+ + N_2$	0.05 ± 0.01
(with 2σ)	$CH_2CN^+ + H + N_2$	0.95 ± 0.01
	$CHCN^+ + H_2 + N_2$	-

Let us now incline our discussion of our reported BRs in light of Titan's ionospheric chemistry and the associated N_2^+-induced ion-molecule reactions. It has been pointed out that nitriles in Titan's atmosphere are more abundantly formed at higher altitudes[174]. In these regions, N_2 is more frequently ionized and/or dissociated by the magnetospheric electrons from Saturn's rapidly rotating magnetosphere and EUV-irradiation than at the lower altitudes. This makes the determination of accurate BRs of N_2^+ ion-molecule reactions with the trace nitrile compounds such as CH_3CN very important as far as supporting the models is concerned. The high proton affinities of nitriles such a CH_3CN allows them to be effectively protonated by the ubiquitous protonated hydrocarbon ions (such as $C_2H_5^+$) in Titan's primitive, reducing ionosphere. Therefore, the accurate low temperature BRs determined in the current study, if incorporated in Titan's models, will assist in the accurate modeling of nitrile chemistry and give insights into the haze formation mechanisms.

5.3 Conclusions and Implications for Titan's atmosphere

The BRs of the reactions of state-prepared N_2^+ ion with CH_4, C_2H_2 and C_2H_4, the main minor hydrocarbon constituents of Titan's upper atmosphere, have been measured at a characteristic temperature of 45 ± 5K. The dominant reaction channels in the $N_2^+ + CH_4$ and $N_2^+ + C_2H_2$ reactions are the non-resonant dissociative CT while for the $N_2^+ + C_2H_2$ reaction, non-dissociative CT channel leading to the sole formation of $C_2H_2^+$ product ion is the only reaction channel. In the $N_2^+ + CH_4$ reaction, a branching ratio of 0.83:0.17 is obtained for the formation of CH_3^+ and CH_2^+ product ions, respectively. The absence of a non-dissociative CH_4^+ charge transfer channel suggest that the dominant process in this

reaction is a near-resonant CT process that is accompanied by simple C-H bond rupture of the nascent CH_4^+ ion. Results for the $N_2^+ + C_2H_4$ reaction indicate that $C_2H_3^+$ and $C_2H_3^+$ product ions are formed at a branching ratio of 0.74:0.26, respectively. The process associated with this observed branching is a simple capture process followed by a non-resonant dissociative CT. For the reaction involving N_2^+ with CH_3CN, a branching ration of 0.95:0.05 is obtained for the formation of CH_2CN^+ and CH_3CN^+ product ions, respectively. This BR overwhelmingly favors the formation of H- loss dissociative charge transfer channel in accordance with the statistical ground state dissociation of the cation. This present study represents the most reliable experimental data on the primary branching ratios of the main product channels in low temperature reaction of N_2^+ with CH_4, C_2H_2, and C_2H_4. This primary branching also gives a direct insight onto the dynamics associated with these ion-molecule reactions in Titan's rich ionospheric chemistry. The reported branching ratio measurements illustrates a new, promising modification of a VMIMS apparatus that allows for direct determination of branching ratios of state specific ion-molecule reactions at low temperatures prevalent in Titan's upper atmosphere.

REFERENCES

1. Atreya, S. K., The significance of trace constituents in the solar system. Faraday Disc. 2010, 147, 9-29.

2. De La Haye, V.; Waite Jr, J. H.; Cravens, T. E.; Robertson, I. P.; Lebonnois, S., Coupled ion and neutral rotating model of Titan's upper atmosphere. Icarus, 2008, 197, (1), 110-136.

3. Owen, T.; Niemann, H. B., The origin of Titan's atmosphere: some recent advances. Phil. Transac. Roy. Soc. Chem. 2009, 367, (1889), 607-615.

4. Vuitton, V.; Yelle, R. V.; McEwan, M. J., Ion chemistry and N-containing molecules in Titan's upper atmosphere. Icarus, 2007, 191, (2), 722-742.

5. Niemann, H. B.; Atreya, S. K.; Demick, J. E.; Gautier, D.; Haberman, J. A.; Harpold, D. N.; Kasprzak, W. T.; Lunine, J. I.; Owen, T. C.; Raulin, F., Composition of Titan's lower atmosphere and simple surface volatiles as measured by the Cassini-Huygens probe gas chromatograph mass spectrometer experiment. J. Geoph. Res.Planet. 2010, 115.

6. Meotner, M., Ion-Molecule Condensation Reactions- Mechanism for Organic Synthesis in Ionized Reducing atmospheres. Origins of Life and Evolution of the Biosphere, 1978, 9, (2), 115-131.

7. Neish, C. D.; Somogyi, A.; Smith, M. A., Titan's Primordial Soup: Formation of Amino Acids via Low-Temperature Hydrolysis of Tholins. Astrob. 2010, 10, (3), 337-347.

8. Owen, T. C.; Niemann, H.; Atreya, S.; Zolotov, M. Y., Between heaven and Earth: the exploration of Titan. Faraday Disc. 2006, 133, 387-391.

9. Lunine, J. I., Titan and habitable planets around M-dwarfs. Faraday Disc. 2010, 147, 405-418.

10. Owen, T., The composition and origin of Titan's atmosphere. Planet. Space Sci. 1982, 30, (8), 833-838.

11. Coustenis, A.; Atreya, S. K.; Balint, T.; Brown, R. H.; Dougherty, M. K.; Ferri, F.; Fulchignoni, M.; Gautier, D.; Gowen, R. A.; Griffith, C. A.; Gurvits, L. I.; Jaumann, R.; Langevin, Y.; Leese, M. R.; Lunine, J. I.; McKay, C. P.; Moussas, X.; Muller-Wodarg, I.; Neubauer, F.; Owen, T. C.; Raulin, F.; Sittler, E. C.; Sohl, F.; Sotin, C.; Tobie, G.; Tokano, T.; Turtle, E. P.; Wahlund, J. E.; Waite, J. H.; Baines, K. H.; Blamont, J.; Coates, A. J.; Dandouras, I.; Krimigis, T.; Lellouch, E.; Lorenz, R. D.; Morse, A.; Porco, C. C.; Hirtzig, M.; Saur, J.; Spilker, T.; Zarnecki, J. C.; Choi, E.; Achilleos, N.; Amils, R.; Annan, P.; Atkinson, D. H.; Benilan, Y.; Bertucci, C.; Bezard, B.; Bjoraker, G. L.; Blanc, M.; Boireau, L.; Bouman, J.; Cabane, M.; Capria, M. T.; Chassefiere, E.; Coll, P.; Combes, M.; Cooper, J. F.; Coradini, A.; Crary, F.; Cravens, T.; Daglis, I. A.; de Angelis, E.; de Bergh, C.; de Pater, I.; Dunford, C.; Durry, G.; Dutuit, O.; Fairbrother, D.; Flasar, F. M.; Fortes, A. D.; Frampton, R.; Fujimoto, M.; Galand, M.; Grasset, O.; Grott, M.; Haltigin, T.; Herique, A.; Hersant, F.; Hussmann, H.; Ip, W.; Johnson, R.; Kallio, E.; Kempf, S.; Knapmeyer, M.; Kofman, W.; Koop, R.; Kostiuk, T.; Krupp, N.; Kuppers, M.; Lammer, H.; Lara, L. M.; Lavvas, P.; Le Mouelic, S.; Lebonnois, S.; Ledvina, S.; Li, J.; Livengood, T. A.; Lopes, R. M.; Lopez-Moreno, J. J.; Luz, D.; Mahaffy, P. R.; Mall, U.; Martinez-Frias, J.; Marty, B.; McCord, T.; Salvan, C.; Milillo, A.; Mitchell, D. G.; Modolo, R.; Mousis, O.; Nakamura, M.; Neish, C. D.; Nixon, C. A.; Mvondo, D.; Orton, G.; Paetzold, M.; Pitman, J.; Pogrebenko, S.; Pollard,

W.; Prieto-Ballesteros, O.; Rannou, P.; Reh, K.; Richter, L.; Robb, F. T.; Rodrigo, R.; Rodriguez, S.; Romani, P.; Bermejo, M.; Sarris, E. T.; Schenk, P.; Schmitt, B.; Schmitz, N.; Schulze-Makuch, D.; Schwingenschuh, K.; Selig, A.; Sicardy, B.; Soderblom, L.; Spilker, L. J.; Stam, D.; Steele, A.; Stephan, K.; Strobel, D. F.; Szego, K.; Szopa, C.; Thissen, R.; Tomasko, M. G.; Toublanc, D.; Vali, H.; Vardavas, I.; Vuitton, V.; West, R. A.; Yelle, R.; Young, E. F., TandEM: Titan and Enceladus mission. Exprerim. Astron. 2009, 23, (3), 893-946.

12. Barr, A. C.; Canup, R. M., Origin of the Ganymede-Callisto dichotomy by impacts during the late heavy bombardment. Nature Geosci. 2010, 3, (3), 164-167.

13. Bezard, B., Composition and chemistry of Titan's stratosphere. Phil. Transac. Roy. Soc. Chem. 2009, 367, (1889), 683-695.

14. Raulin, F.; Owen, T., Organic chemistry and exobiology on Titan. Space Sci. Rev. 2002, 104, (1-2), 377-394.

15. Atreya, S. K.; Adams, E. Y.; Niemann, H. B.; Demick-Montelara, J. E.; Owen, T. C.; Fulchignoni, M.; Ferri, F.; Wilson, E. H., Titan's methane cycle. Planet. Space Sci. 2006, 54, (12), 1177-1187.

16. Waite, J. H.; Niemann, H.; Yelle, R. V.; Kasprzak, W. T.; Cravens, T. E.; Luhmann, J. G.; McNutt, R. L.; Ip, W. H.; Gell, D.; De La Haye, V.; Muller-Wordag, I.; Magee, B.; Borggren, N.; Ledvina, S.; Fletcher, G.; Walter, E.; Miller, R.; Scherer, S.; Thorpe, R.; Xu, J.; Block, B.; Arnett, K., Ion Neutral Mass Spectrometer results from the first flyby of Titan. Science, 2005, 308, (5724), 982-986.

17. Lebreton, J. P.; Coustenis, A.; Lunine, J.; Raulin, F.; Owen, T.; Strobel, D., Results from the Huygens probe on Titan. Astr. Astrophys. Rev. 2009, 17, (2), 149-179.

18. Lavvas, P. P.; Coustenis, A.; Vardavas, I. M., Coupling photochemistry with haze formation in Titan's atmosphere, part I: Model description. Plan. Space Sci. 2008, 56, (1), 27-66.

19. Cravens, T. E.; Robertson, I. P.; Waite, J. H.; Yelle, R. V.; Vuitton, V.; Coates, A. J.; Wahlund, J. E.; Agren, K.; Richard, M. S.; La Haye, V.; Wellbrock, A.; Neubauer, F. M., Model-data comparisons for Titan's nightside ionosphere. Icarus, 2009, 199, (1), 174-188.

20. Morente, J. A.; Molina-Cuberos, G. J.; Portí, J. A.; Schwingenschuh, K.; Besser, B. P., A study of the propagation of electromagnetic waves in Titan's atmosphere with the TLM numerical method. Icarus, 2003, 162, (2), 374-384.

21. Pintassilgo, C. D.; Loureiro, J., Kinetic study of a N_2-CH_4 afterglow plasma for production of N-containing hydrocarbon species of Titan's atmosphere. Advanc. Space Res. 2010, 46, (5), 657-671.

22. Navarro-Gonzalez, R.; Ramirez, S. I.; de la Rosa, J. G.; Coll, P.; Raulin, F., Production of hydrocarbons and nitriles by electrical processes in Titan's atmosphere. Space Life Sciences: Life in the Solar System: Prebiotic Chemistry, Chirality and Space Biology 2001, 27, (2), 271-282.

23. Thissen, R.; Vuitton, V.; Lavvas, P.; Lemaire, J.; Dehon, C.; Dutuit, O.; Smith, M. A.; Turchini, S.; Catone, D.; Yelle, R. V.; Pernot, P.; Somogyi, A.; Coreno, M., Laboratory Studies of Molecular Growth in the Titan Ionosphere. J. Phys. Chem. A. 2009, 113, (42), 11211-11220.

24. Imanaka, H.; Smith, M. A., Formation of nitrogenated organic aerosols in the Titan upper atmosphere. Proc. Nat. Aca. Sci. 2010, 107, (28), 12423-12428.

25. Vuitton, V.; Bonnet, J. Y.; Frisari, M.; Thissen, R.; Quirico, E.; Dutuit, O.; Schmitt, B.; Le Roy, L.; Fray, N.; Cottin, H.; Sciamma-O'Brien, E.; Carrasco, N.; Szopa, C., Very high resolution mass spectrometry of HCN polymers and tholins. Faraday Disc. 2010, 147, 495-508.

26. Faure, A.; Vuitton, V.; Thissen, R.; Wiesenfeld, L.; Dutuit, O., Fast ion-molecule reactions in planetary atmospheres: a semiempirical capture approach. Faraday Disc. 2010, 147, 337-348.

27. Coustenis, A., Formation and evolution of Titan's atmosphere. Space Sci. Rev. 2005, 116, (1-2), 171-184.

28. Owen, T., The Contributions of Comets to Planets, Atmospheres, and Life: Insights from Cassini-Huygens, Galileo, Giotto, and Inner Planet Missions. Space Sci. Rev. 2008, 138, (1), 301-316.

29. Canfield, D. E.; Glazer, A. N.; Falkowski, P. G., The Evolution and Future of Earth's Nitrogen Cycle. Science, 2010, 330, (6001), 192-196.

30. Vinatier, S.; Bézard, B.; Nixon, C. A., The Titan $^{14}N/^{15}N$ and $^{12}C/^{13}C$ isotopic ratios in HCN from Cassini/CIRS. Icarus, 2007, 191, (2), 712-721.

31. Perri, F.; Cameron, A. G. W., Hydrodynamic instability of the solar nebula in the presence of a planetary core. Icarus, 1974, 22, (4), 416-425.

32. McCord, T. B.; Hansen, G. B.; Buratti, B. J.; Clark, R. N.; Cruikshank, D. P.; D'Aversa, E.; Griffith, C. A.; Baines, E. K. H.; Brown, R. H.; Dalle Ore, C. M.; Filacchione, G.; Formisano, V.; Hibbitts, C. A.; Jaumann, R.; Lunine, J. I.; Nelson, R. M.; Sotin, C., Composition of Titan's surface from Cassini VIMS. Plan. Space Sci. 2006, 54, (15), 1524-1539.

33. Trigo-Rodriguez, J. M.; Javier Martín-Torres, F., Clues on the importance of comets in the origin and evolution of the atmospheres of Titan and Earth. Plan. Space Sci. In Press, 2011, Corrected Proof.

34. Mancinelli, R. L.; McKay, C. P., The evolution of nitrogen cycling. Origins of Life and Evolution of Biospheres, 1988, 18, (4), 311-325.

35. McKay, C. P.; Scattergood, T. W.; Pollack, J. B.; Borucki, W. J.; Ghyseghem, H. T. V., High-temperature shock formation of N_2 and organics on primordial Titan. Nature 1988, 332, (6164), 520-522.

36. Griffith, C. A.; Zahnle, K., Influx of cometary volatiles to planetary moons: The atmospheres of 1000 possible Titans. J. Geophys. Res. 1995, 100, (E8), 16907-16922.

37. Bar-Nun, A.; Notesco, G.; Owen, T., Trapping of N_2, CO and Ar in amorphous ice--Application to comets. Icarus, 2007, 190, (2), 655-659.

38. Sekine, Y.; Genda, H.; Sugita, S.; Kadono, T.; Matsui, T., Replacement and late formation of atmospheric N_2 on undifferentiated Titan by impacts. Nature Geosci. 2011, 4, (6), 359-362.

39. Jennings, D. E.; Romani, P. N.; Bjoraker, G. L.; Sada, P. V.; Nixon, C. A.; Lunsford, A. W.; Boyle, R. J.; Hesman, B. E.; McCabe, G. H., C12/C13 Ratio in Ethane on Titan and Implications for Methane's Replenishment. J. Phys. Chem. A. 2009, 113, (42), 11101-11106.

40. Abbas, M. M.; Kandadi, H.; LeClair, A.; Achterberg, R. K.; Flasar, F. M.; Kunde, V. G.; Conrath, B. J.; Bjoraker, G.; Brasunas, J.; Carlson, R.; Jennings, D. E.; Segura, M., D/H Ratio of Titan from Observations of the Cassini/Composite Infrared Spetrometer. Astrophy. J. 2010, 708, (1), 342-353.

41. Lavvas, P.; Yelle, R. V.; Vuitton, V., The detached haze layer in Titan's mesosphere. Icarus, 2009, 201, (2), 626-633.

42. Wilson, E. H.; Atreya, S. K., Chemical sources of haze formation in Titan's atmosphere. Planet. Space Sci. 2003, 51, (14-15), 1017-1033.

43. Wilson, E. H.; Atreya, S. K.; Coustenis, A., Mechanisms for the formation of benzene in the atmosphere of Titan. J. Geoph. Res.Planet. 2003, 108, (E2).

44. Wilson, E. H.; Atreya, S. K., Current state of modeling the photochemistry of Titan's mutually dependent atmosphere and ionosphere. J. Geoph. Res.Planet. 2004, 109, (E6).

45. Cui, J.; Yelle, R. V.; Vuitton, V.; Waite, J. H.; Kasprzak, W. T.; Gell, D. A.; Niemann, H. B.; Muller-Wodarg, I. C. F.; Borggren, N.; Fletcher, G. G.; Patrick, E. L.; Raaen, E.; Magee, B. A., Analysis of Titan's neutral upper atmosphere from Cassini Ion Neutral Mass Spectrometer measurements. Icarus, 2009, 200, (2), 581-615.

46. Vuitton, V.; Yelle, R. V.; Lavvas, P., Composition and chemistry of Titan's thermosphere and ionosphere. Phil. Transac. Roy. Soc. Chem. 2009, 367, (1889), 729-741.

47. Romanzin, C.; Arzoumanian, E.; Es-sebbar, E.; Jolly, A.; Perrier, S.; Gazeau, M. C.; Benilan, Y., Combined experimental and theoretical studies on methane photolysis at 121 6 and 248 nm-implications on a program of laboratory simulations of Titan's atmosphere. Plan. Space Sci. 2010, 58, (13), 1748-1757.

48. Gu, X.; Kim, Y. S.; Kaiser, R. I.; Mebel, A. M.; Liang, M. C.; Yung, Y. L., Chemical dynamics of triacetylene formation and implications to the synthesis of

polyynes in Titan's atmosphere. Proc. Natl. Acad. Sci. U. S. A. 2009, 106, (38), 16078-16083.

49. Huang, C. S.; Zhang, F. T.; Kaiser, R. I.; Kislov, V. V.; Mebel, A. M.; Silva, R.; Gichuhi, W. K.; Suits, A. G., Photodissociation of the Diacetylene Dimer and Implications for Hydrocarbon Growth in Titan's Atmosphere. Astrophy. J. 2010, 714, (2), 1249-1255.

50. Lewis, G. R.; Arridge, C. S.; Linder, D. R.; Gilbert, L. K.; Kataria, D. O.; Coates, A. J.; Persoon, A.; Collinson, G. A.; André, N.; Schippers, P.; Wahlund, J.; Morooka, M.; Jones, G. H.; Rymer, A. M.; Young, D. T.; Mitchell, D. G.; Lagg, A.; Livi, S. A., The calibration of the Cassini-Huygens CAPS Electron Spectrometer. Planet. Space Sci. 2010, 58, (3), 427-436.

51. Wahlund, J. E.; Galand, M.; Muller-Wodarg, I.; Cui, J.; Yelle, R. V.; Crary, F. J.; Mandt, K.; Magee, B.; Waite, J. H.; Young, D. T.; Coates, A. J.; Garnier, P.; Agren, K.; Andre, M.; Eriksson, A. I.; Cravens, T. E.; Vuitton, V.; Gurnett, D. A.; Kurth, W. S., On the amount of heavy molecular ions in Titan's ionosphere. Planet. Space Sci. 2009, 57, (14-15), 1857-1865.

52. Galand, M.; Yelle, R.; Cui, J.; Wahlund, J. E.; Vuitton, V.; Wellbrock, A.; Coates, A., Ionization sources in Titan's deep ionosphere. J. Geophys. Res. Spac. Phys. 2010, 115.

53. Sittler, E. C.; Johnson, R. E.; Smith, H. T.; Richardson, J. D.; Jurac, S.; Moore, M.; Cooper, J. F.; Mauk, B. H.; Michael, M.; Paranicas, C.; Armstrong, T. P.; Tsurutani, B., Energetic nitrogen ions within the inner magnetosphere of Saturn. J. Geophys. Res. Spac. Phys. 2006, 111, (A9).

54. Carrasco, N.; Alcaraz, C.; Dutuit, O.; Plessis, S.; Thissen, R.; Vuitton, V.; Yelle, R.; Pernot, P., Sensitivity of a Titan ionospheric model to the ion-molecule reaction parameters. Planet. Space Sci. 2008, 56, (12), 1644-1657.

55. Carrasco, N.; Plessis, S.; Dobrijevic, M.; Pernot, P., Toward a Reduction of the Bimolecular Reaction Model for Titan's Ionosphere. Int. J. Chem. Kinet. 2008, 40, (11), 699-709.

56. Townsend, D.; Minitti, M. P.; Suits, A. G., DC slice imaging. Abstr. Pap. Am. Chem. Soc. 2003, 225, U438-U439.

57. Leskiw, B. D.; Kim, M. H.; Hall, G. E.; Suits, A. G., Reflectron velocity map ion imaging. Rev. Sci. Instrum. 2005, 76, 104101.

58. Townsend, D.; Minitti, M. P.; Suits, A. G., Direct current slice imaging. Rev. Sci. Instrum. 2003, 74, (4), 2530-2539.

59. Wiley, W. C.; McLaren, I. H., Time-of-flight mass spectrometer with improved resolution (Reprinted from Review of Scientific Instruments vol 26, pg 1150, 1995). J. Mass Spectrom. 1997, 32, (1), 4-11.

60. Hanisco, T. F.; Yan, C.; Kummel, A. C., Resonantly Enhanced Multiphoton Ionization of nitrogen a"1-SIGMA-g+ (v' = v").rarw. X1-SIGMA.g+ (v" = 0, 1, 2) .2. Alignment and Orientation Measurements. J Phys. Chem. 1992, 96, (7), 2982-2993.

61. Hawley, M.; Mazely, T. L.; Randeniya, L. K.; Smith, R. S.; Zeng, X. K.; Smith, M. A., A Free Jet Flow Reactor for Ion Molecule Reaction Studies at Very Low Energies. Int J. Mass Spectrom. 1990, 97, (1), 55-86.

62. Rowe, B. R.; Marquette, J. B., Cresu Studies of Ion Molecule Reactions. Int. J. Mass Spectrom. 1987, 80, 239-254.

63. Hallock, A. J.; Matthews, C. M.; Balzer, F.; Zare, R. N., N_2 product internal-state distributions for the steady-state reactions of NO with H_2 and NH_3 on the Pt (100) surface. J. Phys. Chem. B, 2001, 105, (37), 8725-8728.

64. Mori, H.; Niimi, T.; Akiyama, I.; Tsuzuki, T., Experimental detection of rotational non-Boltzmann distribution in supersonic free molecular nitrogen flows. Phys Fluids, 2005, 17, (11), -.

65. Kato, S.; Bierbaum, V. M.; Leone, S. R., Laser Fluorescence and Mass-Spectrometric Measurements of Vibrational-Relaxation of N_2^+(v) with He, Ne, Ar, Kr, and Xe. nt. J. Mass Spectrom. Ion Processes, 1995, 150, 469-486.

66. Kato, S.; deGouw, J. A.; Lin, C. D.; Bierbaum, V. M.; Leone, S. R., Vibrational enhancement of the charge transfer rate constant of N_2^+(v=0-4) with Kr at thermal energies. J. Chem. Phys. 1996, 105, (13), 5455-5466.

67. Kato, S.; deGouw, J. A.; Lin, C. D.; Bierbaum, V. M.; Leone, S. R., Charge-transfer rate constants for N_2^+ (v=0-4) with Ar at thermal energies. Chem. Phys. Lett. 1996, 256, (3), 305-311.

68. Kato, S.; Frost, M. J.; Bierbaum, V. M.; Leone, S. R., Vibrational Specificity for Charge-Transfer Versus Deactivation in N_2^+ (v=0, 1, 2) + Ar and O_2 Reactions. Can. J. Chem. 1994, 72, (3), 625-636.

69. Pollard, J. E.; Johnson, L. K.; Lichtin, D. A.; Cohen, R. B., State-Selected Reactive Scattering .1. $H_2^+ + H_2 \rightarrow H_3^+ + H$. J. Chem. Phys. 1991, 95, (7), 4877-4893.

70. Glenewinkel-Meyer, T.; Gerlich, D., Single and merged beam studies of the reaction H_2^+(v= 0,1;j= 0,4) + $H_2 \rightarrow H_3^+ + H$. Israel J. Chem. 1997, 37, (4), 343-352.

71. Degouw, J. A.; Ding, L. N.; Frost, M. J.; Kato, S.; Bierbaum, V. M.; Leone, S. R., Vibrational-Energy Dependence of the Reaction $N_2^+(v) + H_2 \rightarrow N_2H^+ + H$ at Thermal Energies. Chem. Phys. Lett. 1995, 240, (4), 362-368.

72. Uiterwaal, C. J. G. J.; Vaneck, J.; Niehaus, A., State-Selected Ion-Molecule Reactions - Charge-Transfer and Atomic Rearrangement Processes in Thermal-Energy Collisions of $H_2^+(X;V) + N_2$ and of N_2^+ (X, A; V) + H_2. J. Chem. Phys. 1995, 102, (2), 744-753.

73. Randeniya, L. K.; Smith, M. A., Gas-Phase Reaction-Rates of N_2^+ with CH_4, O_2, and Normal-H_2 at Very Low-Temperatures. J. Chem. Phys. 1991, 94, (1), 351-356.

74. Wilson, E. H.; Atreya, S. K., Titan's carbon budget and the case of the missing ethane. J. Phys. Chem. A 2009, 113, (42), 11221-6.

75. Coustenis, A.; Bezard, B.; Gautier, D.; Marten, A.; Samuelson, R., Titan's Atmosphere from Voyage Infrared Observations..3. Verticle Distributions of Hydrocarbons and Nitriles near Titan's North Pole. Icarus 1991, 89, (1), 152-167.

76. Yung, Y. L.; Allen, M.; Pinto, J. P., Photochemistry of the atmosphere of Titan: comparison between model and observations. The Astrophysical journal. Supplement series, 1984, 55, (3), 465-506.

77. Arrington, C. A., Aromatic Ring-Forming Reactions of Metastable Diacetylene with 1,3-Butadiene. The journal of physical chemistry. A, Molecules, spectroscopy, kinetics, environment, & general theory, 1998, 102, (19), 3315-3322.

78. Glicker, S.; Okabe, H., Photochemistry of Diacetylene. J. Phys. Chem. 1987, 91, (2), 437-440.

79. Silva, R.; Gichuhi, W. K.; Huang, C.; Doyle, M. B.; Kislov, V. V.; Mebel, A. M.; Suits, A. G., H elimination and metastable lifetimes in the UV photoexcitation of diacetylene. Proc. National Acad. Sci. U.S.A 2008, 105, (35), 12713-12718.

80. Arrington, C. A.; Ramos, C.; Robinson, A. D.; Zwier, T. S., Ultraviolet Photochemistry of Diacetylene with Alkynes and Alkenes: Spectroscopic Characterization of the Products. J. Phys. Chem. A, 1999, 103, (10), 1294-1299.

81. Bandy, R. E.; Lakshminarayan, C.; Frost, R. K.; Zwier, T. S., Direct Detection of C_4H_2 Photochemical Products: Possible Routes to Complex Hydrocarbons in Planetary Atmospheres. Science, 1992, 258, (5088), 1630-1633.

82. Bandy, R. E.; Lakshminarayan, C.; Frost, R. K.; Zwier, T. S., The ultraviolet photochemistry of diacetylene: Direct detection of primary products of the metastable C_4H_2*+ C_4H_2 reaction. J. Chem. Phys. 1993, 98, (7), 5362-5374.

83. Frost, R. K.; Zavarin, G. S.; Zwier, T. S., Ultraviolet Photochemistry of Diacetylene-Metastable C_4H_2* + C_2H_2 reaction with Helium and nitrogen. J. Phys. Chem. 1995, 99, (23), 9408-9415.

84. Armitage, J. B., 373. Researches on acetylenic compounds. Part XXXVII. The synthesis of conjugated tetra-acetylenic compounds. J. Chem. Soc. 1952, 2014.

85. Gu, X. B.; Guo, Y.; Mebel, A. M.; Kaiser, R. I., Chemical dynamics of the formation of the 1,3-butadiynyl radical ($C_4H(X^2\Sigma^+)$) and its isotopomers. J. Phy. Chem. A 2006, 110, (39), 11265-11278.

86. Huang, C. S.; Li, W.; Kim, M. H.; Suits, A. G., Two-color reduced-Doppler ion imaging. J. Chem. Phys. 2006, 125, (12).

87. Stanton, J. F.; Bartlett, R. J., The Equation of motion Coupled-cluster Method-A systematic Biorthogonal approach to molecular-excitation energies, Transition-probabilities and Excited-state properties. J. Chem. Phys. 1993, 98, (9), 7029-7039.

88. Rico, R. J.; Headgordon, M., Single Reference Theories of molecular Excited-states with Single and Double Substitutions. Chem. Phys. Lett. 1993, 213, (3-4), 224-232.

89. Dunning, T. H., Gaussian-Basis Sets for use in Correlated Molecular Calculations.1. The atoms Boron Through Neon and Hydrogen. J. Chem. Phys. 1989, 90, (2), 1007-1023.

90. Hopkins, B. W.; ElSohly, A. M.; Tschumper, G. S., Reliable structures and energetics for two new delocalized π. . . π prototypes: cyanogen dimer and diacetylene dimer. Phys. Chem. Chem. Phys. 2007, 9, (13), 1550-1558.

91. Knowles, P. J.; Werner, H. J., An efficient method for the evaluation of coupling coefficients in configuration-interaction calculations. Chem. Phys. Lett. 1988, 145, (6), 514-522.

92. Knowles, P. J.; Werner, H. J., An efficient second order MC SCF for long configuration expansions. Chem. Phys. Lett. 1985, 115, (3), 259-267.

93. Kawasaki, M.; Sugita, A.; Ramos, C.; Matsumi, Y.; Tachikawa, H., Photodissociation of water dimer at 205 nm. J. Phys. Chem. A 2004, 108, (39), 8119-8124.

94. Mebel, A. M.; Kislov, V. V.; Kaiser, R. I., Ab initio/Rice-Ramsperger-Kassel-Marcus study of the singlet C_4H_4 potential energy surface and of the reactions of $C_2(X\ ^1\Sigma g^+)$ with $C_4H_4(X^1A_{1g})$ and $C(^1D)$ with C_3H_4 (allene and methylacetylene). J. Chem. Phys. 2006, 125, (13).

95. Chastaing, D.; Underwood, J.; Wittig, C., Intracluster superelastic scattering via sequential photodissociation in small HI clusters. J. Chem. Phys. 2003, 119, (2), 928-938.

96. Klippenstein, S. J.; Miller, J. A., The addition of hydrogen atoms to diacetylene and the heats of formation of *i*-C_4H_3 and *n*-C_4H_3. J. Phys. Chem. A 2005, 109, (19), 4285-4295.

97. Stavish, L.; Fondren, L. D.; Adams, N. G., Reactions of N^+ and N_2^+ with several cyclic molecules studied using a selected ion flow tube. Int. J. Mass Spectrom. Ion Processes 2009, 281, (3), 103-107.

98. Singh, P. C.; Shen, L.; Zhou, J.; Schlegel, H. B.; Suits, A. G., Photodissociation Dynamics of Methylamine Cation and its Relevance to Titan's Ionosphere. Astrophys. J. 2010, 710, (1), 112-116.

99. Imanaka, H.; Smith, M. A., EUV Photochemical Production of Unsaturated Hydrocarbons: Implications. to EUV Photochemistry in Titan and Jovian Planets. J. Phys. Chem.A 2009, 113, (42), 11187-11194.

100. Imanaka, H.; Smith, M. A., From the Cover: Formation of nitrogenated organic aerosols in the Titan upper atmosphere. Proc. Natl. Acad. Sci. U. S. A. 2010, 107, (28), 12423-8.

101. Garnier, P.; Wahlund, J. E.; Rosenqvist, L.; Modolo, R.; Agren, K.; Sergis, N.; Canu, P.; Andre, M.; Gurnett, D. A.; Kurth, W. S.; Krimigis, S. M.; Coates, A.; Dougherty, M.; Waite, J. H., Titan's ionosphere in the magnetosheath: Cassini RPWS results during the T32 flyby. Annales Geophysicae 2009, 27, (11), 4257-4272.

102. Waite, J. H., Jr.; Young, D. T.; Cravens, T. E.; Coates, A. J.; Crary, F. J.; Magee, B.; Westlake, J., The Process of Tholin Formation in Titan's Upper Atmosphere. Science 2007, 316, (5826), 870-875.

103. Robertson, I. P.; Cravens, T. E.; Waite, J. H.; Yelle, R. V.; Vuitton, V.; Coates, A. J.; Wahlund, J. E.; Agren, K.; Mandt, K.; Magee, B.; Richard, M. S.; Fattig, E., Structure of Titan's ionosphere: Model comparisons with Cassini data. Planet. Space Sci. 2009, 57, (14-15), 1834-1846.

104. Leclerc, J. C.; Lorquet, J. C., The electronic structure of ionized molecules. VI. n-Alkylamines. J. Phys. Chem., 1967, 71, (4), 787-791.

105. Hubin-Franskin, M. J.; Delwiche, J.; Giuliani, A.; Ska, M. P.; Motte-Tollet, F.; Walker, I. C.; Mason, N. J.; Gingell, J. M.; Jones, N. C., Electronic excitation and optical cross sections of methylamine and ethylamine in the UV-VUV spectral region. J. Chem. Phys. 2002, 116, (21), 9261-9268.

106. Wei, J.; Zhang, B.; Fang, L.; Zhang, L. D.; Cai, J. Y., REMPI time-of-flight mass spectra of C_2H_7N isomers. Opt. Commun. 1998, 156, (4-6), 331-336.

107. Bodi, A.; Kercher, J. P.; Bond, C.; Meteesatien, P.; Sztaray, B.; Baer, T., Photoion photoelectron coincidence spectroscopy of primary amines RCH_2NH_2 (R=H, CH_3, C_2H_5, C_3H_7, i-C_3H_7): Alkylamine and alkyl radical heats of formation by isodesmic reaction networks. J. Phys. Chem. A, 2006, 110, (50), 13425-13433.

108. Traeger, J. C.; Harvey, Z. A., Heat of Formation for the $CH_3CHNH_2^+$ Cation by Photoionization Mass Spectrometryâ€ J. Phys. Chem. A 2006, 110, (27), 8542-8547.

109. Eppink, A. T. J. B.; Parker, D. H., Velocity map imaging of ions and electrons using electrostatic lenses: Application in photoelectron and photofragment ion imaging of molecular oxygen. Rev. Sci. Instrum. 1997, 68, (9), 3477-3484.

110. Leskiw, B. D.; Kim, M. H.; Hall, G. E.; Suits, A. G., Reflectron velocity map ion imaging. Rev. Sci. Instrum. 2005, 76, (10), 104101.

111. Becke, A. D., Density-functional thermochemistry. III. The role of exact exchange. J. Phys. Chem. 1993, 98, (7), 5648-5652.

112. Lee, C.; Yang, W.; Parr, R. G., Development of the Colle-Salvetti correlation-energy formula into a functional of the electron density. Phys. Rev. B 1988, 37, (2), 785.

113. Frisch, M. J. T., G. W.; Schlegel, H. B.; Scuseria, G. E.; Robb, M. A.; Cheeseman, J. R.; Zakrzewski, V. G.; Montgomery, J. A.; Stratmann, R. E.; Burant, J. C.; Dapprich, S.; Millam, J. M.; Daniels, R. E.; Kudin, K. N.; Strain, M. C.; Farkas, O.; Tomasi, J.; Barone, V.; Cossi, M.; Cammi, R.; Mennucci, B.; Pomelli, C.; Adamo, C.; Clifford, S.; Ochterski, J.; Petersson, G. A.; Ayala, P. Y.; Cui, Q.; Morokuma, K.; Salvador, P.; Dannenberg, J. J.; Malick, D. K.; Rabuck, A. D.; Raghavachari, K.; Foresman, J. B.; Cioslowski, J.; Ortiz, J. V.; Baboul, A. G.; Stefanov, B. B.; Liu, G.; Liashenko, A.; Piskorz, P.; Komaromi, I.; Gomperts, R.; Martin, R. L.; Fox, D. J.; Keith, T.; Al-Laham, M. A.; Peng, C. Y.; Nanayakkara, A.; Challacombe, M.; Gill, P. M. W.; Johnson, B.; Chen, W.; Wong, M. W.; Andres, J. L.; Gonzalez, C.; M. Head-Gordon, M.; Replogle, E. S.; Pople, J. A Gaussian 98, revision A.11; Gaussian, Inc: Pittsburgh, PA, 2001.

114. Scuseria, G. E.; Janssen, C. L.; III, H. F. S., An efficient reformulation of the closed-shell coupled cluster single and double excitation (CCSD) equations. J. Chem. Phys. 1988, 89, (12), 7382-7387.

115. Scuseria, G. E.; III, H. F. S., Is coupled cluster singles and doubles (CCSD) more computationally intensive than quadratic configuration interaction (QCISD) J. Chem. Phys. 1989, 90, (7), 3700-3703.

116. Pople, J. A.; Head-Gordon, M.; Raghavachari, K., Quadratic configuration interaction. A general technique for determining electron correlation energies. J. Chem. Phys. 1987, 87, (10), 5968-5975.

117. III, G. D. P.; Bartlett, R. J., A full coupled-cluster singles and doubles model: The inclusion of disconnected triples. J. Chem. Phys. 1982, 76, (4), 1910-1918.

118. Thom H. Dunning, J., Gaussian basis sets for use in correlated molecular calculations. I. The atoms boron through neon and hydrogen. J. Chem. Phys. 1989, 90, (2), 1007-1023.

119. Peterson, K. A.; Dunning, T. H., Intrinsic Errors in Several ab Initio Methods: The Dissociation Energy of N_2. J. Phys. Chem., 1995, 99, (12), 3898-3901.

120. MOLPRO, A package of ab initio programs designed by Werner, H.-J. a. K., P. J.; Amos, R. D.; Bernhardsson, A.; Berning, A.; Celani, P.; Cooper, D. L.; Deegan, M. J. O.; Dobbyn, A. J.; Eckert, F.; Hampel, C.; Hetzer, G.; Knowles, P. J.; Korona, T.; Lindh, R.; Lloyd, A. W.; McNicholas, S. J.; Manby, F. R.; Meyer, W.; Mura, M. E.; Nicklass, A.; Palmieri, P.; Pitzer, R.; Rauhut, G.; Schutz, M.; Schumann, U.; Stoll, H.; Stone, A. J.; Tarroni, R.; Thorsteinsson, T.; Werner, H.-J.

121. Streibel, T.; Hafner, K.; Mühlberger, F.; Adam, T.; Zimmermann, R., Resonance-Enhanced Multiphoton Ionization Time-of-Flight Mass Spectrometry for Detection of Nitrogen Containing Aliphatic and Aromatic Compounds: Resonance-Enhanced Multiphoton Ionization Spectroscopic Investigation and On-Line Analytical Application. Appl. Spectrosc. 2006, 60, (1), 72-79.

122. Andrews, S. R.; Parry, D. E.; Harris, F. M., Combined experimental and computational study of the double ionization of ethylamine, propylamine and butylamine to triplet electronic states of their dications. J. Mass Spectrom. 1995, 30, (12), 1694-1700.

123. Bouma, W. J.; Dawes, J. M.; Radom, L., The methylamine radical cation and its stable isomer the methylenammonium radical cation Org. Mass Spectrom. 1983, 18, (1), 12-15.

124. Krier, C.; Lorquet, J. C.; Berlingin, A., The electronic structure of ionised molecules - VIII: Ethylamine. Org. Mass Spectrom. 1974, 8, (1), 387-401.

125. Gridelet, E.; Dehareng, D.; Locht, R.; Lorquet, A. J.; Lorquet, J. C.; Leyh, B., Ground and Excited State Dissociation Dynamics of Ionized 1,1-Difluoroethene. J. Phys. Chem. A 2005, 109, (37), 8225-8235.

126. Choi, T. H.; Park, S. T.; Kim, M. S., Theoretical and experimental studies of the dissociation dynamics of methaniminium cation, $CH_2NH_2^+ \rightarrow CHNH^+ + H_2$: Reaction path bifurcation. J. Chem. Phys. 2001, 114, (14), 6051-6057.

127. Ng, C.-Y., State-Selected and State-to-State Ion–Molecule Reaction Dynamics. The J. Phys. Chem. A 2002, 106, (25), 5953-5966.

128. Farrar, J. M.; Lee, Y. T., Chemical Dynamics. Ann. Rev. Phys. Chem. 1974, 25, (1), 357-386.

129. Boyle, J. M.; Uselman, B. W.; Liu, J.; Anderson, S. L., Vibrational effects on the reaction of NO_2^+ with C_2H_2: Effects of bending and bending angular momentum. The J. Chem. Phys. 2008, 128, (11), 114304.

130. Dressler, R. A.; Chiu, Y.; Levandier, D. J.; Tang, X. N.; Hou, Y.; Chang, C.; Houchins, C.; Xu, H.; Ng, C.-Y., The study of state-selected ion-molecule reactions using the vacuum ultraviolet pulsed field ionization-photoion technique. J. Chem. Phys. 2006, 125, (13), 132306.

131. Nicolas, C.; Torrents, R.; Gerlich, D., Integral and differential cross section measurements at low collision energies for the $N_2^+ + CH_4$ reactions. J. Chem. Phys. 2003, 118, (6), 2723-2730.

132. Qian, X.-M.; Zhang, T.; Chang, C.; Wang, P.; Ng, C. Y.; Chiu, Y.-H.; Levandier, D. J.; Miller, J. S.; Dressler, R. A.; Baer, T.; Peterka, D. S., High-resolution state-selected ion-molecule reaction studies using pulsed field ionization photoelectron-secondary ion coincidence method. Rev. Sci. Instrum. 2003, 74, (9), 4096-4109.

133. Anicich, V. G.; Wilson, P.; McEwan, M. J., A SIFT ion-molecule study of some reactions in Titan's atmosphere. Reactions of N^+, N_2^+ and HCN^+ with CH_4, C_2H_2, and C_2H_4. J Am. Soc. Mass. Spectr. 2004, 15, (8), 1148-1155.

134. Anicich, V. G.; McEwan, M. J., Ion-molecule chemistry in Titan's ionosphere. Planet. Space Sci. 1997, 45, (8), 897-921.

135. Balucani, N.; Asvany, O.; Osamura, Y.; Huang, L. C. L.; Lee, Y. T.; Kaiser, R. I., Laboratory investigation on the formation of unsaturated nitriles in Titan's atmosphere. Plan. Space Sci. 2000, 48, (5), 447-462.

136. Kaiser, R. I.; Ochsenfeld, C.; Head-Gordon, M.; Lee, Y. T.; Suits, A. G., A Combined Experimental and Theoretical Study on the Formation of Interstellar C_3H Isomers. Science, 1996, 274, (5292), 1508-1511.

137. Sims, I. R.; Smith, I. W. M., Rate constants for the radical-radical reaction between CN and O_2 at temperatures down to 99 K. Chem. Phys. Lett. 1988, 151, (6), 481-484.

138. Smith, I. W. M., Reactions at very low temperatures: Gas kinetics at a new frontier. Angew Chem. Int. Edit. 2006, 45, (18), 2842-2861.

139. Wilson, E. H.; Atreya, S. K., Chemical sources of haze formation in Titan's atmosphere. Planet. Space Sci. 2003, 51, (14-15), 1017-1033.

140. Yelle, R. V.; Borggren, N.; de la Haye, V.; Kasprzak, W. T.; Niemann, H. B.; Müller-Wodarg, I.; Waite, J. J. H., The vertical structure of Titan's upper atmosphere from Cassini Ion Neutral Mass Spectrometer measurements. Icarus 2006, 182, (2), 567-576.

141. McEwan, M. J.; Anicich, V. G., Titan's ion chemistry: A laboratory perspective. Mass. Spectrom. Rev. 2007, 26, (2), 281-319.

142. McEwan, M. J.; Scott, G. B. I.; Anicich, V. G., Ion-molecule reactions relevant to Titan's ionosphere. Int. J. Mass Spectrom. 1998, 172, (3), 209-219.

143. Suits, A. G., Titan: A Strangely Familiar World. J. Phys. Chem. A 2009, 113, (42), 11097-11098.

144. Randeniya, L. K.; Smith, M. A., Gas phase reaction rates of N_2^+ with CH_4, O_2, and n-H_2 at very low temperatures. J. Chem. Phys. 1991, 94, (1), 351-356.

145. Imanaka, H.; Smith, M. A., Formation of nitrogenated organic aerosols in the Titan upper atmosphere. Proc. Natl. Acad. Sci. USA 2010, 107, (28), 12423-12428.

146. Imanaka, H.; Smith, M. A., EUV Photochemical Production of Unsaturated Hydrocarbons: Implications to EUV Photochemistry in Titan and Jovian Planets J. Phys. Chem. A, 2009, 113, (42), 11187-11194.

147. Pollard, J. E.; Lichtin, D. A.; Cohen, R. B., Differential cross sections for state-selected reactions in the $H_2^+ + H_2$ system. Chem. Phys. Lett. 1988, 152, (2-3), 171-176.

148. Glenewinkel-Meyer, T. G., D., Single and Merged Beam Studies of the Reaction $H_2^+ + H_2 \rightarrow H_3^+ + H$. Israel J. of Chem. 1987, 37, 343.

149. Belikov, A. E.; Mullen, C.; Smith, M. A., State-specific reactions HBr^+ ($^2\prod_i$, v^+) + H_2, HBr) $\rightarrow$ H_2Br^+ at low collisional energies. J. Chem. Phys. 2001, 114, (15), 6625-6630.

150. Lykke, K. R.; Kay, B. D., Two-photon spectroscopy of N_2: Multiphoton ionization, laser-induced fluorescence, and direct absorption via the a"$^1\Sigma^+_g$ state. J. Chem. Phys. 1991, 95, (4), 2252-2258.

151. Kim, H.-T.; Anderson, S. L., Multiphoton ionization photoelectron spectroscopy of acetaldehyde via the $\tilde{A}^1$ A", B, C and D states . J. Chem. Phys. 2001, 114, (7), 3018-3028.

152. Conaway, W. E.; Morrison, R. J. S.; Zare, R. N., Vibrational state selection of ammonia ions using resonant 2 + 1 multiphoton ionization. Chem. Phys. Lett. 1985, 113, (5), 429-434.

153. Rijs, A. M.; Backus, E. H. G.; de Lange, C.; Janssen, M. H. M.; Wang, K.; V., M., Rotationally resolved photoelectron spectroscopy of hot N_2 formed in the photofragmentation of N_2O. J. Chem. Phys. 2001, 114, (21), 9413.

154. Stockbauer, R., Threshold electron-photoion coincidence mass spectrometric study of CH_4, CD_4, C_2H_6, and C_2D_6. J. Chem. Phys. 1973, 58, (9), 3800-3815.

155. Bombach, R.; Dannacher, J.; Stadelmann, J.-P., The rate/energy functions for the competitive fragmentation processes of ethylene and ethane cations. Int. J. Mass Spectrom. Ion Processes 1984, 58, 217-231.

156. Berkowitz, J.; Greene, J. P.; Cho, H.; Ruscic, B., The ionization potentials of CH_4 and CD_4. J. Chem. Phys. 1987, 86, (2), 674-676.

157. Frey, R. F.; Davidson, E. R., Potential energy surfaces of CH_4^+. J. Chem. Phys. 1988, 88, (3), 1775-1785.

158. Milhaud, J., On the formation of CH_4^+, CH_3^+, CH_2^+, CH^+ and C^+ secondary ions in methane. Internat. J. Mass Spectrom. Ion Phys. 1975, 16, (3), 327-337.

159. NIST, Data from NIST Standard Reference Database 69: NIST Chemistry WebBook. http://webbook.nist.gov/chemistry/.

160. Tsuji, M.; Kouno, H.; Matsumura, K.-I.; Funatsu, T.; Nishimura, Y.; Obase, H.; Kugishima, H.; Yoshida, K., Dissociative charge-transfer reactions of Ar^+ with simple aliphatic hydrocarbons at thermal energy. J. Chem. Phys. 1993, 98, (3), 2011-2022.

161. Mackie, R. A.; Scully, S. W. J.; Sands, A. M.; Browning, R.; Dunn, K. F.; Latimer, C. J., A photoionization mass spectrometric study of acetylene and ethylene in the VUV spectral region. Int. J. Mass Spectrom. 2003, 223-224, 67-79.

162. D. W. Turner, C. B., A. D. Baker, and C. R. Brundle, Molecular Photoelectron Spectroscopy Wiley-Interscience, New York, 1970.

163. K. Kimura, S. K., Y. Achiba, T. Yamazaki, and S. Iwata, Handbook of HeI Photoelectron Spectra of Fundamental Organic Molecules Japan Sci. Soc., Tokyo. 1981.

164. Pollard, J. E.; Trevor, D. J.; Reutt, J. E.; Lee, Y. T.; Shirley, D. A., Torsional potential and intramolecular dynamics in the C_2H_4 photoelectron spectra. J. Chem. Phys. 1984, 81, (12), 5302-5309.

165. Kim, M. H.; Leskiw, B. D.; Suits, A. G., Vibrationally Mediated Photodissociation of Ethylene Cation by Reflectron Multimass Velocity Map Imaging. J. Phys. Chem. A, 2005, 109, (35), 7839-7842.

166. Brack, A., The molecular Origins of Life. Cambridge University press: Cambridge, Ed. 1998.

167. Nixon, C. A.; Achterberg, R. K.; Teanby, N. A.; Irwin, P. G. J.; Flaud, J.-M.; Kleiner, I.; Dehayem-Kamadjeu, A.; Brown, L. R.; Sams, R. L.; Bezard, B.; Coustenis, A.; Ansty, T. M.; Mamoutkine, A.; Vinatier, S.; Bjoraker, G. L.; Jennings, D. E.; Romani, P. N.; Flasar, F. M., Upper limits for undetected trace species in the stratosphere of Titan. Faraday Disc. 2010, 147, 65-81.

168. Vuitton, V.; Yelle, R. V.; Anicich, V. G., The nitrogen chemistry of Titan's upper atmosphere revealed. ApJ . 2006, 647, (2), L175-L178.

169. Wincel, H.; Wlodek, S.; Bohme, D. K., Acetonitrile in gas-phase ion/molecule chemistry. Int. J. Mass Spectrom. 1988, 84, (1-2), 69-87.

170. Harland, P. W.; McIntosh, B. J., Enthalpies of formation for the isomeric ions H_xCCN^+ and H_xCNC^+ (x = 0-3) by "monochromatic" electron impact on C_2N_2, CH_3CN and CH_3NC. Int. J. Mass Spectrom. 1985, 67, (1), 29-46.

171. Mair, C.; Roithová, J.; Fedor, J.; Lezius, M.; Herman, Z.; Märk, T. D., Surface collisions of the acetonitrile molecular ion: evidence for isomerization of CD_3CN^+ to the ketenimine cation CD_2=C=ND^+. Int. J. Mass Spectrom. Ion Processes, 2003, 223-224, 279-290.

172. Choe, J. C., Isomerization and dissociation of the acetonitrile molecular cation. Int. J. Mass Spectrom. Ion Processes, 2004, 235, (1), 15-23.

173. Wu, C.; Xiong, Y.; Gao, Z.; Kong, F. a.; Lu, H.; Yang, X.; Xu, Z., Ionization and dissociation of acetonitrile by intense femtosecond laser pulse. Chinese Science Bulletin 2000, 45, (21), 1953-1955.

174. Vigren, E.; Semaniak, J.; Hamberg, M.; Zhaunerchyk, V.; Kaminska, M.; Thomas, R. D.; af Ugglas, M.; Larsson, M.; Geppert, W. D., Dissociative recombination of nitrile ions with implications for Titan's upper atmosphere. Planet. Space Sci. In Press, 2011, Corrected Proof.

ABSTRACT

ASTROCHEMICAL DYNAMICS:
FUNDAMENTAL STUDIES RELEVANT TO TITAN'S ATMOSPHERE

by

WILSON K. GICHUHI

August 2011

Advisor: Prof. Arthur G. Suits, PhD

Major: Chemistry (Physical)

Degree: Doctor of Philosophy

This work presents results of primary fundamental photodissociation and state-specific ion-molecule dynamical studies that are relevant to understanding the formation and growth mechanisms of unsaturated hydrocarbon molecules, haze layers and aerosols in Titan's upper atmosphere. In the *diacetylene dimer*, it is shown, via laboratory studies combined with electronic structure calculations that the photodissociation of the dimer readily initiates atomic hydrogen (H) loss and atomic H transfer reactions forming two prototypes of resonantly stabilized free radicals, C_8H_3 and C_4H_3, respectively. In ethylamine cation, high-level ab initio calculations identify the complex dissociation pathways for the ground state $CH_3CH_2NH_2^+$ radical cation at 233.3 nm using Direct current (DC) slice imaging technique, revealing important features of the potential surface that are important in Titan's ion-molecule reactions. Finally, a new technique is implemented to measure the branching ratios for the reactions of state-prepared N_2^+ ions with methane (CH_4), acetylene (C_2H_2) ethylene (C_2H_4), Hydrogen (H_2) and acetonitrile (CH_3CN) under a rotational temperature ~40 ± 5K.

AUTOBIOGRAPHICAL STATEMENT

WILSON K. GICHUHI

The early years of my academic, family and social life were spent in Kenya where I was born and raised. Though my parents did not receive any formal education, they were instrumental in motivating me to pursue education to greater heights so that I could become a teacher and live according to their 'wish and view' of a successful, educated son. The dream of becoming a 'teacher' was finally becoming a reality after I passed my secondary school and got admitted at the University of Nairobi to pursue B.S. in Chemistry where I graduated with a first class honors in 2001. In 2002, I joined the same university to pursue a M.S. in Environmental chemistry and graduated in 2005. In August 2005, I arrived in the U.S.A. to pursue PHD in chemistry. The following year, I joined Suits group where I was involved in carrying out fundamental studies relevant to Titan's atmosphere. While in the group, I encountered very stimulating, exciting and sometimes challenging experimental projects that increased my motivation to pursue fundamental experimental studies that can assist in understanding the chemistry of Titan's atmosphere and other related low temperature reducing environments. I am married with an 18 month old son, Lincoln Gichuhi. Apart from science, I enjoy athletics and cooking.